STATE OF CALIFORNIA DEPARTMENT OF TRANSPORTATION

TECHNICAL REPORT DOCUMENTATION PAGE

TR0003 (REV. 10/98)

1. REPORT NUMBER	2. GOVERNMENT ASSOCIATION NUMBER	3. RECIPIENT'S CATALOG NUMBER
CA13-1983		

4. TITLE AND SUBTITLE	5. REPORT DATE
Tsunami Forces on Selected California Coastal Bridges	June 2013
	6. PERFORMING ORGANIZATION CODE OSU
7. AUTHOR(S) Solomon C. Yim, Mohsen Azadbakht	8. PERFORMING ORGANIZATION REPORT NO. OSU/CA13-1983
9. PERFORMING ORGANIZATION NAME AND ADDRESS School of Civil and Construction Engineering Oregon State University 101 Kearney Hall Corvallis, OR 97331	10. WORK UNIT NUMBER 11. CONTRACT OR GRANT NUMBER 65A0384
12. SPONSORING AGENCY AND ADDRESS California Department of Transportation Engineering Service Center 1801 30th Street, MS 9-2/5i Sacramento, California 95816 California Department of Transportation Division of Research and Innovation, MS-83 1227 O Street Sacramento CA 95814	13. TYPE OF REPORT AND PERIOD COVERED Final Report 3/1/2011 – 2/28/2013 14. SPONSORING AGENCY CODE 913

15. SUPPLEMENTAL NOTES

Prepared in cooperation with the State of California Department of Transportation.

16. ABSTRACT

Tsunami horizontal and vertical forces and overturning moment time histories are computed for selected California coastal bridges. For each tsunami flow condition, the horizontal and vertical forces and overturning moment time histories are computed for four selected time periods containing: a) initial impact, b) occurrence of the maximum tsunami water velocity, c) occurrence of maximum tsunami momentum flux, and d) occurrence of maximum tsunami mass flux. It is found that the initial stage of tsunami loading on a bridge superstructure is a combination of horizontal and uplift forces. Maximum uplift force during the initial impact time period is found to occur when the tsunami water free-surface elevation reaches the top of the bridge barrier right before overtopping the bridge and starting to flow onto the bridge deck. It is observed that the time period representing the initial impact of the tsunami on the bridge superstructure leads to maximum horizontal force, downward vertical force, and overturning moment. Overall maximum uplift force is found to be in tsunami scenarios where the bridge superstructure is already inundated. The maximum horizontal force, downward vertical force, and overturning moment do not change significantly for different water elevations. Maximum uplift force is observed to increase for higher tsunami water free-surface elevations where the corresponding flow velocity is higher. Analyzing a deck-girder bridge considering the failure of the first seaward girder shows a 15% reduction in maximum horizontal force. Uplift force is found to be approximately 25% larger for the bridge with a failed first girder. A set of equations are proposed to compute maximum horizontal and vertical forces on bridge superstructures based on a regression analysis of the simulation results. Comparison between numerical results from simulations and the estimated forces using the recommended approach shows a good agreement between numerical predictions and formula estimations of the tsunami forces.

17. KEY WORDS	18. DISTRIBUTION STATEMENT	
Tsunami load, bridge superstructure, flow velocity, free-surface elevation, California coastal bridges	No restrictions. This document is available to the public through the National Technical Information Service, Springfield, VA 22161	
19. SECURITY CLASSIFICATION (of this report) Unclassified	20. NUMBER OF PAGES 145	21. PRICE

Reproduction of completed page authorized

DISCLAIMER STATEMENT

This document is disseminated in the interest of information exchange. The contents of this report reflect the views of the authors who are responsible for the facts and accuracy of the data presented herein. The contents do not necessarily reflect the official views or policies of the State of California or the Federal Highway Administration. This publication does not constitute a standard, specification or regulation. This report does not constitute an endorsement by the Department of any product described herein.

For individuals with sensory disabilities, this document is available in Braille, large print, audiocassette, or compact disk. To obtain a copy of this document in one of these alternate formats, please contact: the Division of Research and Innovation, MS-83, California Department of Transportation, P.O. Box 942873, Sacramento, CA 94273-0001.

Tsunami Forces on Selected California Coastal Bridges

by
Solomon C. Yim
and
Mohsen Azadbakht

School of Civil & Construction Engineering, Oregon State University

Final Report No. CA13-1983

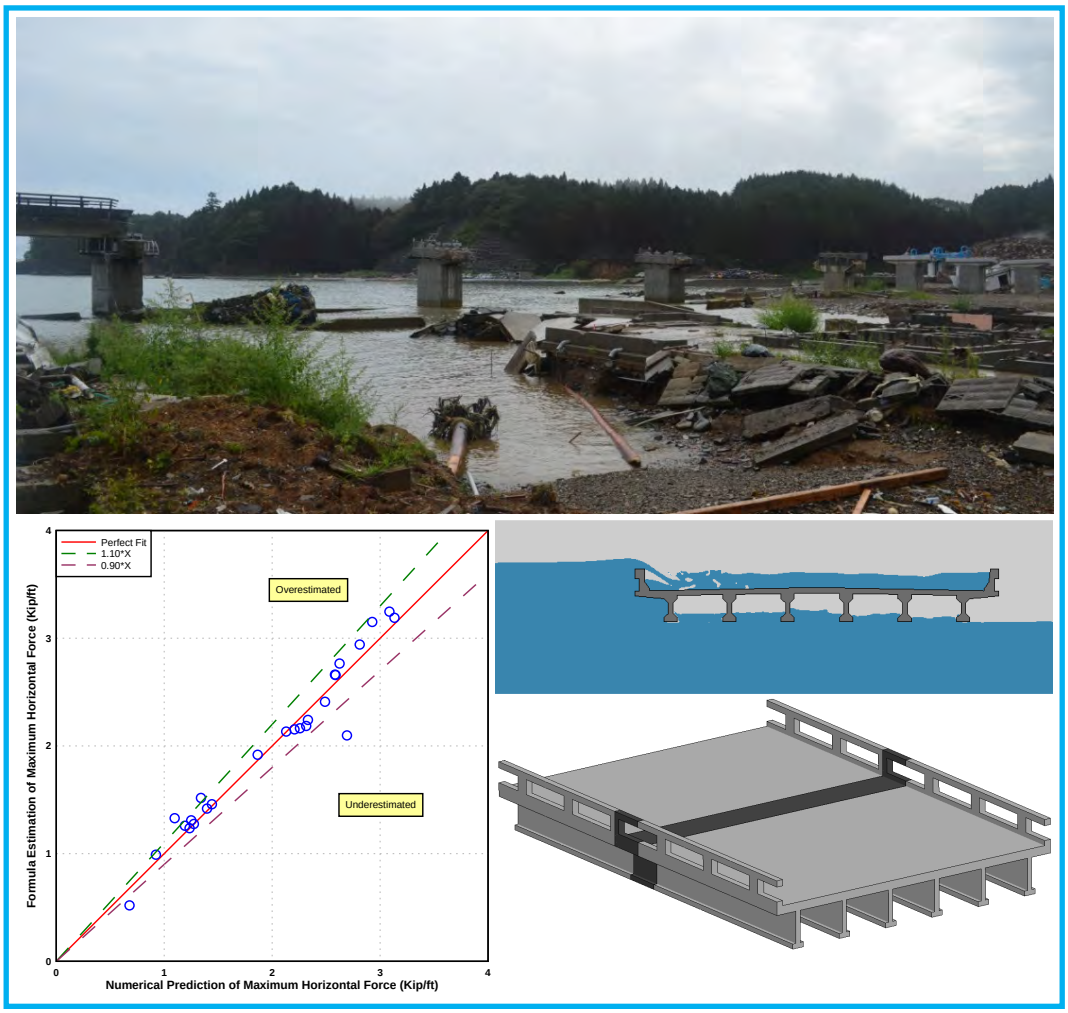

June 2013

Final Report submitted to the California Department of Transportation (Caltrans)
under Contract No. 65A0384

Table of Contents

1 Abstract 1
2 Background 3
2.1 Introduction 3
2.2 Literature review 4
2.2.1 Field surveys and observed bridges failure mechanisms during tsunamis 4
2.2.2 Experimental studies 5
2.2.3 Numerical studies 7
3 Tsunami Flow Field Boundary Condition Generation and Critical Time Periods 9
4 Numerical Modeling and Model Validation 13
4.1 Numerical Modeling 13
4.2 FE Model Validation 15
4.2.1 Experimental setup and measurements 15
4.2.2 Numerical simulations 15
5 Results and Discussion 19
5.1 Mad River Slough Bridge 19
5.2 Salmon Creek Bridge 23
5.3 Old Creek Bridge 26
5.4 Malibu Lagoon Bridge 28
5.5 Agua Hedionda Lagoon Bridge 30
6 The Effect of Failure of the First Seaward Girder in Deck-girder Bridges 33
7 Discussion on Tsunami Downward Vertical Force on Bridge Superstructures 34
8 Conditions for a Net Tsunami Uplift Force on a Bridge Superstructure 35
9 Tsunami Load Estimation Method for Bridge Superstructures 37
9.1 Proposed Tsunami Load Estimation Method 37
9.2 Example Calculation of Proposed Tsunami Load Estimation Method 45
10 A Note on Computational Efforts 47
11 Concluding Remarks 48
12 Acknowledgment 50
13 References 51

Appendix A. Time Histories of Tsunami Water Free-surface Elevation and Horizontal Velocity Components ……. A-1

Appendix B. Time Histories of Tsunami Horizontal and Vertical Forces and Overturning Moments on Selected Bridges ……...…….. B-1

Appendix C. Load Estimation Procedure Input and Results ……..…….. C-1

Appendix D. Screen Captures of CFD Simulations ……...…….. D-1

Appendix E. Drawings of Selected Bridges ……...…….. E-1

List of Figures

Figure 1. Utatsu Bridge failure during 2011 Great East Japan Earthquake and the subsequent Tohoku Tsunami (Photo by Yim). 5
Figure 2. Locations of selected bridges along California coast line (Source: Google Maps). 10
Figure 3. a) Tsunami water free-surface elevation and water velocity components in b) normal to the bridge direction, c) in north direction, and d) in east direction at the location of the Salmon Creek Bridge. 11
Figure 4. Scaled tsunami water free-surface elevation compared to bridge elevation, Salmon Creek Bridge. 12
Figure 5. Finite Element Models of Mad River Slough Bridge Superstructure, a) first approach and b) second approach. 14
Figure 6. Sketch demonstrating positive directions used to calculate the time history of horizontal and vertical forces and overturning moments. 15
Figure 7. Experimental setup to measure the hydrodynamic loads on inundated bridge decks (Kerenyi et al. 2009). 16
Figure 8. a) 3D FE model, b) strip of bridge used for modeling, c) Positive directions used to compute hydrodynamic forces and overturning moment. 17
Figure 9. a) Location of the Mad River Slough Bridge, b) close-up view of the bridge (Source: Google maps). 20
Figure 10. Screen captures of Mad River Slough Bridge, Water surface elevation 5 ft above bridge elevation, initial impact time period. 20
Figure 11. a) Tsunami forces and b) overturning moment time histories on the Mad River Slough Bridge, Water surface elevation 5 ft above bridge elevation, Initial impact time period. 21
Figure 12. Maximum horizontal and vertical forces and overturning moment on Mad River Slough Bridge for five different water elevations. 22
Figure 13. a) Location of the Salmon Creek Bridge, b) close-up view of the bridge (Source: Google maps). 23
Figure 14. Screen captures of Salmon Creek Bridge, Water surface elevation 5 ft above bridge elevation, initial impact time period. 24

Figure 15. a) Tsunami forces and b) overturning moment time histories on the Salmon Creek Bridge, Water surface elevation 5 ft above bridge elevation. 25
Figure 16. a) Maximum horizontal and vertical forces and b) overturning moment on Salmon Creek Bridge for five different water elevations. 26
Figure 17. a) Location of the Old Creek Bridge, b) close-up view of the bridge (Source: Google maps). 26
Figure 18. Screen captures of Old Creek Bridge, Water surface elevation 5 ft above bridge elevation, Initial impact time period. 27
Figure 19. a) Tsunami forces and b) overturning moment time histories on the Old Creek Bridge, Water surface elevation 5 ft above bridge elevation. 28
Figure 20. Maximum horizontal and vertical forces and overturning moment on Old Creek Bridge for five different water elevations. 28
Figure 21. a) Location of the Malibu Lagoon Bridge, b) close-up view of the bridge (Source: Google maps). 29
Figure 22. Screen captures of Malibu Lagoon Bridge, Water surface elevation 5 ft above bridge elevation, Initial impact time period. 29
Figure 23. a) Tsunami forces and b) overturning moment time histories on the Malibu Lagoon Bridge, Water surface elevation 5 ft above bridge elevation. 30
Figure 24. Maximum horizontal and vertical forces and overturning moment on Malibu Lagoon Bridge for five different water elevations. 30
Figure 25. a) Location of the Agua Hedionda Lagoon Bridge, b) close-up view of the bridge (Source: Google maps). 31
Figure 26. Screen captures of Agua Hedionda Lagoon Bridge, Water surface elevation 5 ft above bridge elevation, Initial impact time period. 31
Figure 27. a) Tsunami forces and b) overturning moment time histories on the Agua Hedionda Lagoon Bridge, Water surface elevation 5 ft above bridge elevation. 32
Figure 28. a) Maximum horizontal and vertical forces and b) overturning moment on Agua Hedionda Lagoon Bridge for five different water elevations. 33
Figure 29. a) Maximum horizontal and vertical forces and b) overturning moment on Mad River Slough Bridge for five different water elevations, Intact bridge versus bridge without first girder. 34
Figure 30. Sketch demonstrating the tsunami flow direction on bridge deck. 35
Figure 31. Graphical demonstration of the net forces acting on a bridge superstructure during tsunami strike a) initial impact before overtopping the bridge, b) initial impact after overtopping the bridge, and c) total inundation of the bridge. 37
Figure 32. Sketch demonstrating different parameters used in the tsunami load estimation method. 40
Figure 33. Comparison between formula estimation and numerical prediction of the maximum horizontal forces. 42

Figure 34. Comparison between formula estimation and numerical prediction of the maximum downward vertical forces. 42
Figure 35. Comparison between formula estimation and numerical prediction of the maximum uplift forces. 43
Figure 36. Comparison between formula estimation and numerical prediction of the maximum horizontal forces (Using exact value for h parameter). 44
Figure 37. Comparison between formula estimation and numerical prediction of the maximum downward vertical forces (Using exact value for h parameter). 44

List of Tables

Table 1. Comparison between drag, lift, and moment coefficients measured from the experiment and the numerical simulation 17
Table 2. Empirical coefficients for tsunami load estimation 41
Table 3. Empirical Force coefficients for tsunami load estimation 41

1 Abstract

Tsunami horizontal and vertical forces and overturning moment time histories are computed for selected California coastal bridges. The tsunami input data sets, which includes tsunami water free-surface elevation and horizontal velocity components, were provided by the California Department of Transportation (Caltrans). Tsunami maximum water free-surface elevation data are scaled to 5, 10, 15, 20, and 25 feet above bridge elevation to obtain five tsunami flow conditions for each bridge. For each tsunami flow condition, the horizontal and vertical forces and overturning moment time histories are computed for four selected time periods containing: a) initial impact, b) occurrence of the maximum tsunami water velocity, c) occurrence of maximum tsunami momentum flux, and d) occurrence of maximum tsunami mass flux. Two different modeling approaches are used. To model the initial impact of the tsunami on bridge superstructure, the bridge is placed on top of the body of water then water starts to surge toward it. For the other three time periods as flow depth is higher than the bridge elevation, an already inundated bridge is used for analyses. The resulting horizontal and vertical forces and overturning moments are analyzed and compared for the selected time periods for each tsunami flow condition. From the numerical simulations, it is found that the initial stage of tsunami loading on a bridge superstructure is a combination of horizontal and uplift forces. These forces gradually increase as the tsunami water free-surface elevation rises. The horizontal force is due to hydrostatic force caused by accumulation of water on the seaward side of the bridge superstructure and a drag force due to resistance of the bridge superstructure against the tsunami flow. Maximum uplift force during the initial impact time period is found to occur when the tsunami water free-surface elevation reaches the top of the bridge barrier right before overtopping the bridge and starting to flow onto the bridge deck. After this time, the uplift force acting on a partially inundated bridge is countered by the weight of water ponding on the deck and slamming force caused by the tsunami hitting the upper surface of the bridge deck. The resultant vertical force is a downward force which increases as the tsunami water free-surface elevation and flow velocity increase. It is observed that the time period representing the initial impact of the tsunami on the bridge superstructure leads to maximum horizontal force, downward vertical force, and overturning moment. Overall maximum uplift force is found to be in tsunami scenarios where the bridge superstructure is already inundated. Comparing the

resultant forces from different tsunami water free-surface elevations reveals that the maximum horizontal force, downward vertical force, and overturning moment do not change significantly for different water elevations. This is because they occur in initial impact time period where flow depth is limited to a range from the low chord of the bridge to top of the bridge barrier. Maximum uplift force is observed to increase for higher tsunami water free-surface elevations where the corresponding flow velocity is higher. Analyzing a deck-girder bridge considering the failure of the first seaward girder shows a 15% reduction in maximum horizontal force. Uplift force is found to be approximately 25% larger for the bridge with a failed first girder. A set of equations are proposed to compute maximum horizontal and vertical forces on bridge superstructures based on a regression analysis of the simulation results. Comparison between numerical results from simulations and the estimated forces using the recommended approach shows a good agreement between numerical predictions and formula estimations of the tsunami forces. An example demonstrating how the recommended design procedure can be used to estimate the maximum horizontal force, maximum downward vertical force, and the maximum uplift force on a bridge superstructure during a tsunami event is also provided in section 9.2.

2 Background

This section provides a summary on the importance of the study as well as a comprehensive literature review on response of bridge superstructures during past tsunamis.

2.1 Introduction

Tsunamis have caused significant damage to coastal communities in recent years. The 2011 Great East Japan Earthquake and resulting Tohoku Tsunami destroyed many infrastructures along Japan's east coast including bridge superstructures (Iemura et al. 2005; Kawashima 2012; Yashinsky 2012). More than 300 bridges were reported to be washed away due to the 2011 Tohoku Tsunami where the tsunami wave heights were estimated to be 5 to 15 m in different regions (Akiyama et al. 2012; Maruyama et al. 2012). It was reported that most of the bridges survived the earthquake but were completely destroyed after being hit by tsunami (Akiyama et al. 2012), indicating that the current design specification cannot provide bridges with sufficient strength to resist the tsunami loads. The bridge columns previously retrofitted by steel jackets were observed to perform well during earthquake and tsunami (Kawashima 2012).

Highway bridges, as an important part of transportation system, have a significant role in maintaining access to coastal communities after a tsunami. Therefore, tsunami-resistant design of these superstructures is crucial. Although the scientific community has been interested in behavior of bridges during hurricanes and storm surges over the past few years (e.g. Douglass et al. 2006; Robertson et al. 2007a and b; Okeil and Cai 2008; Cuomo et al. 2009; Sheppard and Marin 2009; Bradner et al. 2011; Jin and Meng 2011; Gullett et al. 2012) few comprehensive studies have been conducted regarding measuring tsunami forces on bridge superstructures. Most of these studies are either limited to surveys conducted after past major tsunamis explaining the failure mechanisms (e.g. Iemura et al. 2005; Akiyama et al. 2012; Kawashima 2012; Kosa 2012) or small scale experimental studies not covering a reasonable range of wave types and bridge configurations (e.g. Kataoka 2006; Sugimoto and Unjoh, 2007; Kosa et al. 2010).

2.2 Literature review

A comprehensive literature review on response of bridge superstructures during past tsunamis is provided here. First, field surveys conducted after the recent major tsunamis and observed bridge failure mechanisms are discussed. Then a review of experimental studies on tsunami loads on bridge superstructures is provided. Finally a brief survey of numerical studies on predicting tsunami loads on coastal bridges is summarized.

2.2.1 Field surveys and observed bridges failure mechanisms during tsunamis

2.2.1.1 Failure of the connections attaching the bridge superstructure to substructure

This type of failure can be considered as the most likely failure of a bridge during tsunami and hurricane events. Figure 1 shows an example of failure of these connections during the 2011 Great East Japan Earthquake and following Tohoku Tsunami. As a typical failure of bridges during tsunami and hurricane events, standing piers along with washed off superstructure are elements which indicate the weakness of connections between superstructure and substructure. This type of failure is a result of both horizontal and uplift forces acting on the bridge superstructure. The damaged shear keys and evidences of dragging bridge girders on piers and pile caps demonstrate that the uplift forces were not high enough, in some cases, to completely lift the bridge decks from its supports. However it has been reported in some cases that the uplift force on a bridge superstructure was responsible for lifting bridge decks from its piers where the drag force subsequently pushed them off the supporting piers. The intact stoppers installed to prevent the bridge superstructure from excessive longitudinal and transverse displacements were believed to prove this hypothesis (Akiyama et al. 2012).

2.2.1.2 Scour around bridge abutments and supporting piers, failure of the foundation, failure of the bridge piers, and failure duo to debris impact

In addition to failure of the connections supporting the bridge superstructure which caused the bridge superstructure to be washed away after being hit by tsunami in many cases, failure of the bridge piers was also reported in some cases (Maruyama et al. 2012).These failures are other types of failure related to the bridge substructure and will not be further discussed in this article as the present work focuses on the behavior of bridge superstructures under tsunami loads.

However, an interesting observation regarding the failure of bridges under tsunami and hurricane induced loads is pertinent to the location of the dislocated bridge decks. In the case of hurricane, although these decks have been found to be dislocated landward to some extent, they are relatively close to the centerline of bridge while for tsunamis the dislocated decks were found to be far from the original bridge centerline indicating the substantial difference between horizontal force components of tsunamis and hurricanes. Failure of a concrete deck at mid-span, as a result of pounding between superstructure and substructure seen during Hurricane Katrina, is believed to be due to repeated lift and drop actions (Okeil and Cai, 2008). This type of failure which has not been reported in past tsunami survey reports (to the best of writers' knowledge) can be considered as another evidence for low horizontal component of the wave force during hurricanes compared to tsunamis.

Figure 1. Utatsu Bridge failure during 2011 Great East Japan Earthquake and the subsequent Tohoku Tsunami (Photo by Yim).

2.2.2 Experimental studies

After the 2004 Indian Ocean Tsunami, a few experimental studies were carried out to evaluate the tsunami loads on bridge superstructures (e.g. Kataoka 2006; Lukkunaprasit et al. 2008; Sugimoto and Unjoh 2008; Kosa et al. 2010; Zhang et al. 2010). These studies were performed using small scale setups where tsunami waves were generated as solitary waves using a wavemaker or releasing water from an elevated water tank. Kataoka (2006) observed a sudden

impulsive force on bridge model due the water impact followed by a slowly decreasing drag force. It was found that the breaking of the wave has a significant effect on the amount of the impulsive force. The results also showed a relatively constant downward force on bridge model after the impact. Sugimoto and Unjoh (2007) found that the higher still water level resulted in higher lift force on bridge model. It was reported that the bridge models were dropped off the supports when the drag force and lift force exceeded a certain threshold value. This threshold was roughly determined as drag force larger than the self-weight of the bridge model and the lift force twice as large as the self-weight. Lukkunaprasit et al. (2008) studied the effect of the perforations in girders and parapets on reducing the tsunami horizontal force. Tsunami waves were generated by releasing water from an elevated water tank to a wave flume. The horizontal force on the bridge deck was computed by subtracting the force acting on the pier, measured from a separate experiment, from the total force acting on the bridge model. Pressures on the perforated model were found to be close to pressures on the solid model while the resulting horizontal forces in the perforated model were smaller compared to the solid model. The amount of reduction in peak horizontal force was close to the amount of area reduction in the perforated model. Araki et al. (2010) compared the uplift force measurements due to impact of the two types of the waves on a bridge model, just breaking wave and post breaking wave. In case of just breaking wave two peaks were observed in the uplift force time history followed by a downward force while for post breaking wave one peak was observed. The results showed that the magnitude of both the horizontal and uplift force was higher in the cases of just breaking wave. Results from the pressure gauges showed that the smaller tsunami waves led to higher pressures on the face of the seaward girder. Similar behavior was observed for the other two pressure gauges representing the uplift force. It was also concluded that the pressure was higher at the bottom of the deck compared to bottom of the girder. The authors also suggested that any study on fluid impact force on bridge should take into account the dynamic response of the bridge as the duration of the impact force is very short. Kosa et al. (2010) investigated the effects of the different wave forms, broken and unbroken, on the resulting tsunami force on bridges. It was observed that the location of the bridge with respect to the point where the wave breaks can affect the resulting forces. It was observed that for two waves with approximately same height the broken wave led to higher horizontal force while the unbroken wave resulted in larger uplift force. It was also observed that the broken wave led to a relatively constant downward force

while water was overtopping the bridge. Zhang et al. (2010) provided the results of a study on using fairing to reduce the tsunami hydrodynamic force on bridges. For a bridge model without fairing, a high horizontal surge force followed by a relatively constant drag force was measured. The magnitude of the drag force was found to be 1/3 of the peak surge force. Similar behavior was observed for vertical force time history. A downward vertical force was measured after the wave overtopped the bridge. The results showed a significant reduction in maximum horizontal surge force after using the fairing. No obvious reduction pattern for maximum vertical force was observed. Kerenyi et al. (2009) studied the hydrodynamic loads on the inundated bridge decks. More information of this study is provided in the numerical model validation section.

2.2.3 Numerical studies

Lau et al. (2011) provided experimental study and numerical investigations to find tsunami force on bridge decks. The studied model composed of both superstructure and supporting pier. Force time history was divided into two parts, the impulsive phase referring to the maximum force and the slowly-varying phase showing the relatively constant force after wave impact on bridge. The impulsive force was found to be higher for models with less clearance while the slowly-varying force was almost the same for all clearances. The vertical force time history showed an uplift force during the wave impingement on model and a relatively constant downward force when wave overtops the model. This trend was similar for all clearances although the models with less clearance underwent relatively higher uplift and downward forces. Yim et al. (in progress) computed tsunami loads on the Spencer Creek Bridge on the US Highway-101 at Newport, Oregon. Tsunami scenarios were generated based on the possible rupture models of Cascadia subduction zone. Both two and three dimensional models were developed. Maximum tsunami vertical forces were found to be 1.6 to 2.7 times larger than the corresponding horizontal forces. Cheung et al. (2011) developed a set of tsunami scenarios for probabilistic design of bridge superstructures. These tsunami scenarios were used to numerically estimate the tsunami loading on four bridges located on Highway 101 in the Siletz Bay area on the Oregon Coast (Yim et al. 2011). The slamming force on the box girder bridge was found to be approximately 1.5 to 3 times the drag force while this number was approximately one for deck girder bridges. The loads on the box girder bridge were reported to be higher than those of the deck girder bridge. The results also showed that rigid closed rails on

the superstructure could increase horizontal and vertical tsunami forces up to 20% and 15%, respectively, compared to open railing system.

This report presents results of a study on numerically simulating tsunami forces on selected bridge superstructures along California coast line. The locations of these bridges are shown in Figure 2. Tsunami flow conditions for these selected bridges were provided by the California Department of Transportation (Caltrans). These tsunami flow condition data sets contain water free-surface elevation and horizontal velocity components in the north and the east directions. These flow depth and velocity data sets are used as a boundary condition in a finite element model (FEM) to calculate the fluid flow field surrounding the bridge superstructure and the resulting horizontal and vertical forces time histories as well as overturning moment acting on bridge superstructures due to uneven distribution of the tsunami horizontal and vertical loads.

3 Tsunami Flow Field Boundary Condition Generation and Critical Time Periods

Tsunami flow fields including water free-surface elevation and horizontal velocity components near the bridge sites were provided by Caltrans. These tsunami flow fields were developed for various return periods up to 2500 years based on distant tsunami sources, and were calculated based on earthquakes sources only. In this method deformation and displacement of the ocean floor caused by earthquake are used to compute the change in water free-surface elevation. Long wave approximation is used to model the propagation of the tsunami towards the coast. According to this theory the vertical acceleration of water is negligible compared to gravity acceleration resulting in uniform velocity in water column which travels in horizontal direction. The finite difference method is used to solve the equations of motion and continuity (Caltrans, 2010).

Time histories of tsunami water free-surface elevation and horizontal velocity components are used as the boundary condition to generate tsunami flow field at the location of the bridge superstructure. This boundary is set sufficiently far away from the bridge superstructure such that the domain of influence of the presence of the bridge superstructure does not overlap the input boundary but as close as possible to maximize the tsunami loads and minimize the computational domain. Since the tsunami water free-surface elevations in provided data sets were lower than the elevation of the bridges, the maximum water free-surface elevation was scaled up to 5, 10, 15, 20, and 25 feet above bridge elevation, and the rest of the tsunami water free-surface elevation time history was scaled up accordingly. The tsunami horizontal velocity components at the boundary were scaled using square root of the scale factor used to increase the tsunami water free-surface elevation (based on dimensional analysis and similitude theory). Figure 3 shows, for example, the tsunami free-surface elevation and the water velocity component normal to the bridge superstructure at the location of the Salmon Creek Bridge. Considering the location of the State of California, negative normal velocities in tsunami profiles (i.e. Figure 3b) generally represent the tsunami flow during the drawdown where water travels from east to west. In some cases the absolute values of these negative velocities were higher than the positive ones and, therefore, were used in the tsunami load simulations.

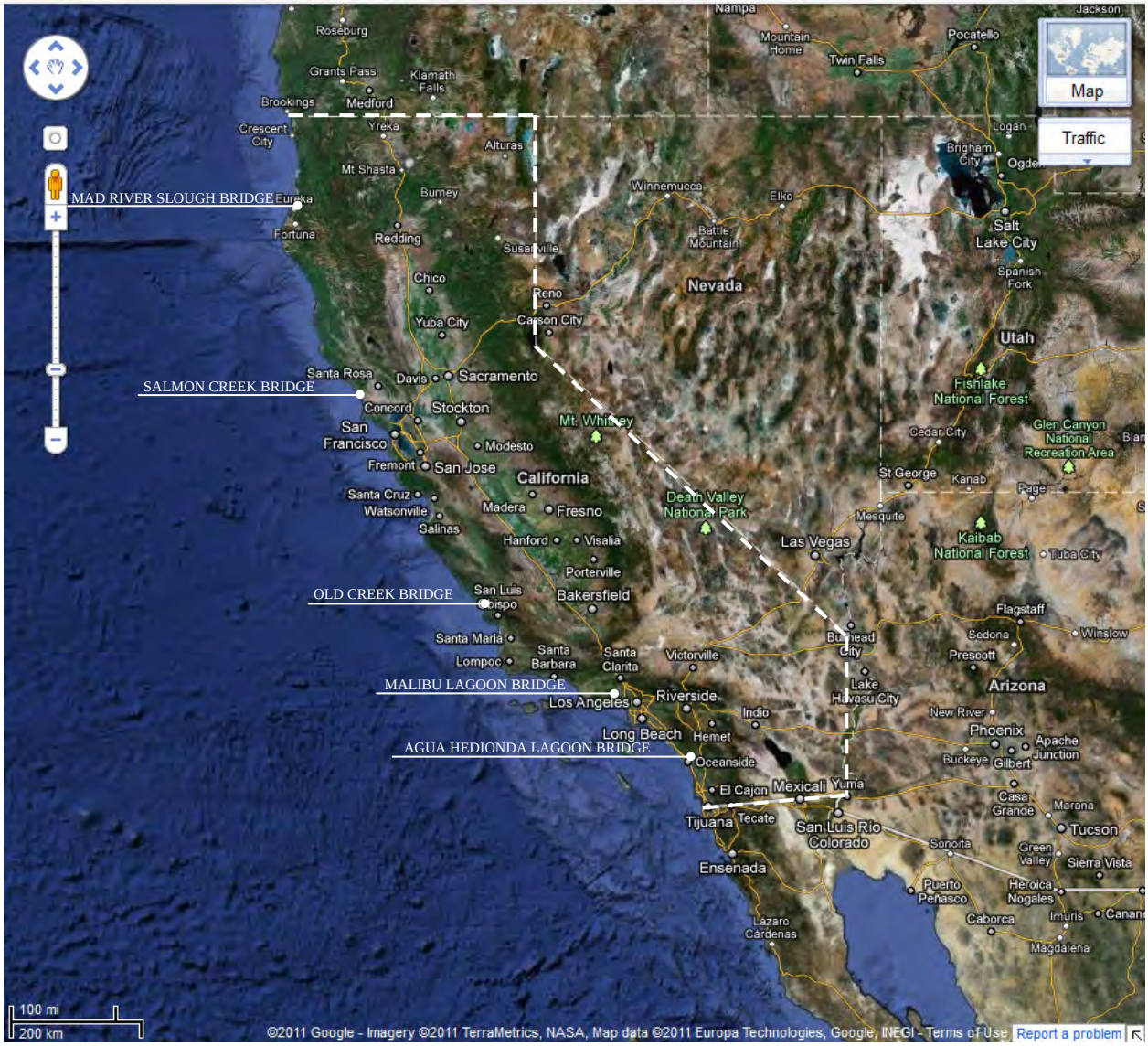

Figure 2. Locations of selected bridges along California coast line (Source: Google Maps).

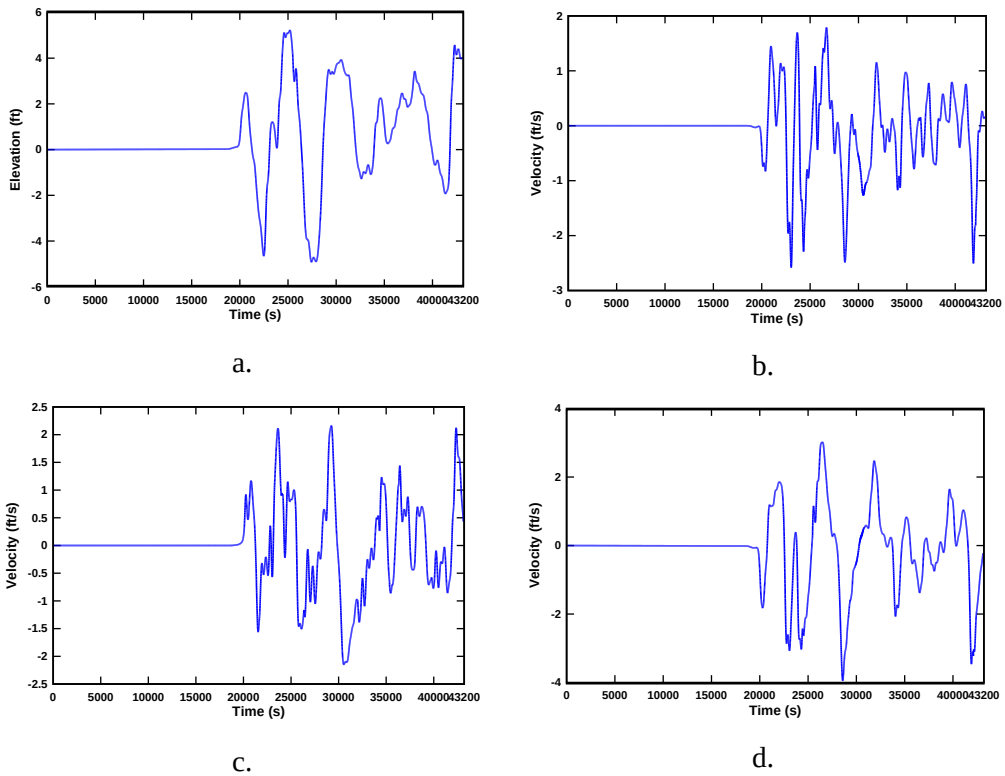

Figure 3. a) Tsunami water free-surface elevation and water velocity components in b) normal to the bridge direction, c) in north direction, and d) in east direction at the location of the Salmon Creek Bridge.

Tsunami flow durations are usually on the order of hours, thus in order to capture the behavior of the structure under several impacts and inundations during the entire process, multiple time durations should be analyzed in detail. Since it is impractical to perform a large-domain computational fluid dynamics (CFD) analysis from beginning to end for such a long duration, it is decided to perform the simulations for a set of time periods representing the most critical scenarios such that the simulation time periods essentially cover all the important features of the entire tsunami load duration. Followings are the time periods studied:

a. initial impact; the duration when tsunami water free-surface elevation reaches the low chord of the bridge superstructure and rises from there until it reaches the top of the bridge barrier where it overtops the bridge and starts to flow on the bridge deck;
b. the time when maximum flow velocity (V) occurs;
c. the time when the maximum momentum flux ($H*V^2$) occurs; and
d. the time when the maximum mass flux (H*V) occurs.

where H is the tsunami water free-surface elevation and V is the tsunami horizontal velocity. Initial impact time period represents a period during which the first interaction between

tsunami water and the seaward side of the bridge cross-section occurs. Since there may be several initial impacts during a tsunami due to different number of tsunami waves hitting the bridge superstructure during a tsunami, the time period that contained the highest flow velocity is selected to perform the CFD analysis. The maximum flow velocity duration represents a time period in which the tsunami water reaches its highest velocity during the tsunami. The maximum momentum flux and maximum mass flux time periods refer to durations in which the maximum momentum flux and maximum mass flux were recorded, respectively. For cases that initial impact on the bridge superstructure occur at the same time as the maximum water velocity, momentum flux, and mass flux occurred a single model is utilized to calculate the resulting forces induced by tsunami on the bridge superstructure from initial impact to total submergence of the structure. In other cases separate analyses are performed. Figure 4, for example, shows the scaled tsunami water free-surface elevation compared to the bridge elevation for Salmon Creek Bridge.

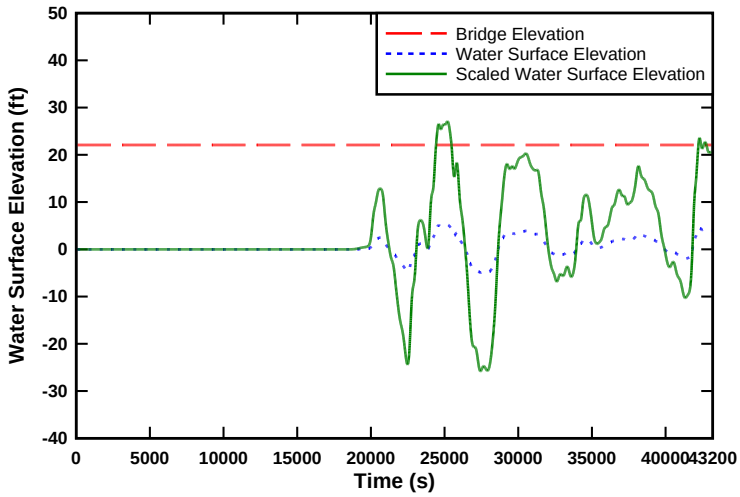

Figure 4. Scaled tsunami water free-surface elevation compared to bridge elevation, Salmon Creek Bridge.

4 Numerical Modeling and Model Validation

4.1 Numerical Modeling

A finite element analysis (FEA) code, LS-DYNA, is used to perform the CFD analysis and calculate the horizontal and vertical forces and overturning moments on selected bridge superstructures due to tsunami loading. The numerical code solves the Navier-Stokes (N-S) equations to obtain the pressure field and consequently forces on the structure. An arbitrary Lagrangian-Eulerian (ALE) formulation was used to track the fluid particles on the fluid free surface. The advantages of using this model over other available CFD analysis codes is its ability to solve the N-S equations and accurately model multi-physics contact and impact instead of potential flow equations which widely used in the ocean and coastal engineering community. The ability to solve the N-S equations allows the model to capture all the effects related to fluid viscosity and rotation of the fluid particles which are neglected in potential-theory based codes. This feature, for example, makes the numerical code able to model wave breaking and fluid impact on the structure, which are crucial in modeling the tsunami and its effects on the structure (Hallquist 2006).

Two different modeling approaches are used. To model the initial impact of the tsunami on bridge superstructure, the bridge is placed on top of the body of water then the water surges toward it. For the other three time periods, as the flow depth is higher than the bridge elevation, an already submerged bridge is used as an initial condition for analyses. The reason two different models are used is because of the different tsunami flow fields for each type. In the model developed for initial impact time period both water free-surface elevation and flow velocity change with time while in the other time periods the goal is to achieve a constant tsunami flow depth and velocity as the bridge is already fully inundated. Figure 5 show these two FE models. The different parts of the FE model domains in both models are also shown in Figure 5. For both models, the domain consists of the two parts: a) a fluid part which includes both water and air domains and b) a bridge superstructure. Solid brick elements are used to model the entire domain. In this study, the bridge superstructure is modeled as a rigid body. The bridge superstructure considered in this study comprises of the bridge deck, supporting girders, and the end barriers which are continuous along the bridge longitudinal direction. Bridge rails are not modeled considering the fact that 2-D FE models are not able to capture the 3-D effects related

to open-gap bridge railings. This assumption was opted because in reality tsunami flow can pass through an open railing system facing minimal resistance except in the presence of debris possibly carried by tsunami water blocking the open spaces between rails. Note that the effect of debris is not included in this study.

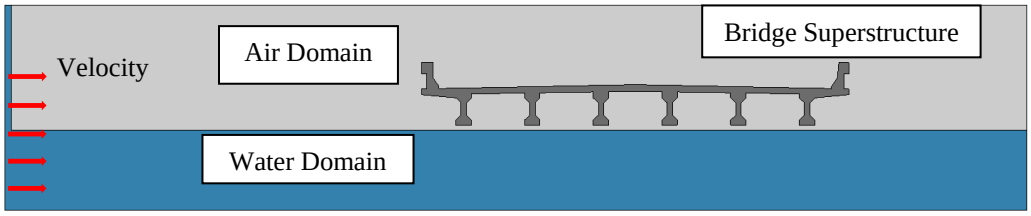

a.

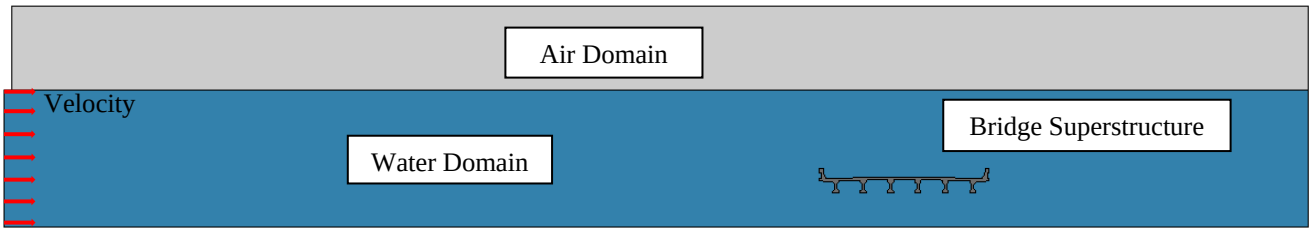

b.

Figure 5. Finite Element Models of Mad River Slough Bridge Superstructure, a) first approach and b) second approach.

Two different approaches are used to model the air in the FE domain. Since in the model developed for initial impact time period the effect of the air trapped under the bridge and between girders is very important in increasing the uplift force, a material representing the real air is modeled. In the second type of the models the bridge model is totally inundated during the simulation and the presence of the air on top of the water free-surface does not affect the resulting hydrodynamic loads and moments. For this modeling, a single-phase simulation is performed and the air domain is modeled as a void part. This void part has no materialistic representation by itself and simply provides an empty mesh domain for the adjacent fluid material to flow in during the simulation if needed. The use of this method over the conventional water-air domain results in significantly less computational time. The resulting overturning moment is computed about the center of gravity of bridge.

A sketch demonstrating the positive directions used to calculate the time history of horizontal and vertical forces is shown in Figure 6.

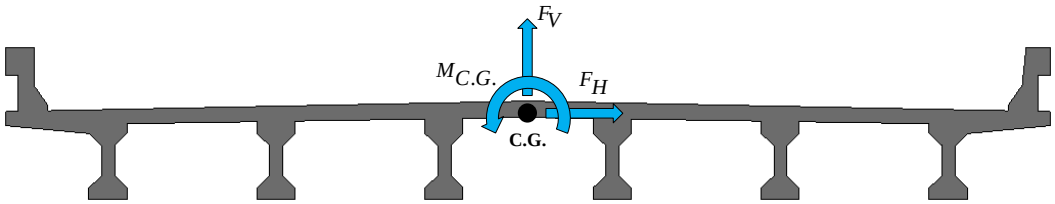

Figure 6. Sketch demonstrating positive directions used to calculate the time history of horizontal and vertical forces and overturning moments.

4.2 FE Model Validation

This section provides the results of a study conducted to evaluate the accuracy of the developed FE model. The predictions of the FE model are compared to experimental measurements of drag, lift, and moment coefficients. The study conducted by Kerenyi et al. (2009) is used here to validate the accuracy of the numerical modeling approach.

4.2.1 Experimental setup and measurements

Kerenyi et al. (2009) studied the hydrodynamic loads on the inundated bridge decks. The experimental results for a 6-Girder bridge model showed the minimum drag coefficients about one while the bridge was totally inundated but close to water free-surface. For higher inundations depths, drag coefficients of approximately 2 were measured. The measured coefficients were sensitive to Froude number as higher Froude numbers led to higher drag coefficients. Lift coefficients were found to be negative for all cases meaning that the inundated bridge decks were subjected to downward hydrodynamic forces. The values of lift coefficients about -1to -1.5 were found to be at the threshold when the bridge is being totally inundated. These lift coefficients approached zero for higher inundation depths. Drag coefficients were found to be relatively smaller in a 3-Girder bridge model compared with the 6-Girder model while the lift coefficients were slightly higher (in the 3-Girder model). Drag coefficients for a streamlined model were found to be approximately half of the 6-Girder model while the lift coefficient at the inundation threshold was almost 20-25% less than those of girder models.

4.2.2 Numerical simulations

A 3D FE model was developed for the verification study. Since the experiments were conducted on a bridge whose cross section was variable along the bridge direction, a 3D numerical

modeling was deemed necessary to provide accurate results. The 3D FE model is shown in Figure 8a. In order to minimize the computational time, a strip of the bridge consisting of half of the bridge length with rail and half of bridge length without rail was modeled. This strip is shown in Figure 8b. Figure 8c shows the positive directions of the computed tsunami forces and overturning moment. A FE domain similar to the one shown in Figure 5b is developed in accordance to the dimensions of the flume in which the experiments were carried out.

Figure 7. Experimental setup to measure the hydrodynamic loads on inundated bridge decks (Kerenyi et al. 2009).

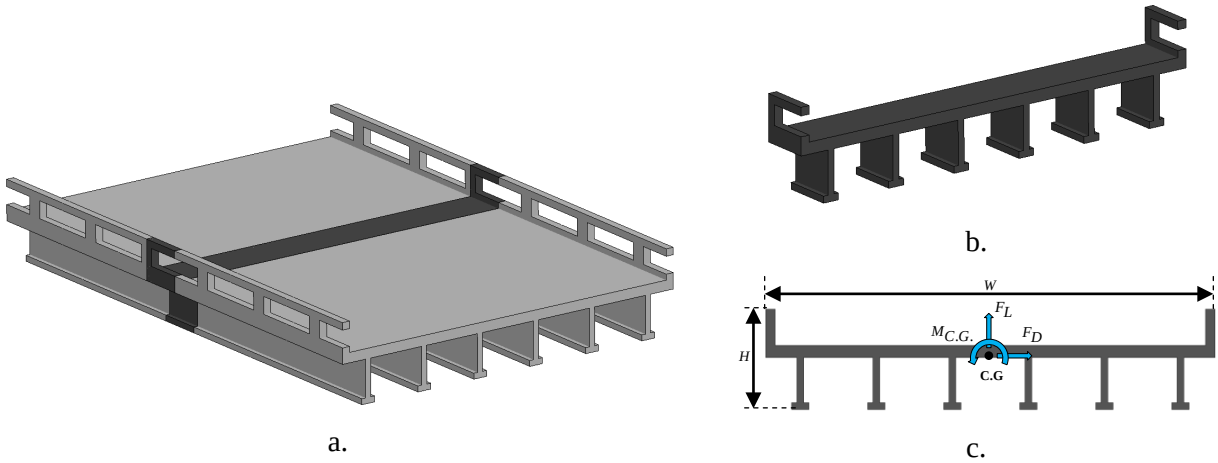

Figure 8. a) 3D FE model, b) strip of bridge used for modeling, c) Positive directions used to compute hydrodynamic forces and overturning moment.

A comparison between drag, lift, and moment coefficients measured from the experiment and the numerical simulation is presented in Table 1. The experimental measurements are from a case with Froude number equal to 0.28 and the inundation ratio of 3 meaning that the difference between water level and the low chord elevation of the bridge is 3 times the height of the bridge specimen. The modeling here has been compared to experimental results for the bridge with the lowest elevation. This is because for the tsunami scenarios in which the bridge is close to water free-surface a different type of modeling is used to study the impact forces on the bridge. Drag, lift, and moment coefficients were obtained from the computed horizontal and vertical forces and moment through Equations 1-3. Table 1 shows good agreement between experimental measurements and numerical simulation results.

Table 1. Comparison between drag, lift, and moment coefficients measured from the experiment and the numerical simulation

	Experimental Measurements	Numerical Results
Drag coefficient ( )	2.00	2.11
Lift coefficient ( )	-0.080	-0.067
Moment coefficient ( )	-0.022	-0.027

(1)

(2)

(3)

where:

: Drag coefficient,

: Lift coefficient,

: Moment coefficient,

: Drag Force,

: Lift Force,

: Moment Force,

ρ: Density of water,

v: flow velocity,

W: Width of the bridge section,

L: Length of the bridge section,

H: Height of the bridge section.

5 Results and Discussion

The results of the FE analyses performed to calculate the tsunami forces on the selected bridges are presented in this section. The bridges studied are: Mad River Slough Bridge, Salmon Creek Bridge, Old Creek Bridge, Malibu Lagoon Bridge, and Agua Hedionda Lagoon Bridge. Note that the maximum values of horizontal and vertical loads and overturning moment obtained for each water free-surface elevation come from possibly different time periods with different amounts of water free-surface elevation and flow velocity. The work presented here should not be considered as a parametric study in which the effect of varying a single parameter is assessed by keeping all other parameters unchanged. As the main purpose of this study was to estimate the tsunami loading under different conditions on five selected bridges and eventually evaluating the vulnerability of the bridges under provided tsunami conditions, we suggest that maximum values representing the critical situations be used for the final design loads consideration.

5.1 Mad River Slough Bridge

The Mad River Slough Bridge is a precast I girder bridge with a reference elevation 8 foot – 8 inches above the mean sea level (MSL). Figure 9 illustrates the location of the bridge with respect to the coast line and a close-up view of the bridge. A total of 15 simulations are performed in order to study the tsunami loading on this bridge. For each water free-surface elevation three simulations were performed, first for the initial impact time period, second for the time when maximum tsunami flow velocity occurs, and third for the time when maximum tsunami momentum flux and mass flux occur. Tsunami free-surface elevation and velocity profiles show that both the maximum tsunami momentum flux and the mass flux occur at a same time, thus requiring only one simulation to cover both time periods. Since the maximum free-surface elevation might occur at different times than the maximum momentum flux, mass flux, and velocity, the water free-surface elevation should not be expected to be at exactly, for example, 5 ft above the bridge in the simulation representing the scaled free-surface elevation of 5 ft above bridge elevation. For this particular bridge the time that maximum momentum flux, mass flux, and velocity occur is close to that of maximum free-surface elevation creating a large hydrostatic pressure and consequently large horizontal force. A set of screen captures of the initial impact time period simulation of the Mad River Slough Bridge for a free-surface elevation

of 5 ft above bridge elevation is shown in Figure 10.

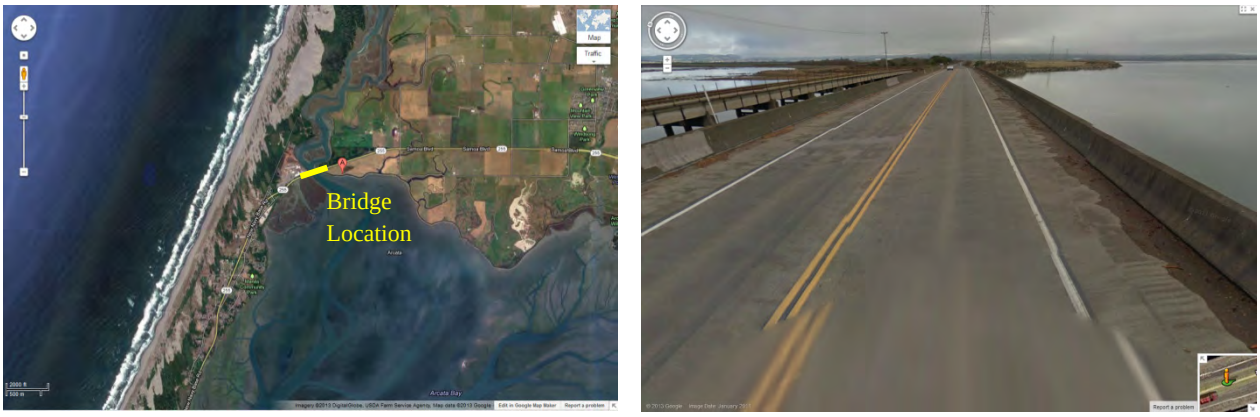

a. b.

Figure 9. a) Location of the Mad River Slough Bridge, b) close-up view of the bridge (Source: Google maps).

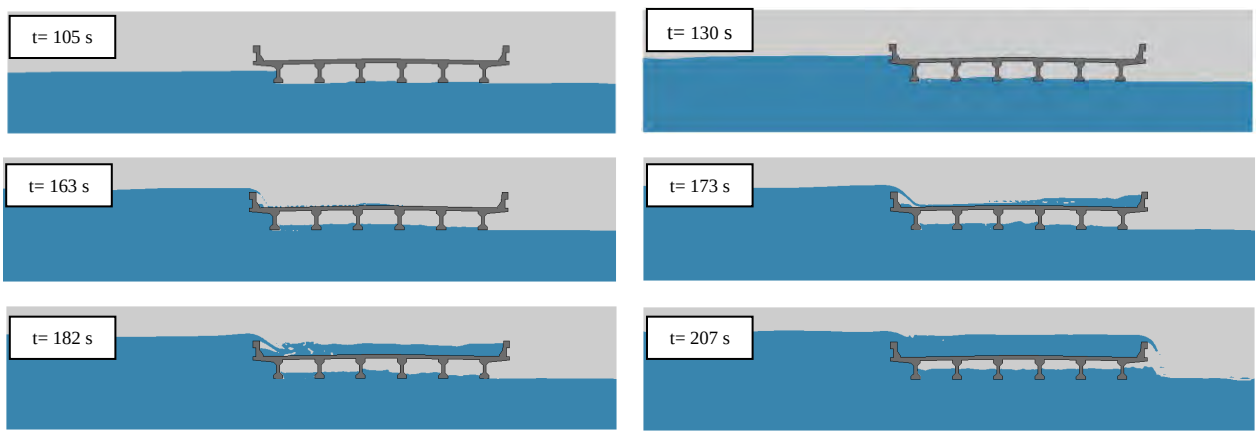

Figure 10. Screen captures of Mad River Slough Bridge, Water surface elevation 5 ft above bridge elevation, initial impact time period.

Three different aspects of these simulations are examined here:

- Resulting force time history obtained in each simulation
- Comparison between different force time histories obtained from different time periods
- Comparison between different force time histories obtained from different water free-surface elevations

Tsunami force time histories obtained from all 15 simulations for this bridge can be classified in two categories. The first is associated with the simulation of tsunami impact during

the initial impact time period. Flow depth for all of the studied initial impacts of the elevations ranges from the low chord of the bridge up to top of the bridge barrier where the tsunami water overtops the bridge. Figure 11 show the tsunami force time history on the Mad River Slough Bridge for the scaled tsunami water free-surface elevation of 5 ft above bridge elevation. The resulting horizontal and vertical forces for the initial impact time period are shown.

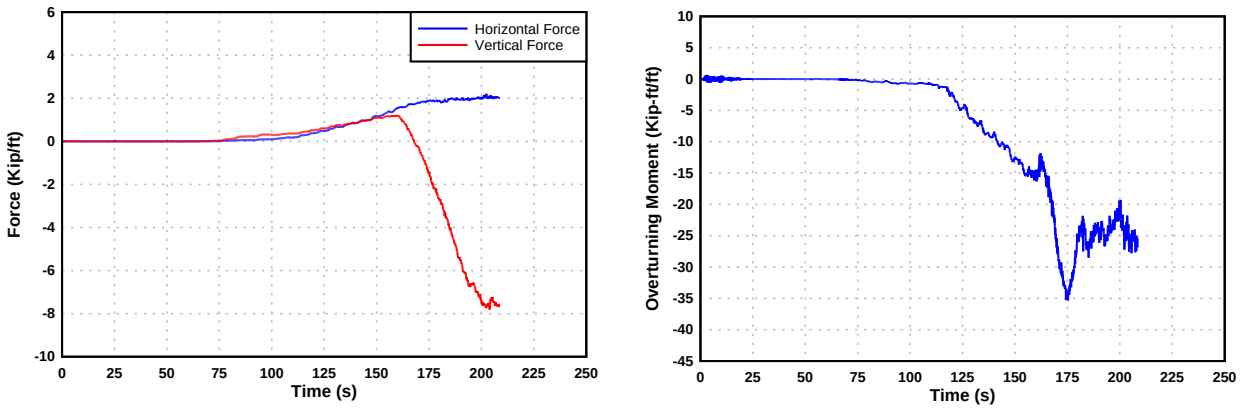

a. b.

Figure 11. a) Tsunami forces and b) overturning moment time histories on the Mad River Slough Bridge, Water surface elevation 5 ft above bridge elevation, Initial impact time period.

Figure 11a shows a gradual increase in both horizontal and uplift forces due to tsunami impact and accumulation of water on the seaside of the bridge superstructure. During this time the horizontal force is a combination of a hydrostatic force caused by the presence of the water, and a drag force due to resistance of the bridge superstructure against the tsunami flow. The uplift force continues to increase as the water free-surface elevation rises and air between the bridge girders is trapped. These forces increase with time until the free-surface elevation reaches the top of the bridge barrier and water start to overtop the bridge and pond on the deck. At this time the horizontal force reaches a relatively steady state and the vertical force begins to change the direction from upward (uplift force) to downward. This downward vertical force, as explained later, is a result of water overtopping the bridge. Since this downward vertical force is caused by the water overtopping the bridge, increasing the tsunami free-surface elevation by the amount of the water which overtops the bridge increases resulting in higher downward vertical force. The simulation continues until the water reaches and overtops the landward bridge barrier. The same trend was observed for tsunami loads on other bridges during the initial impact time period.

The second category is related to simulations performed to determine the tsunami forces

on bridge superstructure when maximum tsunami flow velocity, momentum flux, and mass flux occur. As the main goal in these simulations is to achieve a certain flow velocity and depth representing the afore-mentioned critical time periods, the simulation is run until it reaches a steady state. The results are horizontal and vertical forces and overturning moment on the bridge superstructure for a certain tsunami flow depth and velocity.

A comparison between resultant forces and moments on bridge for different time periods reveals that the maximum horizontal force, downward vertical force, and overturning moment always occur during the initial impact time period. The maximum uplift force is found to occur in simulations where the bridge is already inundated, the time period representing maximum momentum flux and mass flux in this case. Results also show that the maximum absolute overturning moment is negative meaning that, considering a flow from left to right, a clockwise moment is applied to bridge. Figure 12 shows the maximum horizontal and vertical forces and overturning moments on Mad River Slough Bridge for five different tsunami free-surface elevations. Results do not show a substantial difference between maximum horizontal force, downward vertical force, and overturning moment for 5 tsunami free-surface elevations. This suggests that these loads are primarily controlled by the tsunami flow depth during the initial impact time period when the velocity is relatively low and does not change drastically during the simulation. As shown in Figure 12, the maximum uplift force gradually increases as the tsunami free-surface elevation increases. This increase in the maximum uplift force is due to higher flow velocity for tsunami scenarios with higher water free-surface elevations.

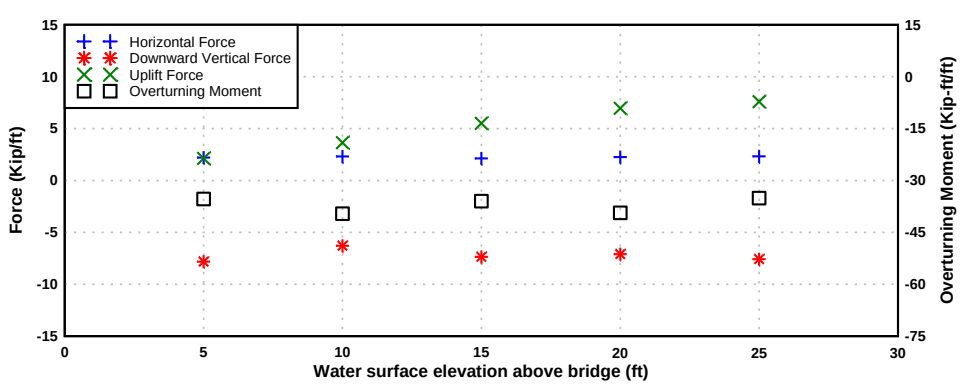

Figure 12. Maximum horizontal and vertical forces and overturning moment on Mad River Slough Bridge for five different water elevations.

5.2 Salmon Creek Bridge

The Salmon Creek Bridge is a concrete slab bridge with elevation approximately 15 foot - 9 inches above MSL. Location of the bridge with respect to the coast line and a close-up view of the bridge are provided in Figure 13. Fourteen simulations are performed and analyzed for this bridge. For the tsunami water free-surface elevations of 5 and 10 ft above bridge, all four different time periods occur at the same time requiring two simulations to calculate tsunami force time histories for these tsunami free-surface elevations. For the free-surface elevations of 15, 20, and 25 ft above the bridge elevation four simulations are conducted for each tsunami water free-surface elevation as the critical time periods occur at different times. A set of screen captures of the simulation of the Salmon Creek Bridge for free-surface elevation of 5 ft above the bridge elevation are shown in Figure 14.

a. b.

Figure 13. a) Location of the Salmon Creek Bridge, b) close-up view of the bridge (Source: Google maps).

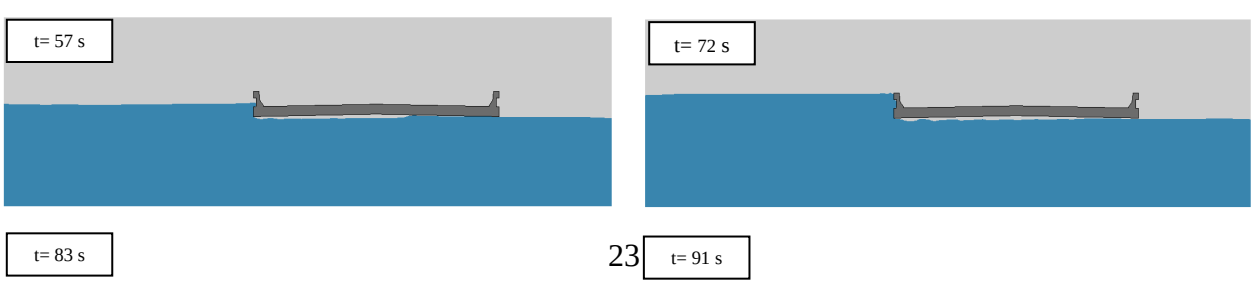

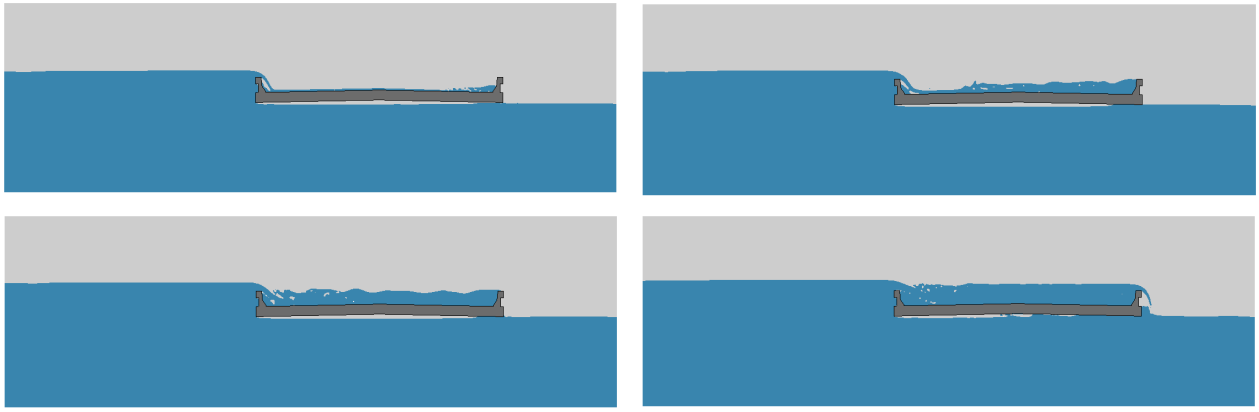

Figure 14. Screen captures of Salmon Creek Bridge, Water surface elevation 5 ft above bridge elevation, initial impact time period.

Figure 15 displays tsunami force time history on the Salmon Creek Bridge for the scaled tsunami free-surface elevation of 5 ft above the bridge elevation. According to Figure 15, both horizontal and vertical forces increase gradually with time. When the tsunami free-surface elevation reaches the top of the bridge barrier, a downward vertical force starts to overcome the buoyancy force resulting in a net downward vertical force due to water flow in the bridge deck. The horizontal force is found to be relatively constant as the bridge starts to be completely inundated. At this time, tsunami water overtops the landward bridge barrier, resulting in a reduction of the downward force. Results show that the maximum horizontal force, downward vertical force, and overturning moment always occur during the initial impact time period. The time period representing the maximum tsunami mass flux is found to produce the highest uplift forces even though the resultant forces are almost identical to those of the maximum momentum flux time period.

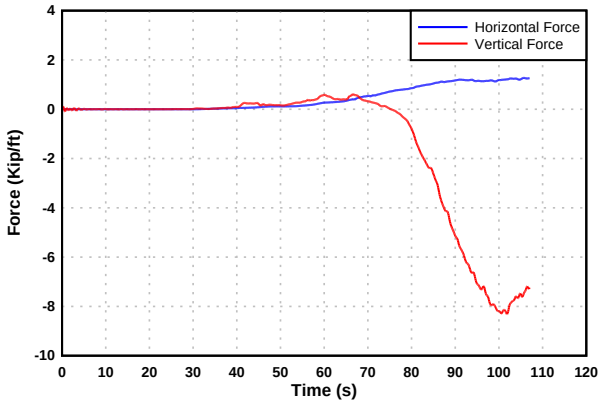

a.

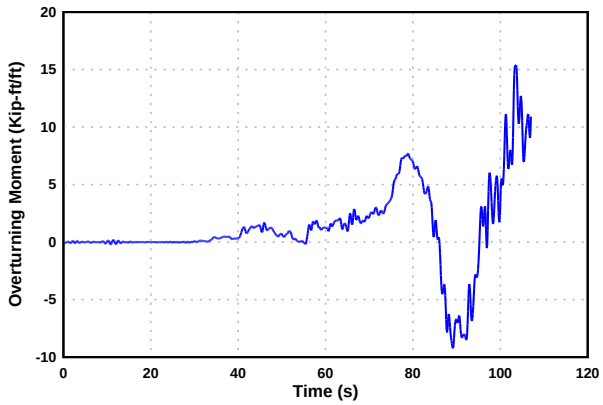

b.

Figure 15. a) Tsunami forces and b) overturning moment time histories on the Salmon Creek Bridge, Water surface elevation 5 ft above bridge elevation.

Figure 16 shows the maximum horizontal and vertical forces and overturning moments on Salmon Creek Bridge for five different tsunami free-surface elevations. As shown in Figure 16, the maximum horizontal force and downward vertical force do not change significantly for different water elevations while the uplift force increases as the tsunami water free-surface elevation and associated flow velocity increase. Overturning moments in both directions are observed to be significant as the different flow conditions from the time tsunami reaches the low chord of the bridge to the time when it overtops the landward bridge barrier create different moments.

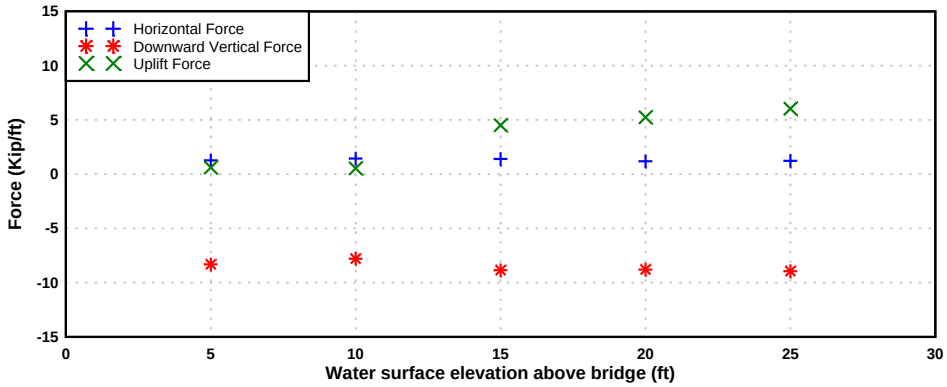

a.

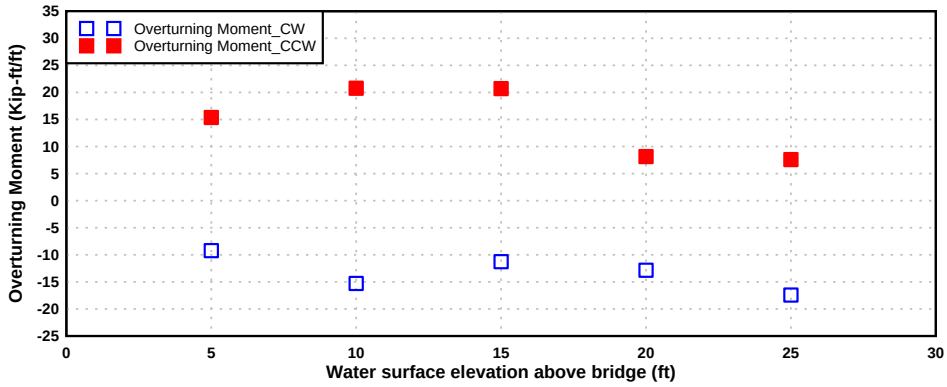

b.

Figure 16. a) Maximum horizontal and vertical forces and b) overturning moment on Salmon Creek Bridge for five different water elevations.

5.3 Old Creek Bridge

The Old Creek Bridge is a T-Girder bridge with a reference elevation 18 foot – 6 inches above the MSL. Figure 17 depicts the location of the bridge with respect to the coast line and a close-up view of the bridge. Sixteen simulations are performed for this bridge, one for tsunami free-surface elevation 5 ft above bridge, three for tsunami water free-surface elevation 10 ft above bridge as maximum tsunami flow velocity occurs during the initial impact time period, and four simulations for tsunami water free-surface elevations 15, 20, and 25 ft above the bridge as all time periods occur at different times. A set of screen captures of the simulation of Old Creek Bridge for free-surface elevation of 5 ft above the bridge elevation are shown in Figure 18.

a. b.

Figure 17. a) Location of the Old Creek Bridge, b) close-up view of the bridge (Source: Google maps).

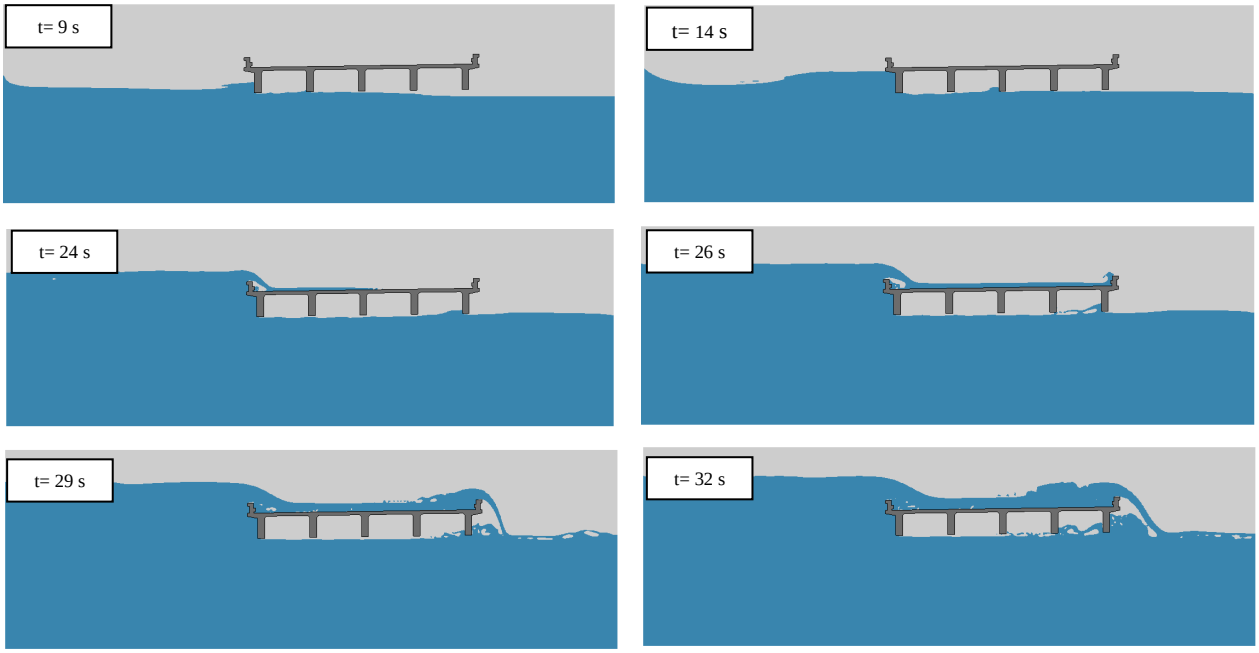

Figure 18. Screen captures of Old Creek Bridge, Water surface elevation 5 ft above bridge elevation, Initial impact time period.

Figure 19 shows the tsunami force time history on the Old Creek Bridge for the scaled tsunami free-surface elevation of 5 ft above the bridge elevation. Similar patterns were obtained for tsunami forces on this bridge during the initial impact time periods for each tsunami free-surface elevation. Both horizontal and uplift forces increase gradually with time as the tsunami free-surface elevation rises in seaside of the bridge superstructure. When the tsunami free-surface elevation reaches the top of the bridge barrier, water starts to flow on bridge deck and the uplift force begins to turn into a downward vertical force while the horizontal force continues to increase. Results show that the maximum horizontal force, downward vertical force, and overturning moment occur during the initial impact time period, while the maximum uplift force is found to be larger in the time period representing the tsunami maximum mass flux. Determination of the reasons for forces are larger in the tsunami maximum mass flux time period than in the tsunami maximum momentum flux time period could be difficult. Since the bridges are completely submerged in these time periods, one might think of the flow velocity as the dominant factor in determining the tsunami forces while results show that the inundation ration has a significant effect on the predicted forces. Figure 20 shows the maximum horizontal and vertical forces and overturning moments on Old Creek Bridge for five different water free-surface elevations. Negative overturning moments are found to be dominant as tsunami generates

clockwise moment on bridge considering that the tsunami travels from left to right. According to Figure 20, both uplift and downward vertical forces gradually increase in magnitude as free-surface elevation increases while horizontal forces and overturning moments do not show a significant change.

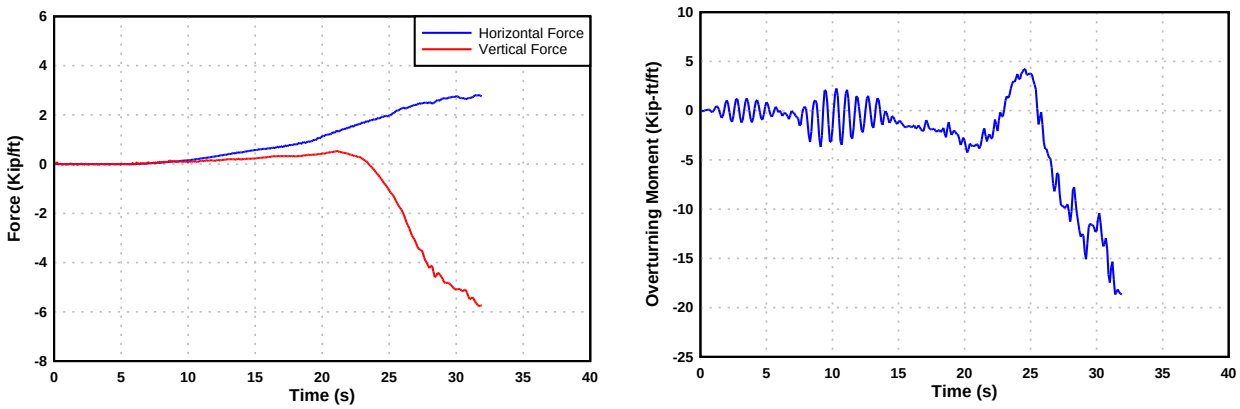

a. b.

Figure 19. a) Tsunami forces and b) overturning moment time histories on the Old Creek Bridge, Water surface elevation 5 ft above bridge elevation.

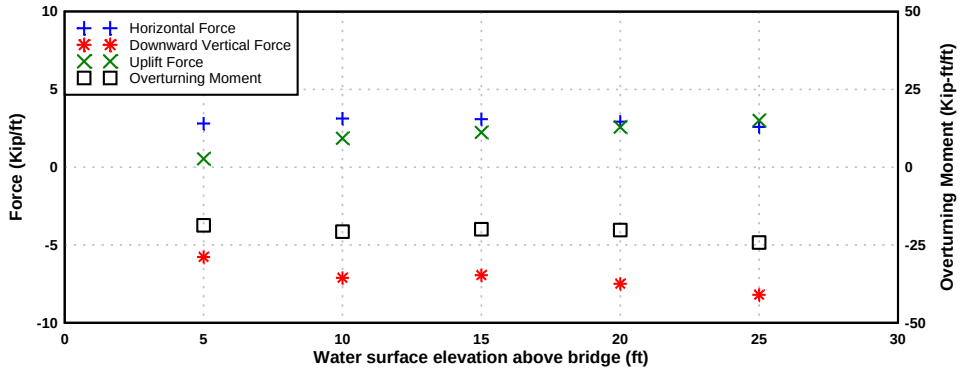

Figure 20. Maximum horizontal and vertical forces and overturning moment on Old Creek Bridge for five different water elevations.

5.4 Malibu Lagoon Bridge

The Malibu Lagoon Bridge is a CIP (cast in place) box-girder bridge with elevation approximately 16 foot - 4 inches above MSL. Location of the bridge with respect to the coast line and a close-up view of the bridge are shown in Figure 21.

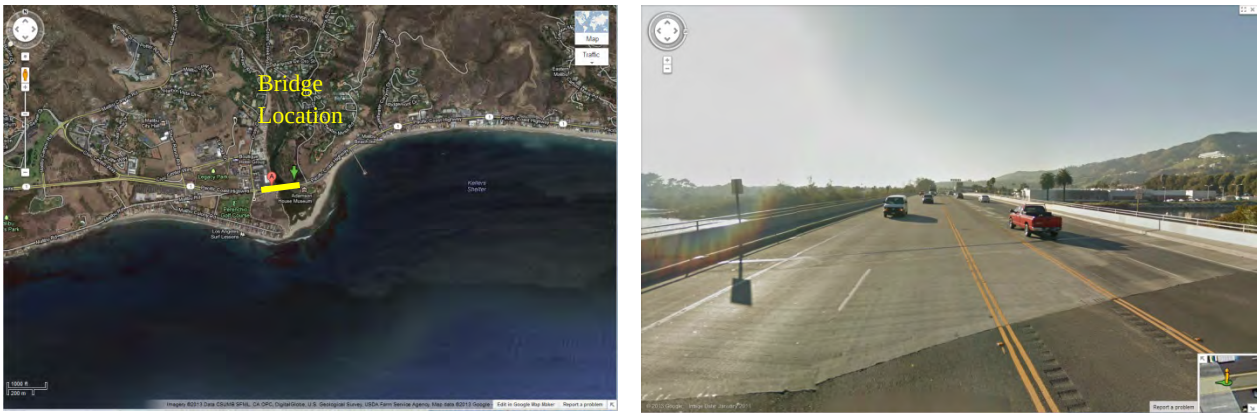

a. b.

Figure 21. a) Location of the Malibu Lagoon Bridge, b) close-up view of the bridge (Source: Google maps).

A total of 14 simulations were performed for this bridge. A set of screen captures of the simulation of the Malibu Lagoon Bridge for tsunami free-surface elevation of 5 ft above bridge elevation are shown in Figure 22. Figure 23 shows the tsunami force time history on the Malibu Lagoon Bridge for the scaled tsunami free-surface elevation of 5 ft above the bridge elevation. The tsunami force pattern on this bridge is similar to previous bridges. As shown in Figure 23, there is a gradual increase in uplift force until free-surface elevation reaches the top of the bridge. The uplift force is found to be much larger than the downward force here as the tsunami water barely overtops the bridge. Results show that the maximum horizontal force, downward vertical force, and overturning moment occur during the initial impact time period while maximum uplift force is found to be larger in the time period representing the tsunami maximum mass flux and momentum flux.

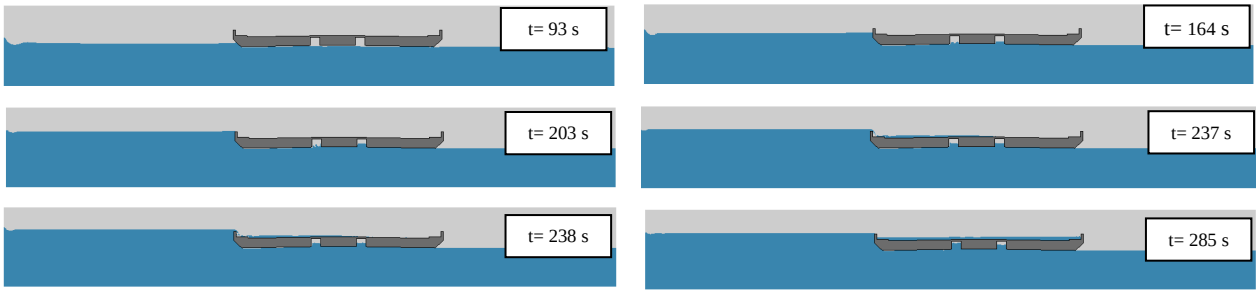

Figure 22. Screen captures of Malibu Lagoon Bridge, Water surface elevation 5 ft above bridge elevation, Initial impact time period.

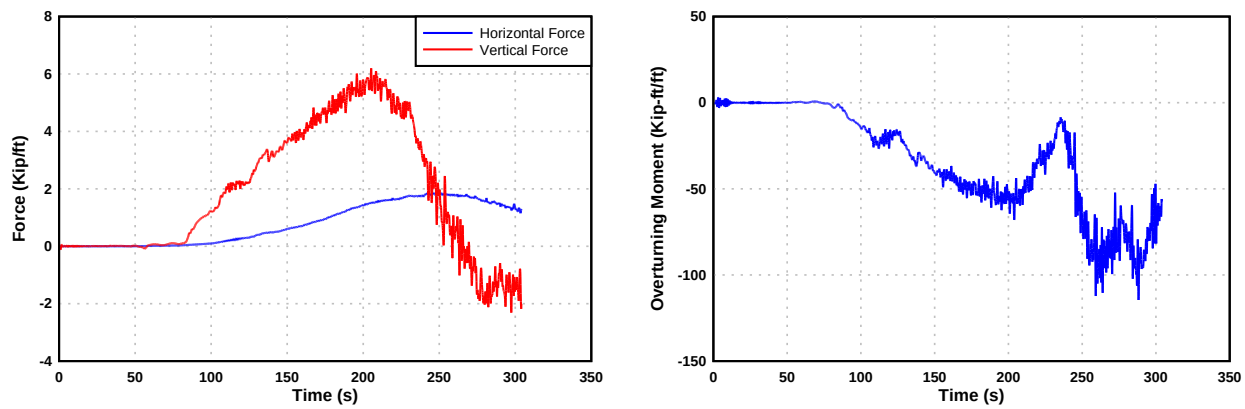

a. b.

Figure 23. a) Tsunami forces and b) overturning moment time histories on the Malibu Lagoon Bridge, Water surface elevation 5 ft above bridge elevation.

Figure 24 shows the maximum horizontal and vertical forces and overturning moments on the Malibu Lagoon Bridge for five different water elevations. As shown in Figure 24, resultant force and moments are on the same order except the results for tsunami free-surface elevation 5 ft above bridge.

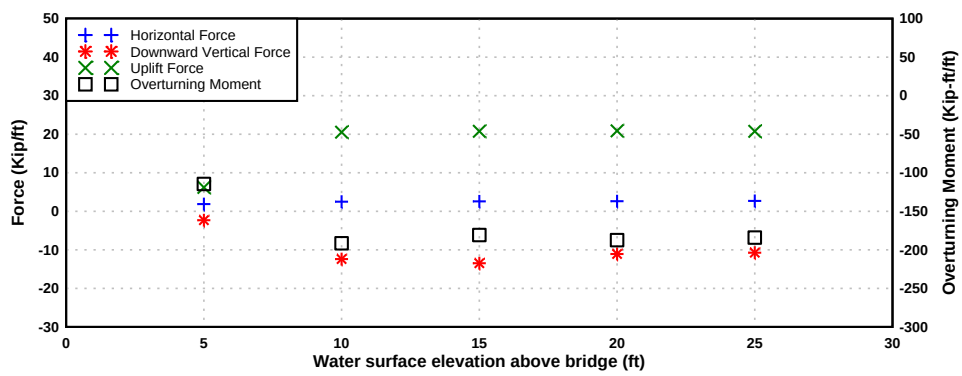

Figure 24. Maximum horizontal and vertical forces and overturning moment on Malibu Lagoon Bridge for five different water elevations.

5.5 Agua Hedionda Lagoon Bridge

The Agua Hedionda Lagoon Bridge is a Concrete Slab bridge with a reference elevation 23 foot – 8 inches above the MSL. The location of the bridge with respect to the shore line and a close-up view of the bridge are shown in Figure 25. A total of 10 simulations are performed for this bridge, two for each tsunami water free-surface elevation. A set of screen captures of the simulation of Agua Hedionda Lagoon Bridge for free-surface elevation of 5 ft above bridge elevation are provided in Figure 26.

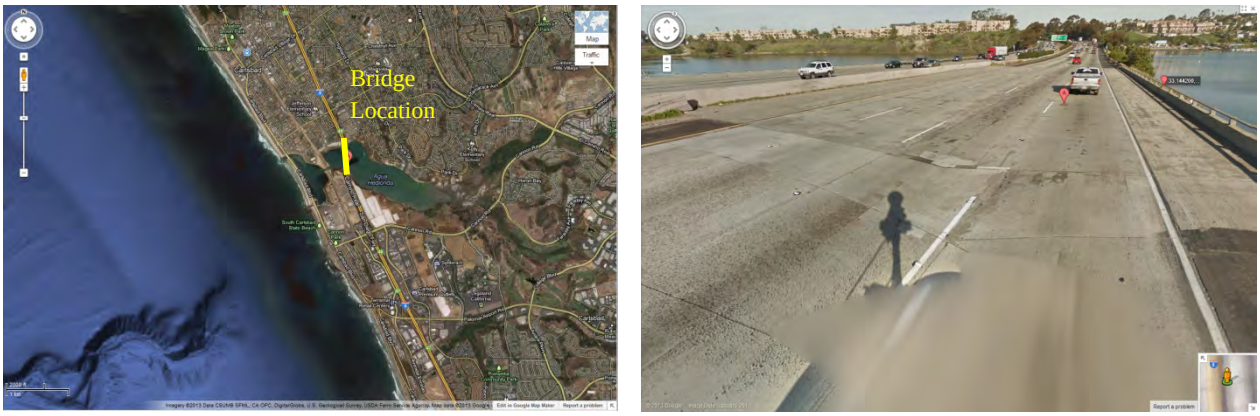

a. b.

Figure 25. a) Location of the Agua Hedionda Lagoon Bridge, b) close-up view of the bridge (Source: Google maps).

Figure 27 provides the computed time histories of horizontal and vertical force for free-surface elevation 5 ft above the bridge. Results show an increase in both horizontal and uplift forces until water surface reaches the top of the bridge. A relatively constant drag force is observed for horizontal force while downward vertical force due to tsunami overtopping the bridge starts to overcome the uplift force.

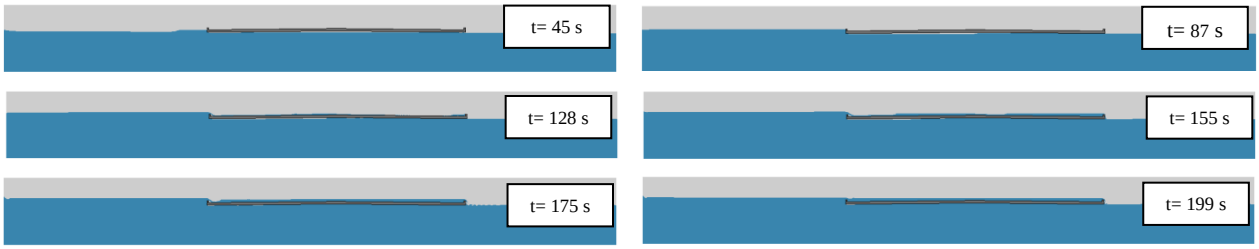

Figure 26. Screen captures of Agua Hedionda Lagoon Bridge, Water surface elevation 5 ft above bridge elevation, Initial impact time period.

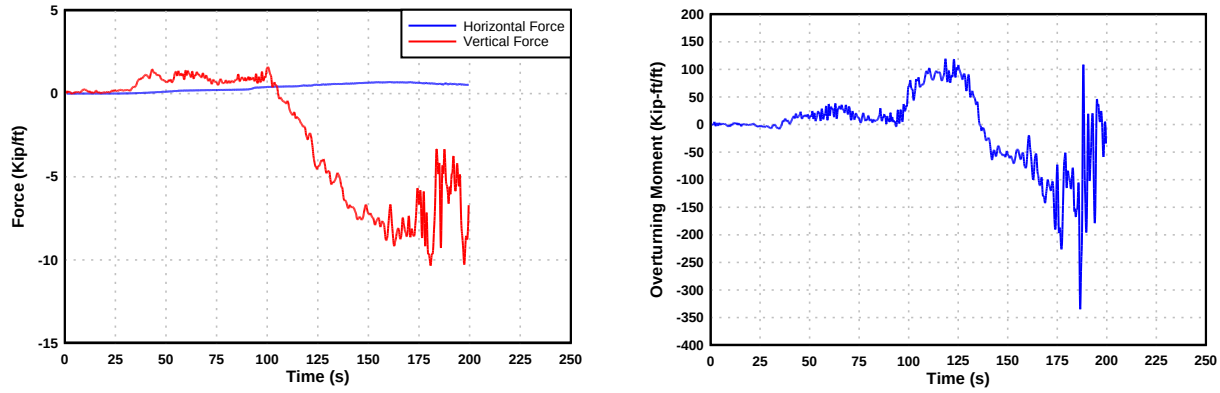

a. b.

Figure 27. a) Tsunami forces and b) overturning moment time histories on the Agua Hedionda Lagoon Bridge, Water surface elevation 5 ft above bridge elevation.

Figure 28 shows the maximum horizontal and vertical forces, and overturning moments for each tsunami free-surface elevation. As shown in Figure 28, the horizontal force and uplift force do not change significantly for the range of tsunami free-surface elevations considered. Results show a gradual increase in the downward vertical force as the tsunami water free-surface elevation rises. As shown in Figure 28, overturning moments in both directions (clock wise and counter clock wise) are important. This is a result of the geometry of the bridge. Large width of the bridge provides large moments arms for vertical forces acting on the both end of the bridge. These forces could be a result of ponding the tsunami water on bridge deck or slamming forces due to tsunami water pouring on the seaside of the bridge deck or water climbing the right end barrier. Magnitude of these forces with respect to each other defines the direction of the final overturning moment. Considering the tsunami flow from left to right, ponding of water on seaside (left) of the bridge deck can result in a positive overturning moment (counter clock wise). As the simulation progresses and the entire deck begins to be inundated, the horizontal velocity of the tsunami flow could create a negative overturning moment (clock wise).

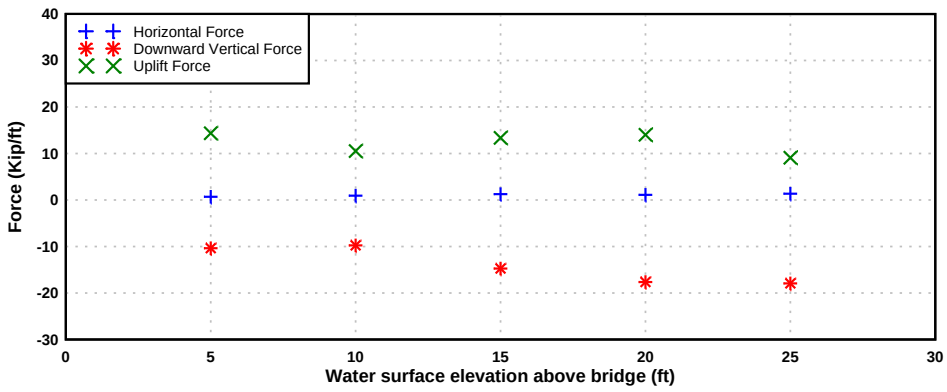

a.

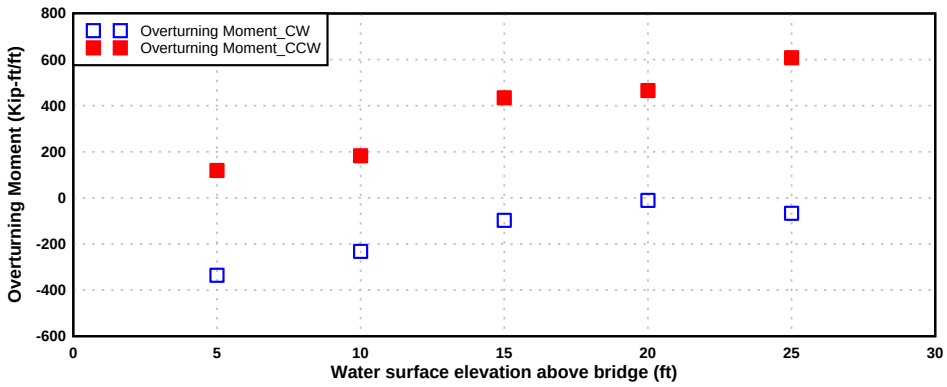

b.

Figure 28. a) Maximum horizontal and vertical forces and b) overturning moment on Agua Hedionda Lagoon Bridge for five different water elevations.

6 The Effect of Failure of the First Seaward Girder in Deck-girder Bridges

A deck girder bridge, Mad River Slough Bridge, is also analyzed in the case of failure of the first seaward girder. The main objective is to evaluate the effect of the failure of the first seaward girder and bridge geometry on resulting tsunami forces. Another set of 10 simulations is conducted to study the tsunami loads on Mad River Slough Bridge in the case of the failure of the first seaward girder. Figures 29a and b show the comparison between maximum computed

horizontal and vertical forces and the overturning moment. A 15% reduction in maximum horizontal force is observed for the bridge with removal of the first girder. The uplift force is found to be approximately 25% larger for the bridge with a failed first girder. This is because the removal of the first bridge girder creates a space beneath the bridge which increases the uplift force due to the flow around the bridge. The substantial change in overturning moment is believed to be a result of higher uplift force at the location of the failed girder. Since this force acts at the seaward end of the bridge, considering the large moment arm between this end and the center of gravity of the bridge, it exerts a much larger overturning moment on the damaged bridge compared to that of the intact bridge.

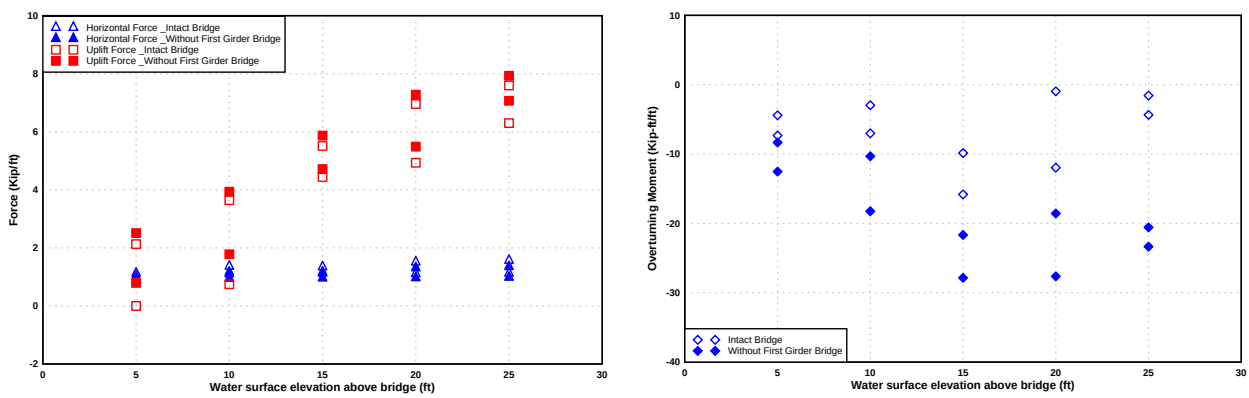

a. b.

Figure 29. a) Maximum horizontal and vertical forces and b) overturning moment on Mad River Slough Bridge for five different water elevations, Intact bridge versus bridge without first girder.

7 Discussion on Tsunami Downward Vertical Force on Bridge Superstructures

The downward vertical load obtained from the numerical simulations is a combination of the following components:

1. Hydrostatic load due to weight of the water one the bridge deck while the bridge is not totally inundated and the effect of the buoyancy force has not come into picture yet;

2. Hydrodynamic load at the entry end (left end, with the overall tsunami flow going from left to right) due to rapid vertical deceleration as the horizontal flow hugs the bridge barrier (as shown using red arrows in Figure 30), and the vertical velocity quickly becomes zero at the

top face of the deck when the flow becomes horizontal again. This vertical deceleration adds a large hydrodynamic downward force on the deck at that end;

3. Similarly, the hydrodynamic load at the exit end (right end) where the horizontal flow bends upward, exerting a very high local pressure at the surface of the deck as it provides the reaction force needed to accelerate the water from zero to high vertical velocity;

4. Downward vertical force due to the current of water passing around the bridge superstructure. This force remains relatively unchanged as the bridge superstructure starts to be totally inundated; and

5. Hydrodynamic pressure at the outer edge of a curved flow. This hydrodynamic pressure at the outer edge is significantly higher than that in the middle and particularly compared to that in the inner edge (NCFMF, 1969). This higher pressure at the outer edge adds to the downward force. These causes are believed to be responsible for the hydrodynamic load induced by the highly nonlinear complex flow resulting in a larger load than the hydrostatic load, as one might expect.

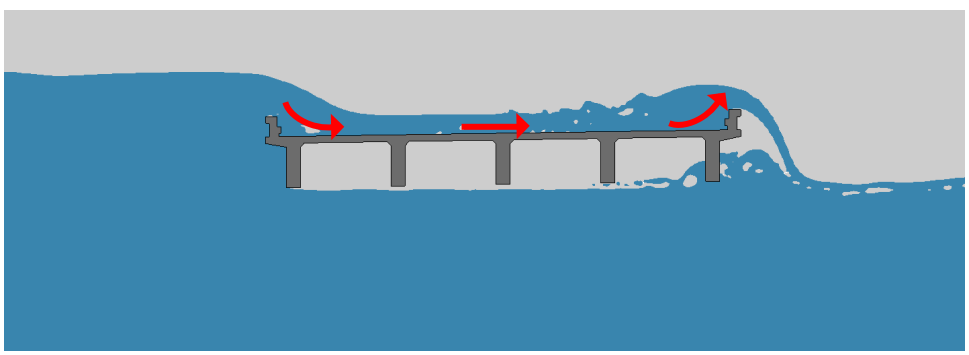

Figure 30. Sketch demonstrating the tsunami flow direction on bridge deck.

8 Conditions for a Net Tsunami Uplift Force on a Bridge Superstructure

Most of the experimental studies conducted to evaluate the tsunami forces on bridge superstructures have used solitary waves to model the tsunami (e.g. Kataoka 2006 and Araki et al. 2010). This approach might not be the most complete way to examine the interaction between tsunami and a bridge superstructure as it covers a part of the entire phenomenon.

The interaction between tsunami and a bridge superstructure can be divided into two phases. Phase one, which is called the initial impact in this study, refers to the first interaction

between tsunami and bridge superstructure. During this time period, the tsunami free-surface elevation reaches the low chord of the bridge superstructure and rises from there until it reaches the top of the bridge barrier where it overtops the bridge and starts to flow on the bridge. Phase two represents the time periods in which the tsunami has completely inundated the bridge superstructure. In this phase the tsunami behaves like a current.

The resulting tsunami load components acting on the bridge superstructure during these two phases could be different. The initial impact can lead to a net uplift force as the rise of the tsunami free-surface and impact on the bridge superstructure from below creates an uplift force. In addition to the hydrodynamic component of the uplift force, partial inundation of the bridge superstructure can also create an uplift force. This uplift force can be magnified due to the effect of air trapped below the deck between girders and diaphragms. However, when tsunami water reaches the top of the bridge barrier and overtops it uplift force becomes a downward force due to fluid impact on the upper surface of the bridge deck and the weight of the water on bridge deck when the bridge is partially inundated. Representing the inundation time periods, phase two could result in both uplift and downward vertical force depending on bridge geometry, flow velocity, and inundation depth of the bridge superstructure. For completely inundated bridges, the uplift force is mainly the buoyancy force due to pressure difference between top and bottom of the bridge superstructure, as the results of the current study show that vertical hydrodynamic forces are much smaller than the buoyancy force due to low tsunami flow velocity.

Therefore, it can be concluded that two flow conditions can lead to a net uplift force on bridges:

1. In the initial impact time period when tsunami hits the bridge as the first interaction between tsunami and bridge and right before tsunami water free-surface elevation reaches the top of the bridge barrier and overtops it, and

2. Under flow condition in which the bridge superstructure is completely inundated and the buoyancy force is the dominant vertical force acting on the bridge superstructure.

Figure 31 provides a graphical demonstration of the net forces acting on bridge superstructures during these two phases of tsunami strike on a bridge superstructure.

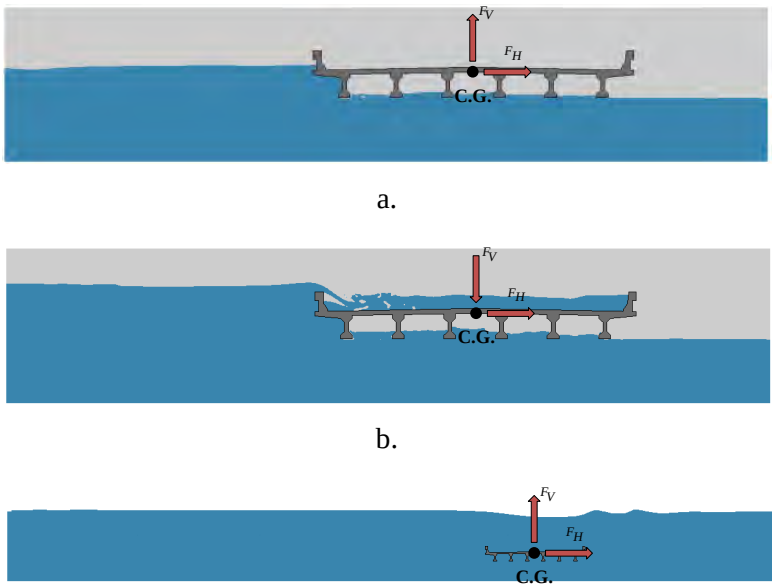

Figure 31. Graphical demonstration of the net forces acting on a bridge superstructure during tsunami strike a) initial impact before overtopping the bridge, b) initial impact after overtopping the bridge, and c) total inundation of the bridge.

9 Tsunami Load Estimation Method for Bridge Superstructures

9.1 Proposed Tsunami Load Estimation Method

There is a lack of technical literature on measurement or estimation of tsunami loads on bridge superstructures for practical design. Existing empirical formulas are available to determine wave loads on bridge decks, but they are limited to storm waves under hurricane conditions that have much smaller temporal and spatial scales than tsunami waves (e.g., Bea et al. 1999; Douglass et al. 2006; AASHTO 2008; Cuomo et al. 2009; Sheppard and Marin, 2009;

Jin and Meng, 2011; Gullett et al. 2012).

As a complex phenomenon, a tsunami can impose a wide range of loads on bridge superstructures as it contains different types of waves from a single solitary wave to a complex pattern of breaking waves. It can also be considered as a current when it completely inundates a bridge superstructure. Thus, due to constantly changing fluid loads, a load estimation method should cover this wide range as much as possible. Although in some cases the already available wind-induced wave load estimation methods could be modified to serve as a preliminary method to predict tsunami loads, but the tsunami load estimation methods should not be limited to that.

The method proposed here estimates the maximum horizontal and vertical loading on a bridge superstructure in a tsunami event and considers both initial impact and total inundation time periods as the critical time periods representing the entire process were modeled in simulations. Note that debris loading is not included in the proposed method. After analyzing the simulation results of different bridges under various tsunami scenarios, it is found that the maximum horizontal and downward vertical loads occur approximately at the same time for many of the cases studied here. At this time the tsunami flow has overtopped the bridge and the flow has reached the second (farther) bridge barrier generating a slamming load on the bridge barrier. Figure 32 shows this situation and the different parameters used in the load estimation method discussed later in this section. At this time, since the bridge is not totally inundated, both hydrostatic load due to the weight of the water on the bridge deck and hydrodynamic slamming load caused by tsunami wave impacting the top surface of the deck generate a downward vertical load. After the bridge is completely inundated, the buoyancy force will take the place of the hydrostatic force.

Proposed formulas to estimate the maximum horizontal and vertical loads are presented in Equations 4-7:

(4)

(5)

(6)

(7)

where:

: Maximum *horizontal Force,*

: Maximum *downward vertical Force,*

: Maximum *uplift Force,*

: Empirical downward vertical force coefficient,

: Empirical uplift force coefficient,

: Hydrostatic horizontal Force,

: Hydrostatic downward vertical Force,

: Drag Force,

: Slamming vertical Force,

: Buoyancy Force,

: Lift Force,

: Drag coefficient,

: Lift coefficient,

: Slamming coefficient in vertical direction,

ρ: Density of water,

g: Acceleration of gravity,

V: Volume of the bridge per 1 ft length,

: Height of the bridge superstructure,

: Width of the bridge superstructure,

: Height of the bridge barrier,

: Effective length of bridge deck for vertical slamming force,

: Height of the bridge girder,

: Thickness of the bridge deck,

: Low chord elevation of the bridge superstructure,

h: Tsunami water free-surface elevation resulting in maximum horizontal and downward vertical hydrostatic forces.

v: Tsunami flow velocity,

: Difference between tsunami water free-surface elevation and low chord of the bridge.

Note that for box-section bridges the height of girder ( ) is zero and low chord elevation ( ) is calculated from the bottom of the bridge deck.

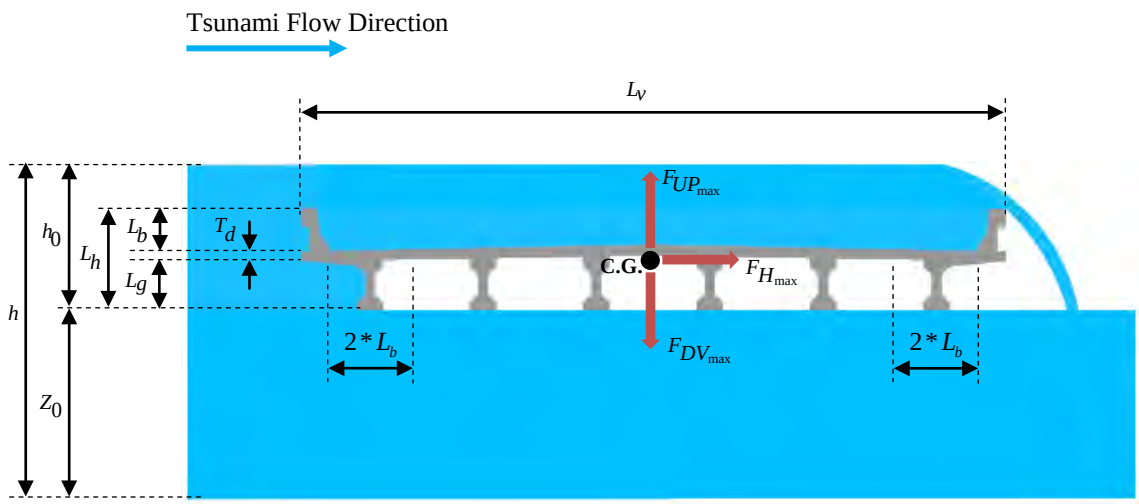

Figure 32. Sketch demonstrating different parameters used in the tsunami load estimation method.

A tsunami "wave length" is usually much larger than a normal bridge width. Therefore, it is reasonable to assume that, in most cases, the entire bridge is inundated when the tsunami free-surface elevation (h) reaches a certain elevation. Here h is tsunami water free-surface elevation resulting in maximum horizontal and downward vertical hydrostatic forces during the initial impact time period. This parameter is found to have a significant effect on the maximum horizontal and downward vertical forces. In addition, this value is found to be very difficult to predict as it represents a threshold where tsunami can result in maximum horizontal and downward vertical forces. As shown from simulations, it varies from seaside of the bridge superstructure where it is responsible for maximum horizontal force to the top of the bridge deck where it generates the maximum downward vertical load. In order to simplify the proposed tsunami load estimation method, the value of h is assumed to be constant across the bridge width. This value is recommended to be considered a height of a bridge barrier higher than the bridge elevation at the top of the bridge barrier. It is observed from the simulations that when the tsunami free-surface elevation rises above this value, the landward side of the bridge (right end in simulations) begins to be totally inundated resulting in a significant reduction in both the

maximum horizontal force and the downward vertical force. However, this assumption might conservatively lead to a slightly higher downward vertical force as simulations showed that the free-surface elevation on top of the bridge deck responsible for maximum downward vertical force is usually less than the free-surface elevation in the seaside of the bridge.

According to Equation 5, the slamming force is proportional to 4 times the bridge barrier height. This factor is considered as the vertical slamming force caused by flow overtopping bridge is practically horizontal at the middle section of the bridge deck and generates little or no hydrodynamic vertical force. Table 2 and Table 3 provide the empirical coefficients used in Equation 4 and 5. The empirical force coefficients are mainly used here to obtain best possible correlation between analytical results and formula estimations.

Table 2. Empirical coefficients for tsunami load estimation

Drag coefficient ( )	2.00
Lift coefficient ( )	1.00
Slamming coefficient in vertical direction ( )	2.00

Table 3. Empirical Force coefficients for tsunami load estimation

Uplift force coefficient ( )	0.77
Downward vertical force coefficient ( )	0.53

Figure 33-35 show the comparison between formula estimation and numerical prediction of the maximum horizontal, uplift, and downward vertical forces. According to Figure 33, in 92% of the tsunami scenarios studied here, maximum horizontal forces can be estimated with less than 30% error using the recommended approach. Maximum downward forces are found to be estimated with less than 40% error in 64% of the cases. Figure 35 shows that the recommended approach can estimate the maximum uplift forces with less than 30% error in 72% of the tsunami scenarios analyzed in this research.

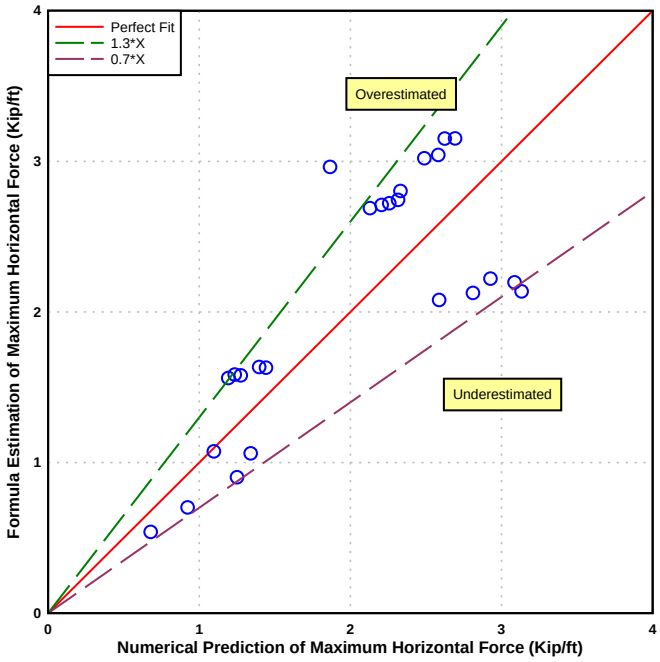

Figure 33. Comparison between formula estimation and numerical prediction of the maximum horizontal forces.

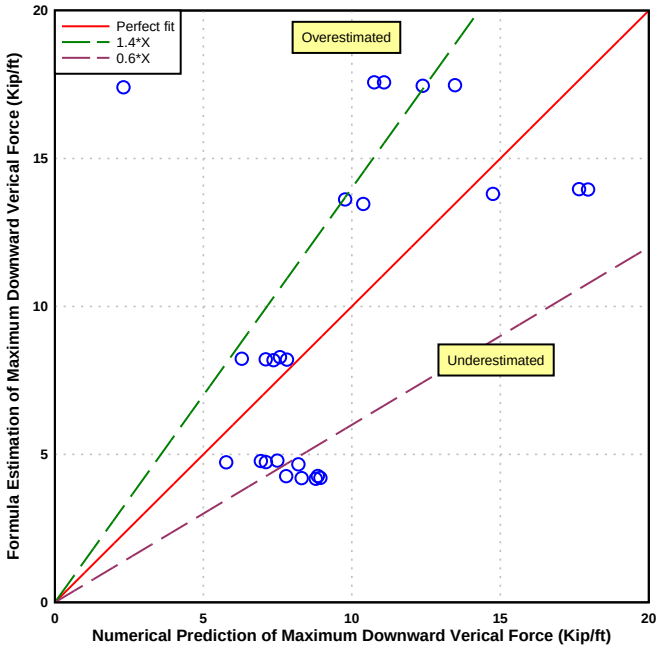

Figure 34. Comparison between formula estimation and numerical prediction of the maximum downward vertical forces.

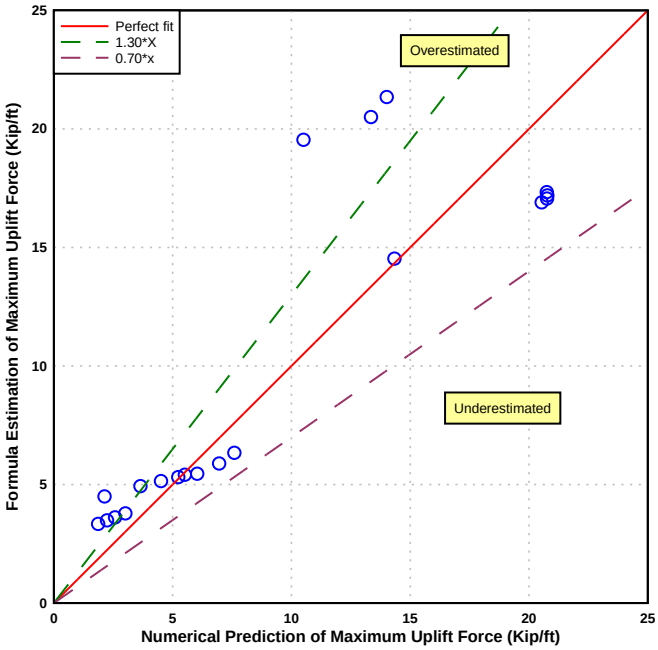

Figure 35. Comparison between formula estimation and numerical prediction of the maximum uplift forces.

The main source of disparity between numerical results and the load estimation method results of maximum horizontal force and downward force is the estimation of the h parameter. The load estimation method is shown to provide much more accurate prediction of the tsunami loads if more precise estimation of the h parameter is available. For Figure 36 and Figure 37, the value of h parameter is directly obtained from the simulations. According to these Figures, tsunami load estimation results are much closer to the numerically predicted forces using exact value for h parameter and updated empirical force coefficients based on the new h parameters.

Note that in the load estimation method proposed in this section, an attempt is made to use the known hydrostatic and hydrodynamic forces such as buoyancy, slamming, and drag to reach the best possible agreement between the numerical simulation results and the formula estimations while keeping it simple and easy for design engineers to use. All the empirical coefficients are calibrated with these goals in mind. Designers may include their own load factors and design parameters depending on the nature of the problem to ensure that the load capacity is always consistent with the demand.

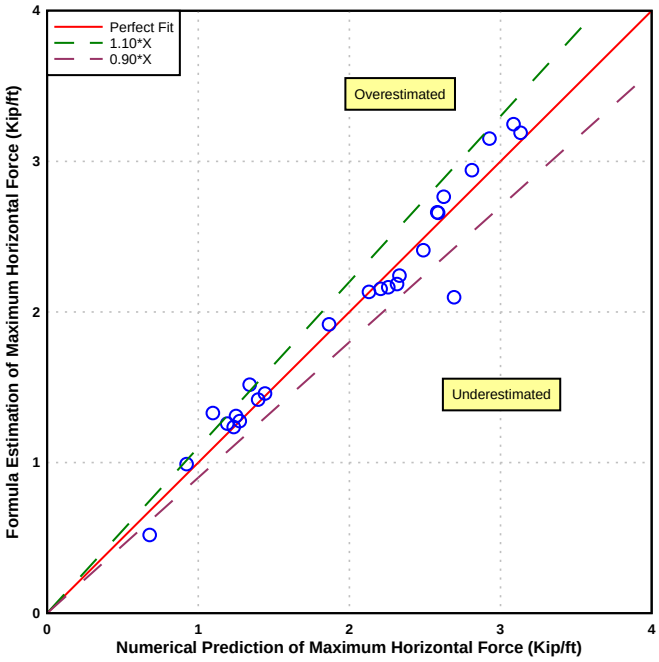

Figure 36. Comparison between formula estimation and numerical prediction of the maximum horizontal forces (Using exact value for h parameter).

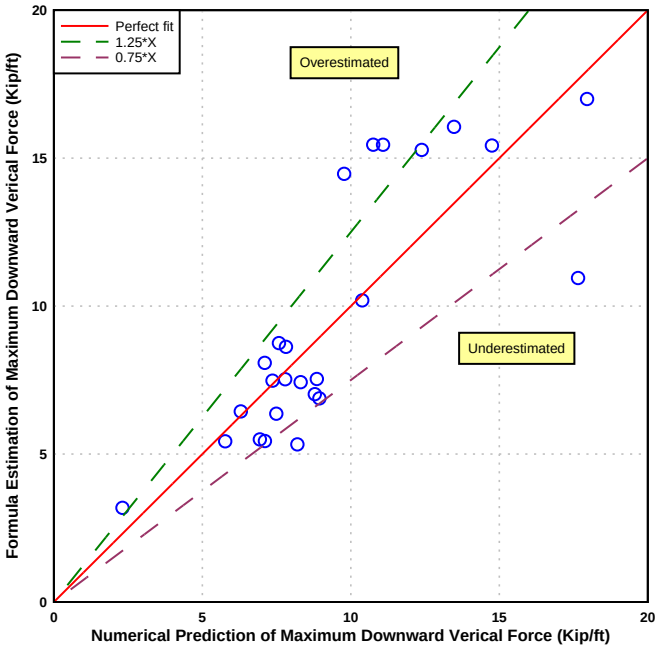

Figure 37. Comparison between formula estimation and numerical prediction of the maximum downward vertical forces (Using exact value for h parameter).

9.2 Example Calculation of Proposed Tsunami Load Estimation Method

This section provides an example demonstrating how the recommended equations can be used to estimate the maximum horizontal force, maximum downward vertical force, and the maximum uplift force on a bridge superstructure during a tsunami event.

First the tsunami flow field condition should be defined. This includes the tsunami free-surface elevation and flow velocity normal to the bridge cross section. These two values should be defined for several time periods. As the simulations showed, maximum horizontal force and maximum downward vertical force occur during the initial impact time period. Thus, the tsunami flow field condition required to estimate these force should be selected based on tsunami free-surface elevation and flow velocity during the initial impact time period. To determine the maximum uplift force, time periods in which maximum tsunami mass flux and momentum flux were recorded should be considered. The maximum uplift force obtained from these two time periods is the overall maximum uplift force.

The methodology is explained below step by step:

1. Define the tsunami free-surface elevation time history and horizontal velocity time histories in north and east directions.
2. Define the horizontal velocity time history normal to bridge cross section.
3. Determine the durations in which tsunami water free-surface elevation reaches the low chord of the bridge and continues to rise and overtops the bridge. These durations are called initial impact time periods.
4. Determine the maximum tsunami velocity during the initial impact time periods. This is the flow velocity during the initial impact time period.
5. Determine the time periods in which the maximum tsunami mass flux and momentum flux occur. Tsunami free-surface elevation during these time periods should be higher than the bridge elevation so that the entire bridge is inundated.
6. Determine the maximum horizontal force and maximum downward vertical force according to flow velocity obtained from initial impact time period.
7. Determine the maximum uplift force from maximum tsunami mass flux and momentum flux time periods.

Suppose a bridge is located in tsunami zone. Density of water is 64 lb/ft^3 (or 0.002 Kip-

s^2/ft^4) and acceleration of gravity is 32.17 ft/s^2. Bridge geometry characteristics are provided below:

bridge reference elevation ( ): 9 ft,

girder height ( ): 3 ft,

deck thickness ( ): 0.7 ft,

barrier height ( ): 2.5 ft,

width of bridge cross section ( ): 50 ft,

height of bridge cross section ( ): 6.2 ft.

bridge volume per foot: 70 ft^3/ft

Tsunami flow conditions are as follows:

flow velocity during the initial impact time period: 15 ft/s.

flow velocity during the maximum tsunami mass flux (or momentum flux) time period: 8 ft/s.

$= 3 + 0.7 + 2.5 = 6.2\ ft$

Therefore, the estimated maximum tsunami horizontal force, downward vertical force, and uplift force are:

10 A Note on Computational Efforts

The simulations were performed on three computing platforms. First is a parallel cluster system of 1,344 compute nodes. Each compute node has 20 GB memory and consists of 2.8 GHz dual Intel Xeon Nehalem-EP quad-core processors. The simulations were conducted on 8 or 16 compute nodes depending on the problem and simulation time. The second is a 2.8 GHz 2-processsor Intel Xeon X5660 workstation having 6 cores per CPU and the 192 GB memory in total. The third one is a 3.1 GHz 2-processsor Intel Xeon E5-2687W workstation having 8 cores per CPU and the 256 GB memory in total. More than 200 simulations were performed over a year and half including preliminary modeling and troubleshooting. Each simulation took 3-7 days to complete.

11 Concluding Remarks

The results of this study on tsunami loading on selected coastal bridges in California are summarized here. The tsunami horizontal and vertical forces and overturning moment time histories were computed for five different tsunami free-surface elevations representing five tsunami scenarios. For each tsunami scenario four time periods were examined. A new method of estimation the tsunami load on bridge superstructures was also proposed. The main findings are as follows:

1. The initial stage of tsunami loading on a bridge superstructure leads to a combination of horizontal and uplift forces. These forces gradually increase as the tsunami free-surface elevation rises.
2. The horizontal force is due to hydrostatic force caused by an accumulation of water on the seaside of the bridge superstructure and a drag force due to resistance of the bridge superstructure against the tsunami flow.
3. The maximum uplift force during the initial impact time period is found to occur when the tsunami free-surface elevation reaches the top of the bridge barrier right before overtoping the bridge and starts to flow on the bridge deck. After this, the uplift force acting on a partially inundated bridge is counterbalanced by the weight of water ponding on the deck and slamming force caused by tsunami hitting the upper surface of the bridge deck. The resultant vertical force is a downward force which increases as the tsunami free-surface elevation and flow velocity increase.
4. It is observed that the time period representing the initial impact of the tsunami on the bridge superstructure leads to the maximum horizontal force, downward vertical force, and overturning moment.
5. Comparing the resultant forces from different tsunami free-surface elevations reveals that the maximum horizontal force, downward vertical force, and overturning moment do not change significantly for different water elevations. This is because they occur in the initial impact time period where flow depth is limited to the range from low chord of the bridge to top of the bridge barrier.
6. The overall maximum uplift force is found to be in tsunami scenarios where the bridge superstructure is already inundated.

7. The maximum uplift force is observed to increase for higher tsunami free- surface elevations where the corresponding flow velocity is higher.
8. The analysis of a deck-girder bridge considering the failure of the first seaward girder shows a 15% reduction in maximum horizontal force. The uplift force is found to be approximately 25% larger for the bridge with failed first girder.
9. A set of equations are proposed to estimate the maximum horizontal and vertical forces on bridge superstructures based on the simulation results. A comparison between numerical results from simulations and the estimated forces using recommended approach shows good agreement between numerical predictions and the proposed approximate estimations of the tsunami forces.

12 Acknowledgment

The authors would like to thank the California Department of Transportation (Caltrans) for the financial support of the project which made this study possible. They would also like to thank the staff of the Caltrans Office of Earthquake Engineering for their constructive comments during course of the project.

13 References

AASHTO. (2008). Guide Specifications for Bridges Vulnerable to Coastal Storms. American Association of State Highway and Transportation Officials, Washington, D.C.

Akiyama, M., Frangopol, D. M., Arai, M., and Koshimura, S. (2012). Probabilistic Assessment of Structural Performance of Bridges under Tsunami Hazard. 43rd Structures Congress. March 29-31, 2012, Chicago, Illinois.

Araki, S., Ishino, K., and Deguchi, I. (2010). Stability of girder bridge against tsunami fluid force. Proceedings of 32nd International Conference on Coastal Engineering (ICCE), June 30-July 5 2010, Shanghai, China.

Bea, R.G., Xu, T., Stear, J., and Ramos, R. (1999). Wave Forces on Decks of Offshore Platforms. Journal of Waterway, Port, Coastal, and Ocean Engineering, 125(3), 136-144.

Bradner, C., Schumacher, T., Cox, D., Higgins, C. (2011). Experimental Setup for a Large-Scale Bridge Superstructure Model Subjected to Waves. Journal of Waterway, Port, Coastal, and Ocean Engineering, 137(1), 3-11.

Caltrans (2010). Probabilistic Tsunami Hazard in California. Technical Report Prepared for Caltrans/PEER.

Cheung, K.F., Wei Y., Yamazaki Y., and Yim S.C. (2011). Modeling of 500-year Tsunamis for Probabilistic Design of Coastal Infrastructure in the Pacific Northwest. Coastal Engineering, 970-985.

Cuomo, G., Shimosako, K., and Takahashi, S. (2009).Wave-in-deck loads on coastal bridges and the role of air. Coastal Engineering. 793-809.

Douglass, S.L., Chen, Q., Olsen, J.M., Edge, B.L., Brown, D. (2006). Wave Forces on Bridge Decks. Final Report Prepared for U.S. Department of Transportation and Federal Highway Administration Office of Bridge Technology, Washington, D.C.

Gullett, P.M., Dickey, M-M., and Howard, I.L. (2012). Numerical modeling of bridges subjected to storm surge for mitigation of hurricane damage. SERRI Report 70015-005. Report Prepared for U.S. Department of Homeland Security.

Hallquist, J.O. (2006). LS-DYNA Theory Manual. Livermore Software Technology Corporation, Livermore, California.

Iemura, H., Pradono, M.H., and Takahashi, Y. (2005) Report on the tsunami damage on the bridges in Banda Aceh and some possible countermeasures. Proceedings of 28th JSCE

Earthquake engineering symposium, Vol.28, No.214.

Jin, J and Meng, B. (2011). Computation of Wave Loads on the Superstructures of Coastal Highway Bridges. Ocean Engineering, 38(17-18), pp.2185-2200

Kataoka, S. (2006). Scenarios of Earthquake and Tsunami Disaster Including Damage to Road Bridges. 22th US - Japan Bridge Engineering Workshop, October 23-25, 2006, Seattle, WA, USA.

Kawashima, K. Damage of Bridges due to the 2011 Great East Japan Earthquake," Proceedings of the International Symposium on Engineering Lessons Learned from the 2011 Great East Japan Earthquake. March 1-4, 2012, Tokyo, Japan.

Kerenyi, K., Sofu, T., and Guo, J. (2009). Hydrodynamic Forces on Inundated Bridge Decks. Report No. FHWA-HRT-09-028. Federal Highway Administration.

Kosa, K., Nii, S., Miyahara, K., and Shoji, M. (2010). Experimental Study for Estimating Tsunami Forces Acting on Bridge Girders. 26th US - Japan Bridge Engineering Workshop, September 20-22, 2010, New Orleans, Louisiana, USA.

Kosa, K. (2012). Damage analysis of bridges affected by tsunami due to Great East Japan Earthquake. Proceedings of the International Symposium on Engineering Lessons Learned from the 2011 Great East Japan Earthquake, March 1-4, 2012, Tokyo, Japan.

Lau, T. L., Ohmachi, T., Inoue, S., and Lukkunaprasit, P. (2011). Experimental and Numerical Modeling of Tsunami Force on Bridge Decks. DOI: 10.5772/23622.

Lukkunaprasit, P., Lau, T.L., Ruangrassamee, A., and Ohmachi, T. (2008). Tsunami wave loading on a bridge deck with perforations. The 14th World Conference on Earthquake Engineering, October 12-17, 2008, Beijing, China.

Maruyama, K., Tanaka, Y., and Hosoda, A. (2012). Damage of Bridges Structures by Huge Tsunami and Evaluation of Tsunami Force on Bridges. The 8th International Symposium on Social Management Systems, SSMS2012- Disaster Prevention and Reconstruction Management. 2-4 May 2012, Kaohsiung, Taiwan, R.O.C.

NCFMF, National Committee for Fluid Mechanics Films. (1969). Pressure Fields and Fluid Acceleration," Available from: http://web.mit.edu/hml/ncfmf.html 1969

Okeil, A. M., and Cai, C. S. (2008). Survey of Short- and Medium-Span Bridge Damage Induced by Hurricane Katrina. Journal of Bridge Engineering, 13 (4), 377–387.

Padgett, J., DesRoches, R., Nielson, B., Yashinsky, M., Kwon, O.-S., Burdette, N., and Tavera,

E. (2008). Bridge damage and repair costs from Hurricane Katrina. Journal of Bridge Engineering. 13 (1), 6–14.

Robertson, I.N., Yim, S., Riggs, H.R., Young, Y.L. (2007). Coastal bridge performance during Hurricane Katrina. Proceedings of Structural Engineering, Mechanics and Computation 3,pp. 1864-1870.

Robertson, I.N., Riggs, H.R., Yim, S.C.S., Young, Y.L. (2007). Lessons from Hurricane Katrina storm surge on bridges and buildings. Journal of Waterway, Port, Coastal, and Ocean Engineering, Vol. 133, pp. 463-483.

Sheppard, D.M., and Marin, J. (2009). Wave Loading on Bridge Decks. Final Report BD545-58, Florida Department of Transportation, Tallahassee, FL.

Sugimoto, T. and Unjoh, S. (2007). Hydrolic Model Tests on the Bridge Structures Damaged by Tsunami and Tidal Wave. 23th US - Japan Bridge Engineering Workshop, November 5-7, 2007, Tsukuba Science City, Japan.

Yim, S. C., Cheung, K.F., Nimmala, S., and Azadbakht, M. (in progress). Tsunami Design Load Estimate for Coastal Infrastructures: A Case Study for Spencer Creek Bridge, Oregon.

Yim, S. C., Boon-intra S, Nimmala S.B., Winston H. M., Azadbakht M., Cheung K.F. (2011) Development of a Guideline for Estimating Tsunami Forces on Bridge Superstructures. Technical Report prepared for Oregon Department of Transportation (ODOT). Salem, OR.

Yashinsky, M. (2012). Lessons for Caltrans from the 2011 great Japan earthquake and tsunami, Proceedings of the International Symposium on Engineering Lessons Learned from the 2011 Great East Japan Earthquake, March 1-4, 2012, Tokyo, Japan.

Zhang, G., Hoshikuma, J-I., and Usui, T. (2010). A study on countermeasure for reducing the effect of tsunami on highway bridges. 26th US - Japan Bridge Engineering Workshop, September 20-22, 2010, New Orleans, Louisiana.

A. Appendix A. Time Histories of Tsunami Water Free-surface Elevation and Horizontal Velocity Components

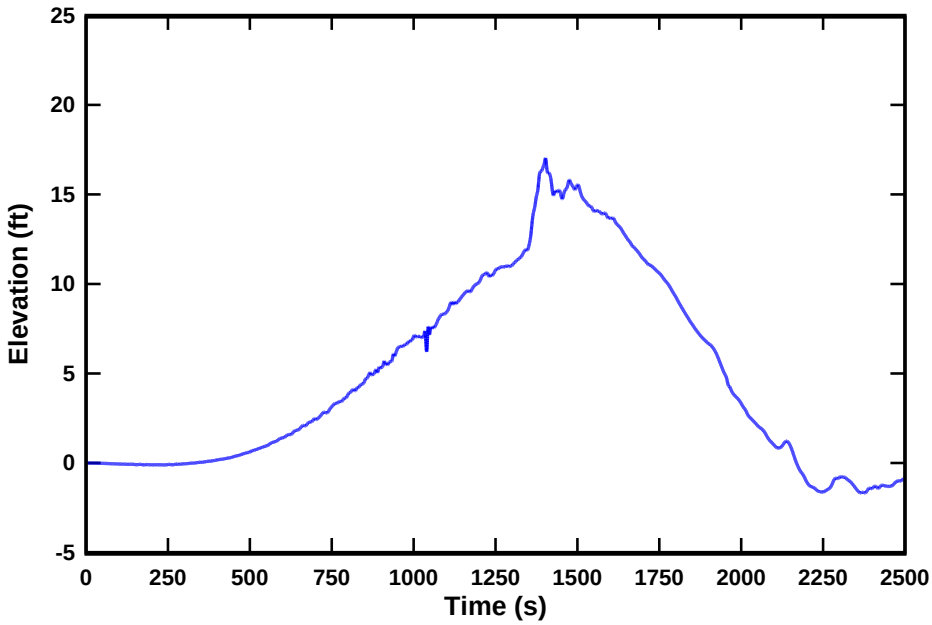

Figure A-1. Tsunami water free-surface elevation at the location of the Mad River Slough Bridge.

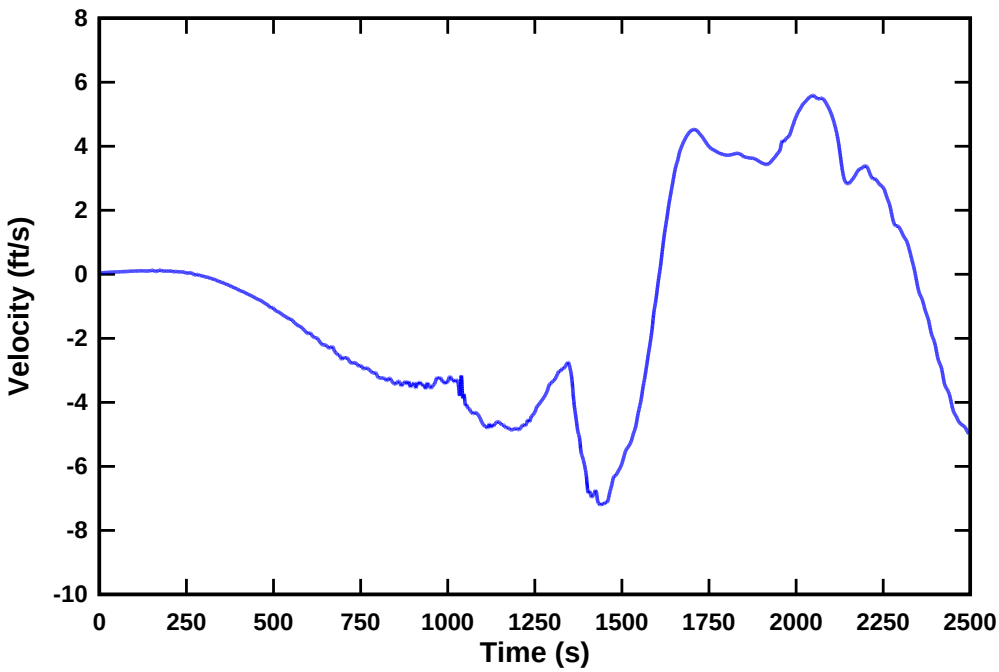

Figure A-2. Tsunami water velocity component normal to bridge direction at the location of the Mad River Slough Bridge.

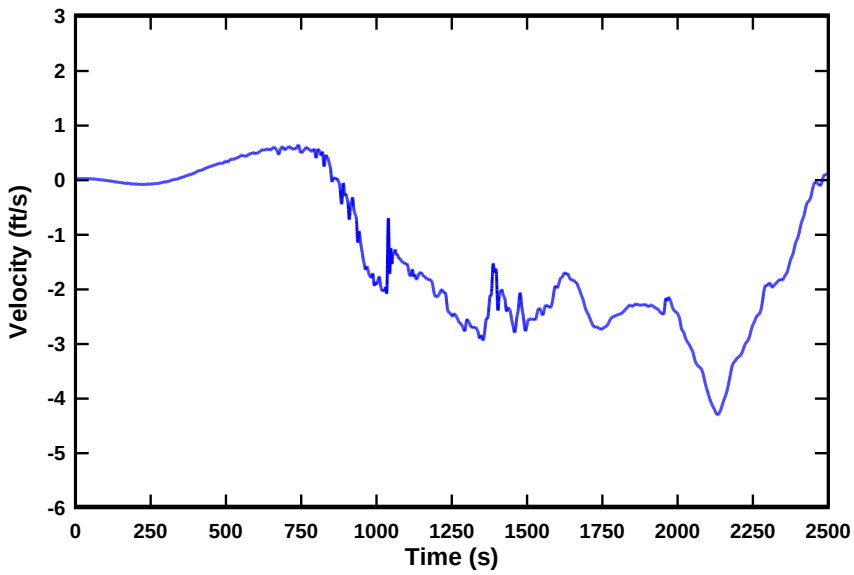

Figure A-3. Tsunami water velocity component in east direction at the location of the Mad River Slough Bridge.

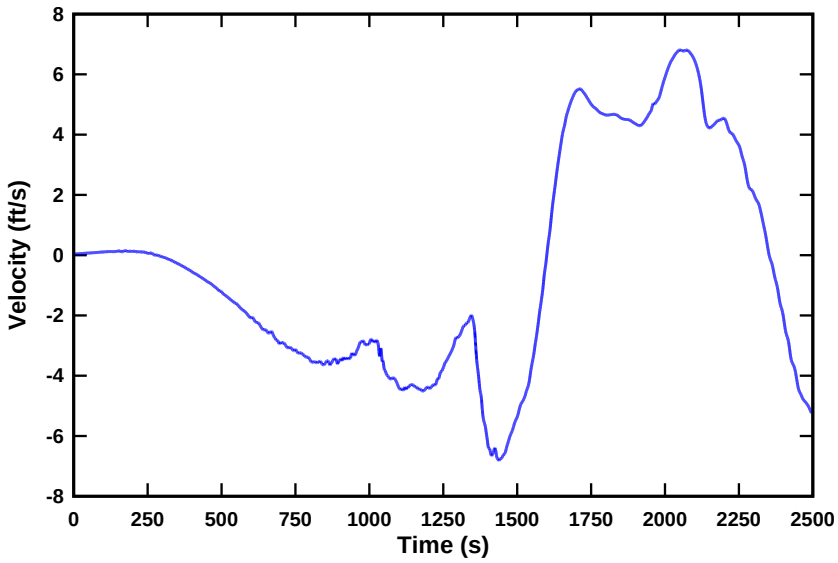

Figure A-4. Tsunami water velocity component in north direction at the location of the Mad River Slough Bridge.

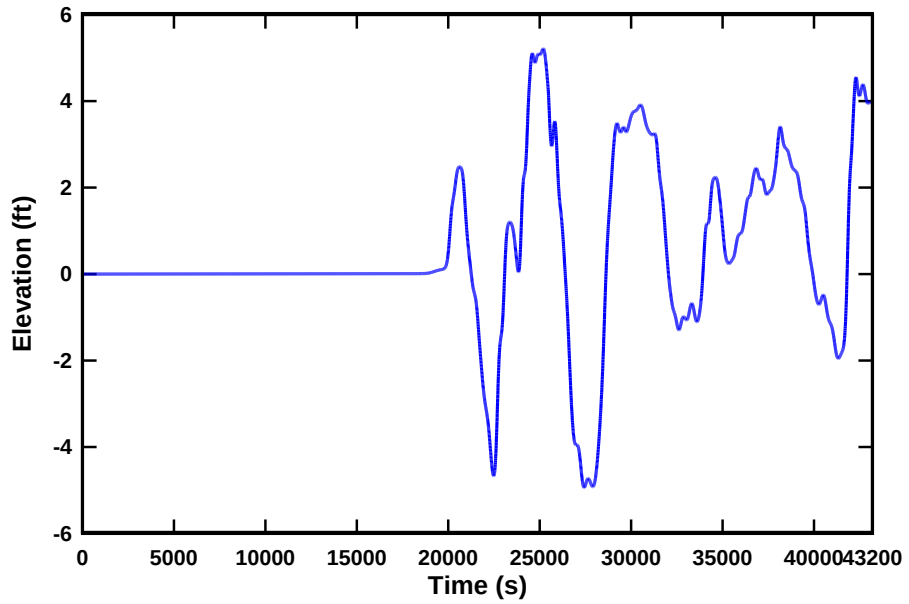

Figure A-5. Tsunami water free-surface elevation at the location of the Salmon Creek Bridge.

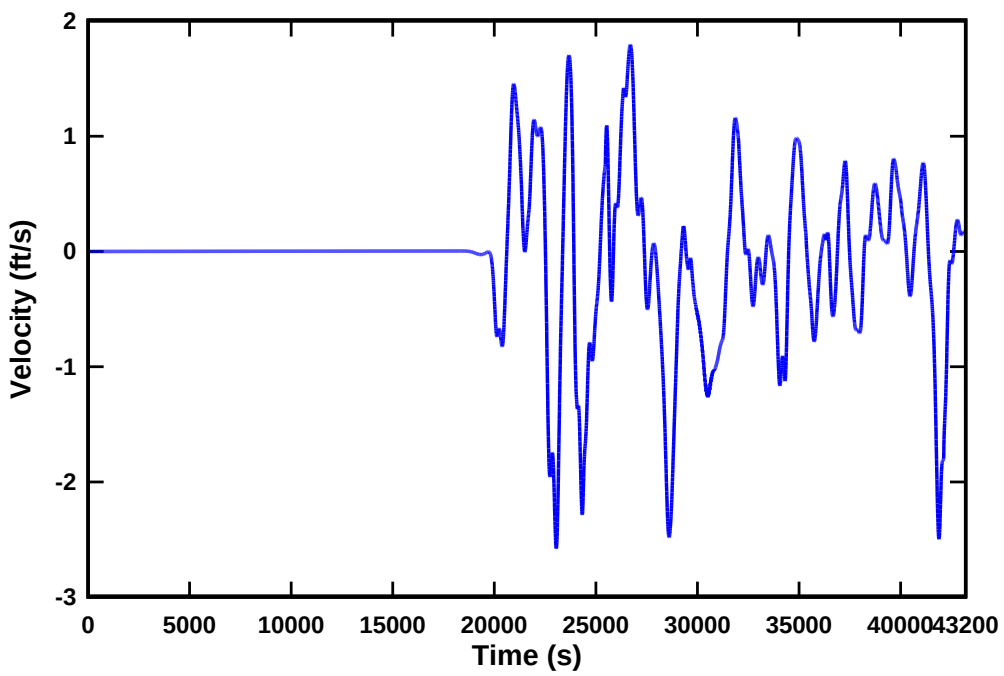

Figure A-6. Tsunami water velocity component normal to bridge direction at the location of the Salmon Creek Bridge.

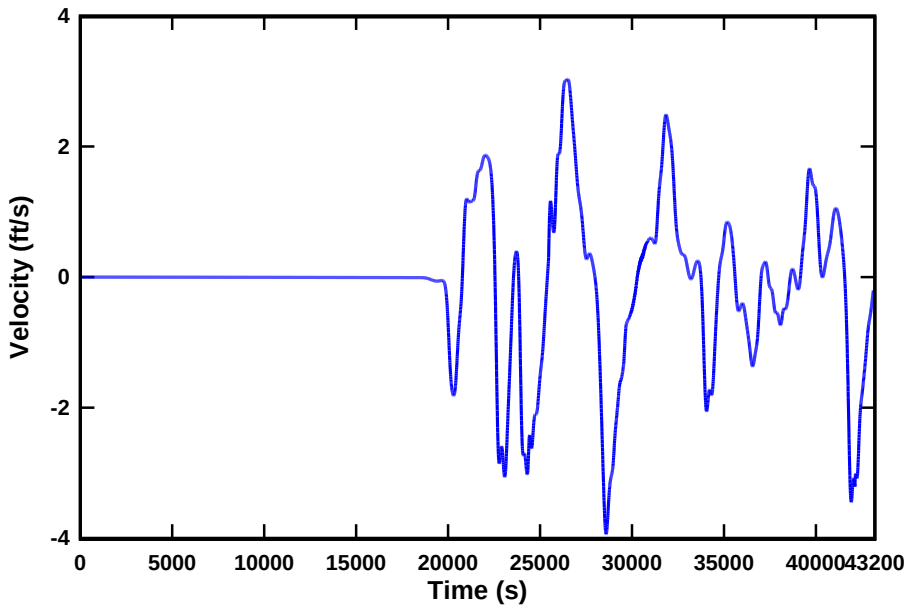

Figure A-7. Tsunami water velocity component in east direction at the location of the Salmon Creek Bridge.

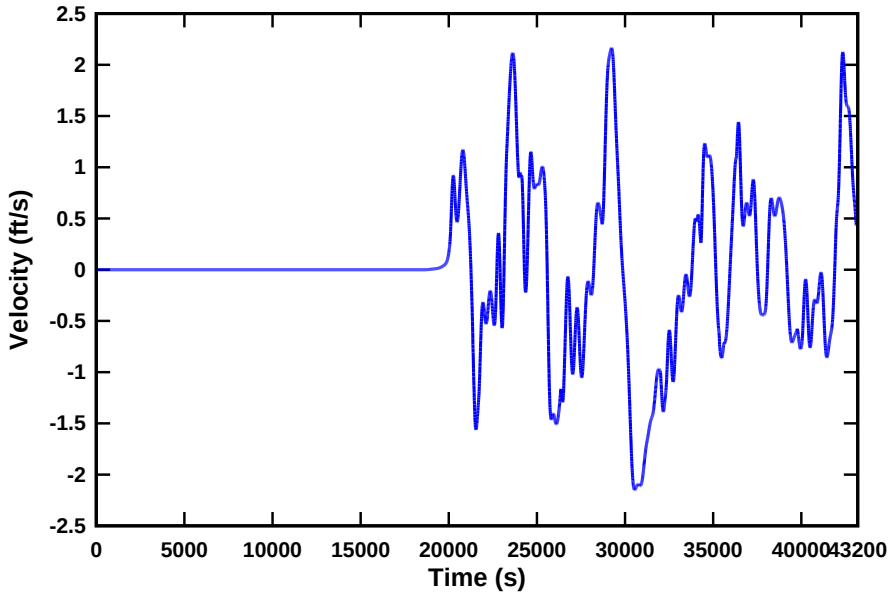

Figure A-8. Tsunami water velocity component in north direction at the location of the Salmon Creek Bridge.

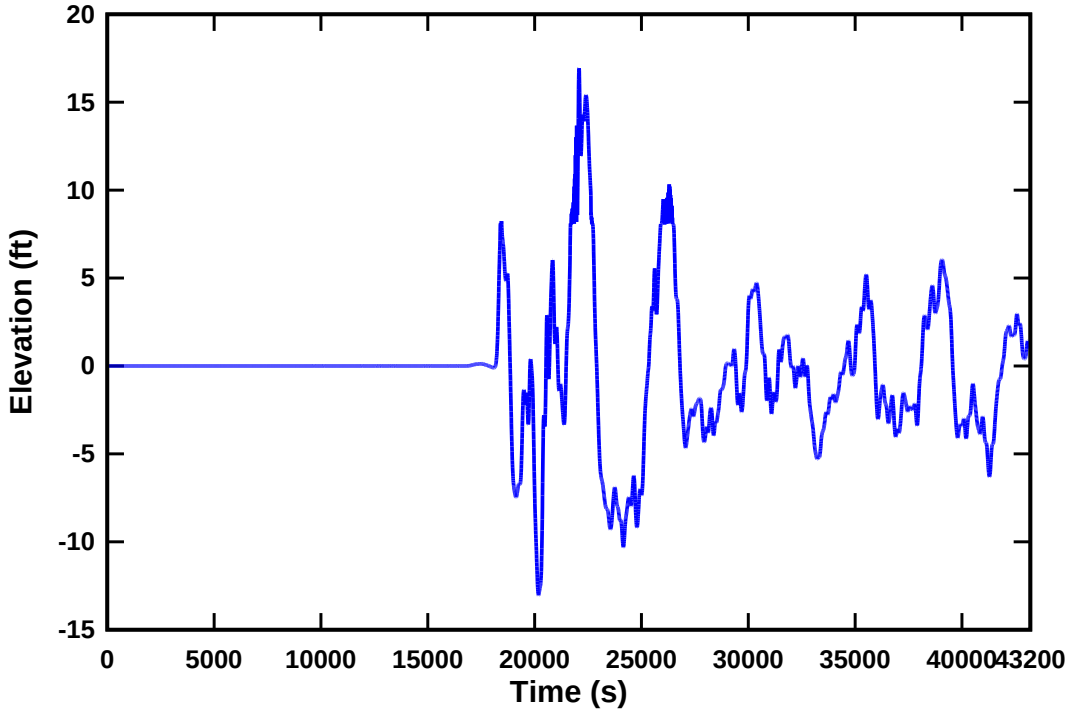

Figure A-9. Tsunami water free-surface elevation at the location of the Old Creek Bridge.

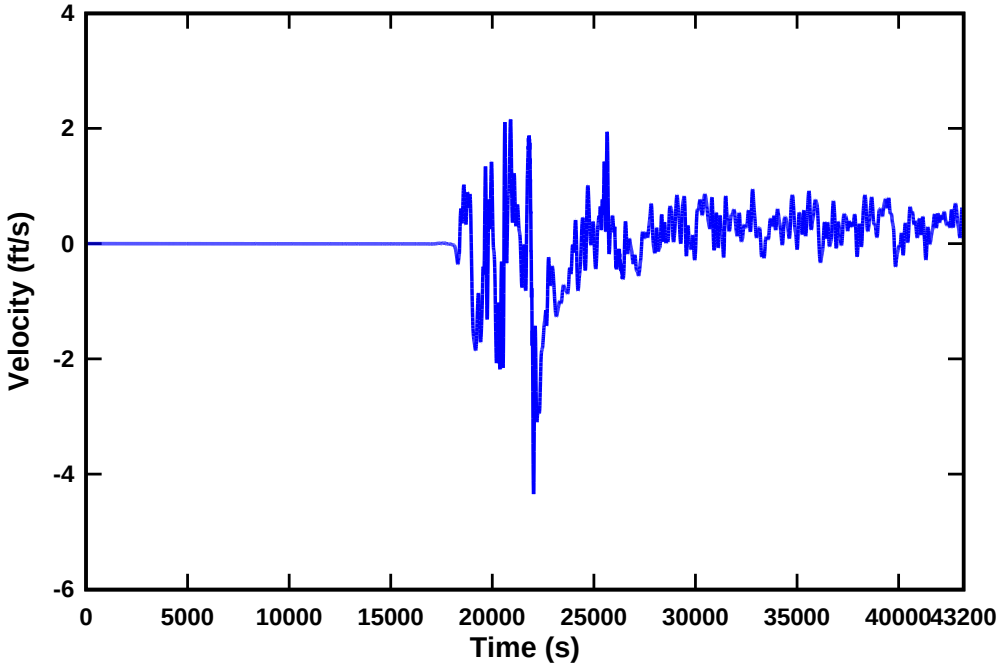

Figure A-10. Tsunami water velocity component normal to bridge direction at the location of the Old Creek Bridge.

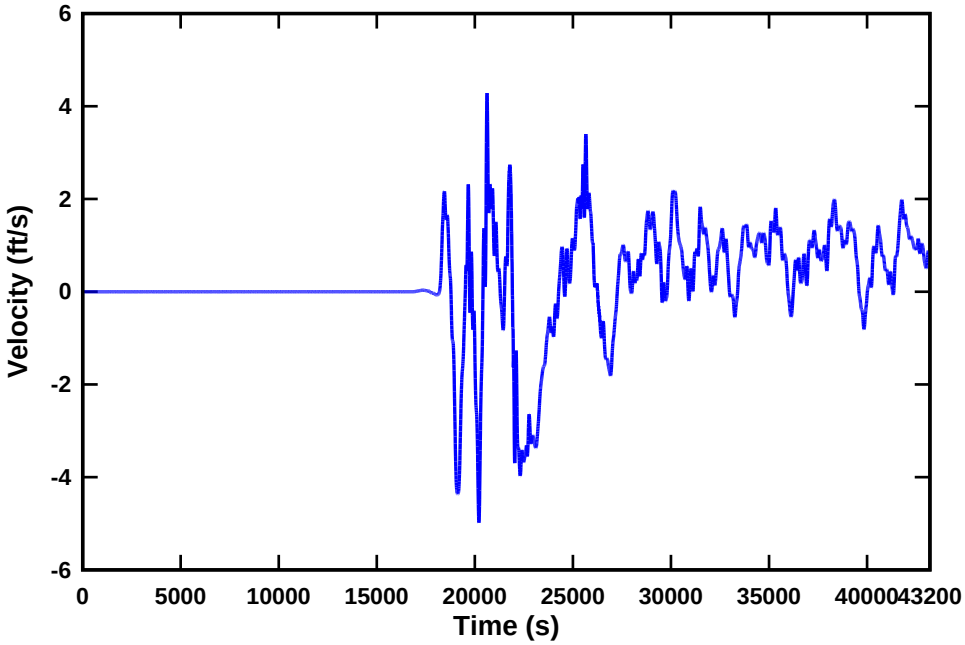

Figure A-11. Tsunami water velocity component in east direction at the location of the Old Creek Bridge.

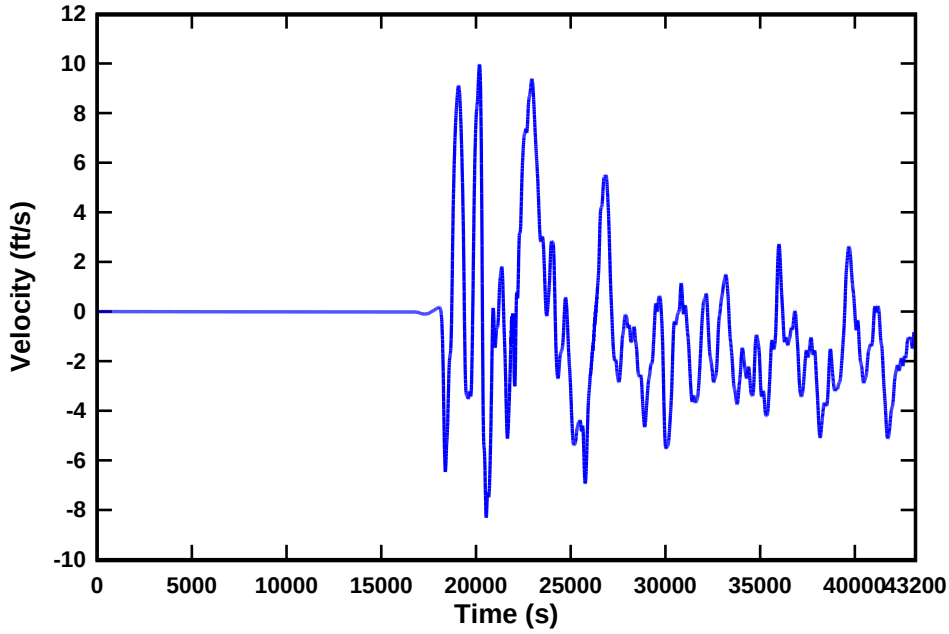

Figure A-12. Tsunami water velocity component in north direction at the location of the Old Creek Bridge.

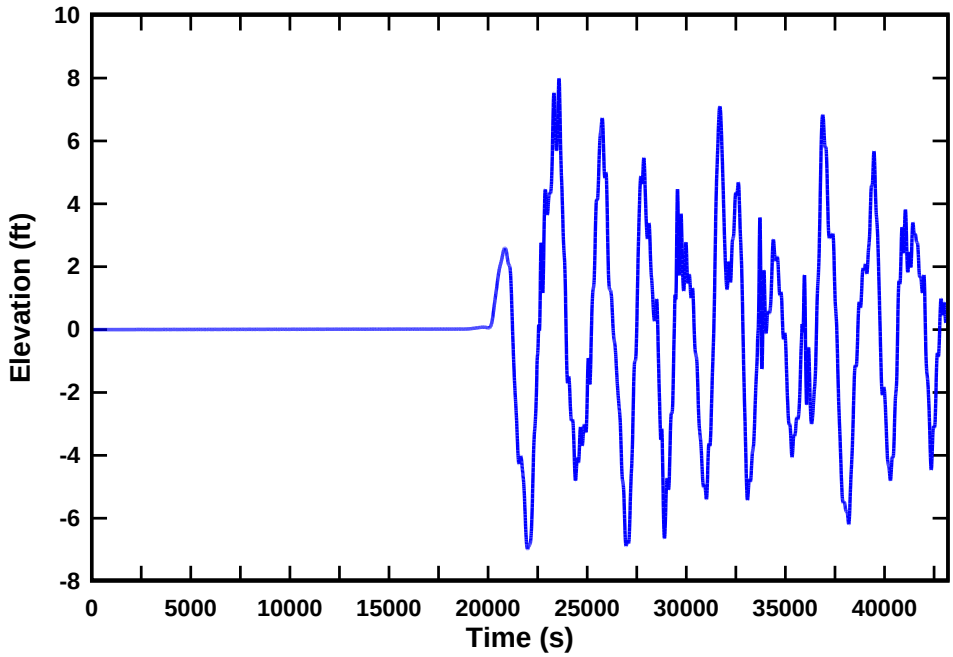

Figure A-13. Tsunami water free-surface elevation at the location of the Malibu Lagoon Bridge.

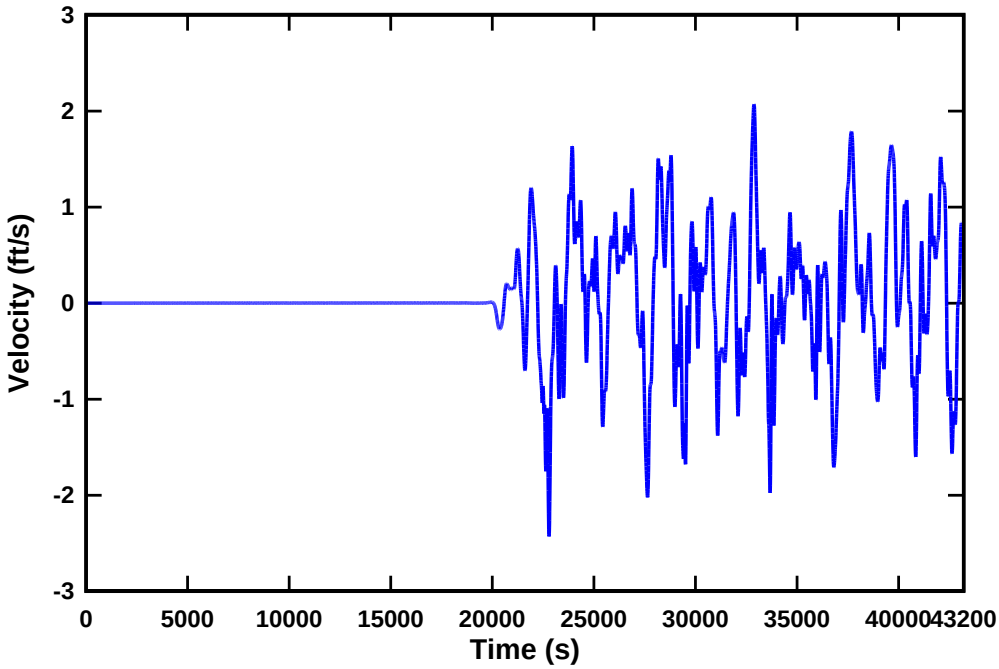

Figure A-14. Tsunami water velocity component normal to bridge direction at the location of the Malibu Lagoon Bridge.

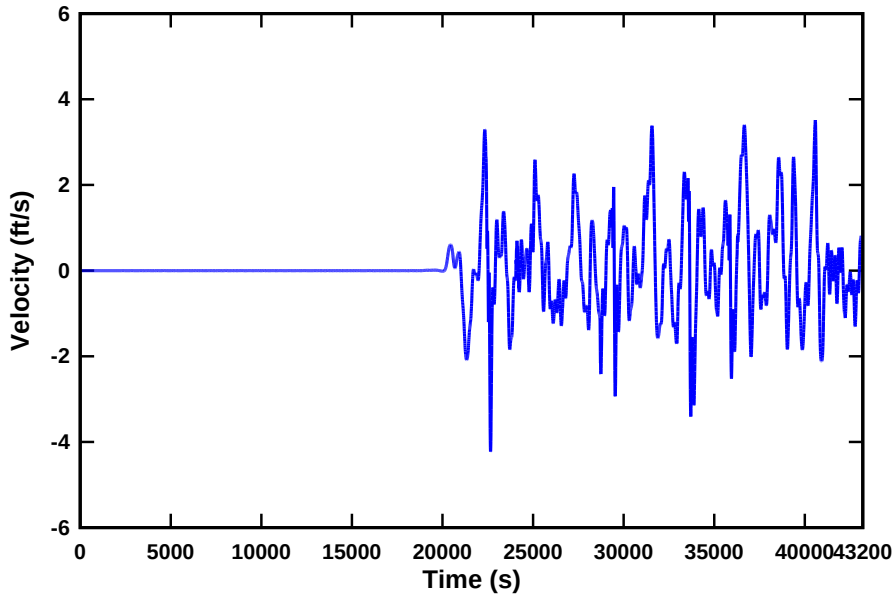

Figure A-15. Tsunami water velocity component in east direction at the location of the Malibu Lagoon Bridge.

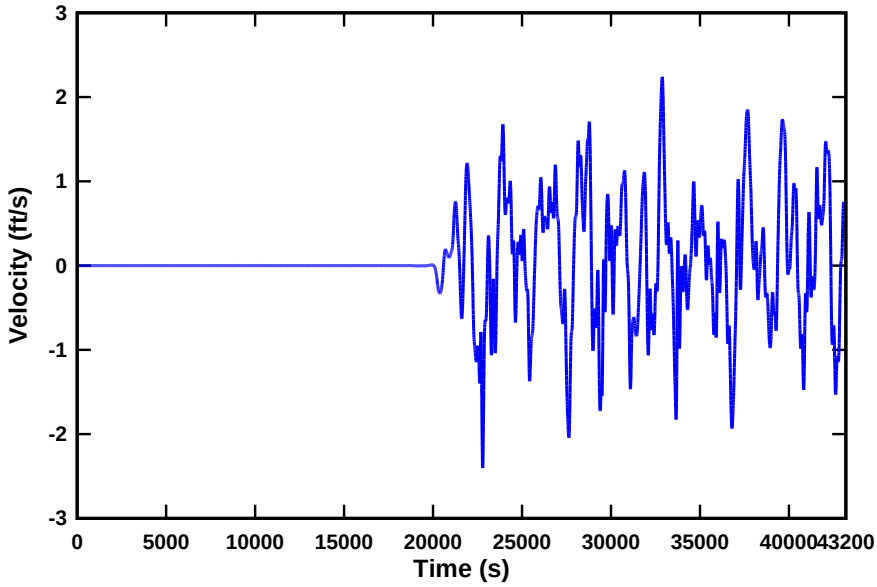

Figure A-16. Tsunami water velocity component in north direction at the location of the Malibu Lagoon Bridge.

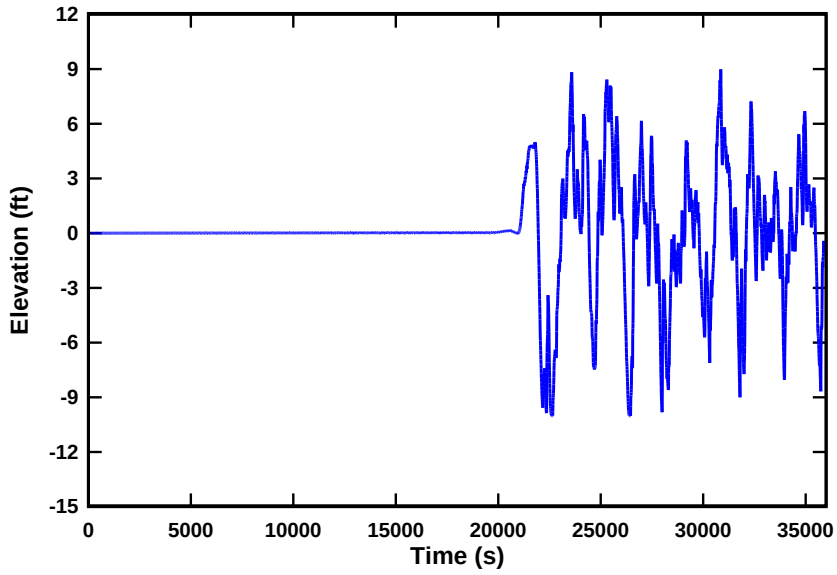

Figure A-17. Tsunami water free-surface elevation at the location of the Agua Hedionda Lagoon Bridge.

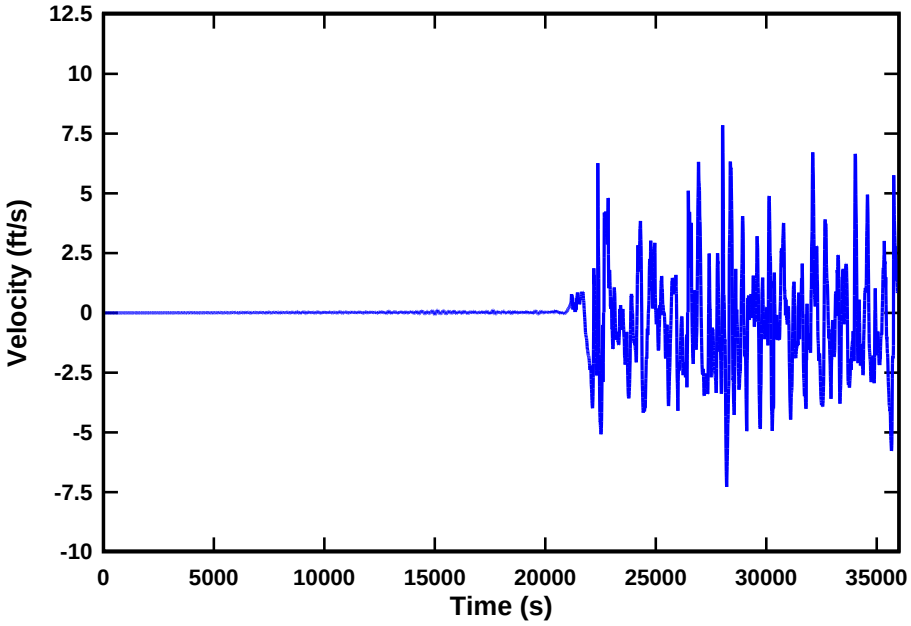

Figure A-18. Tsunami water velocity component normal to bridge direction at the location of the Agua Hedionda Lagoon Bridge.

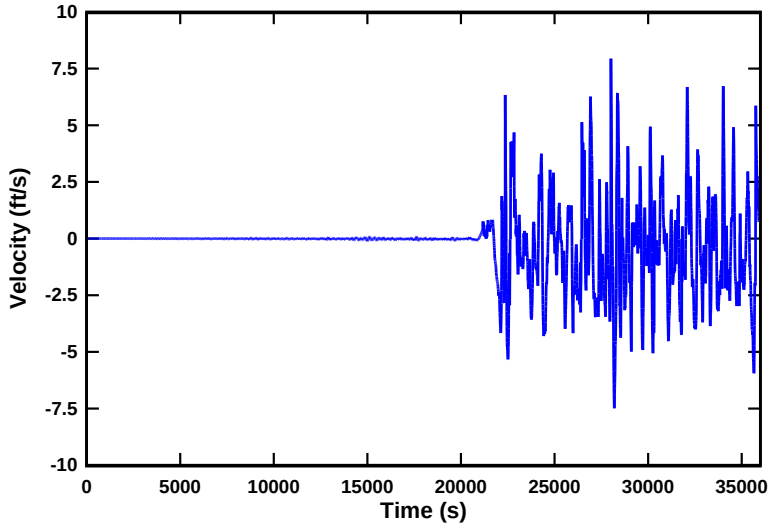

Figure A-19. Tsunami water velocity component in east direction at the location of the Agua Hedionda Lagoon Bridge.

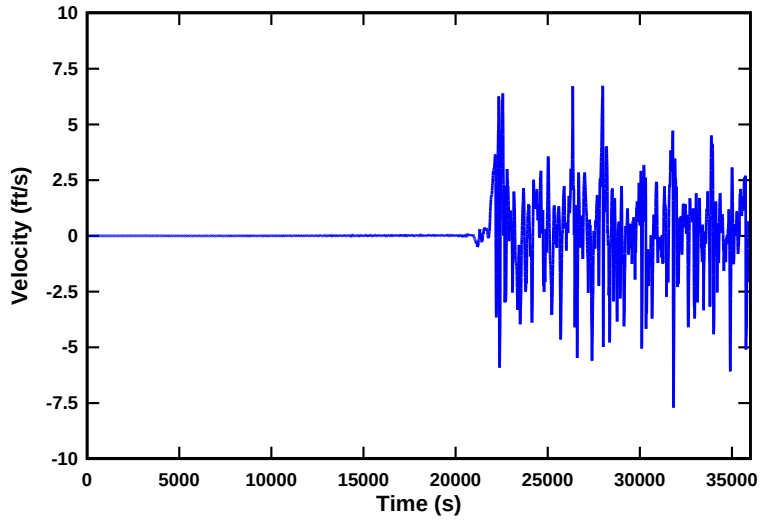

Figure A-20. Tsunami water velocity component in north direction at the location of the Agua Hedionda Lagoon Bridge.

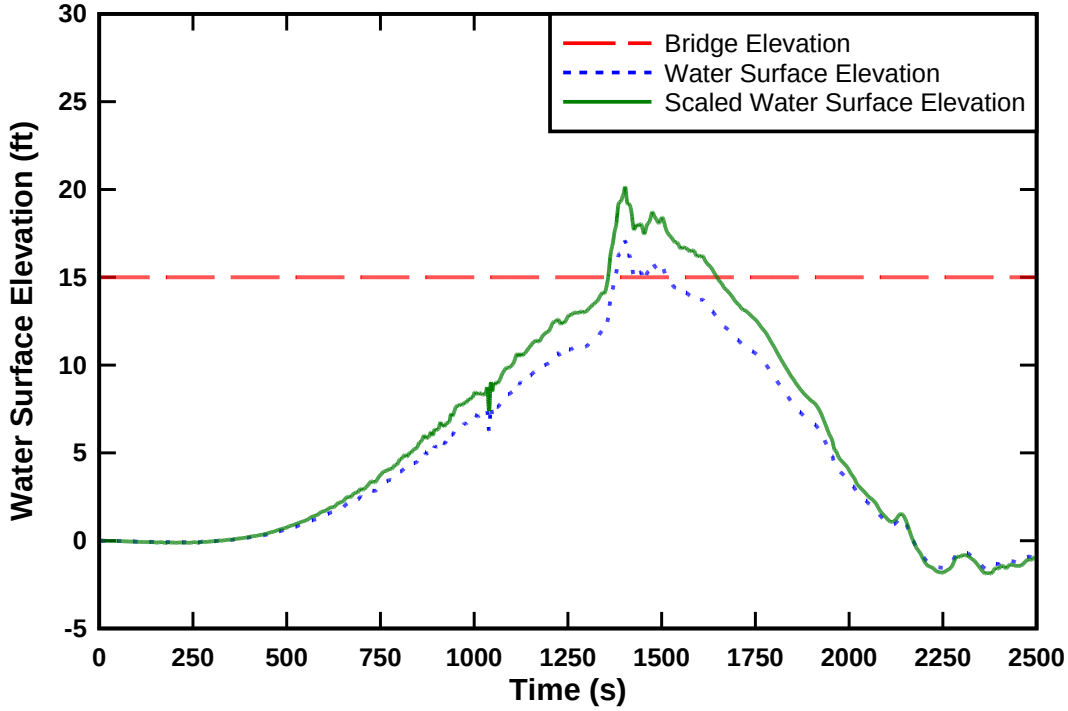

Figure A-21. Scaled tsunami water free-surface elevation compared to Mad River Slough Bridge elevation, water free-surface elevation 5 ft above bridge.

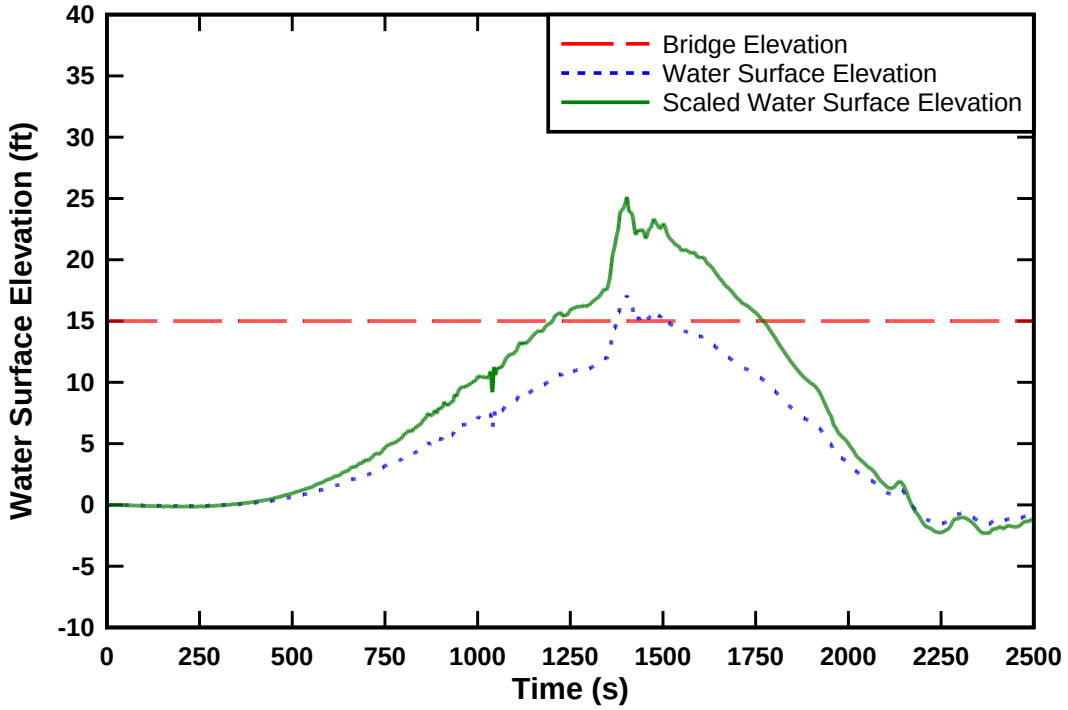

Figure A-22. Scaled tsunami water free-surface elevation compared to Mad River Slough Bridge elevation, water free-surface elevation 10 ft above bridge.

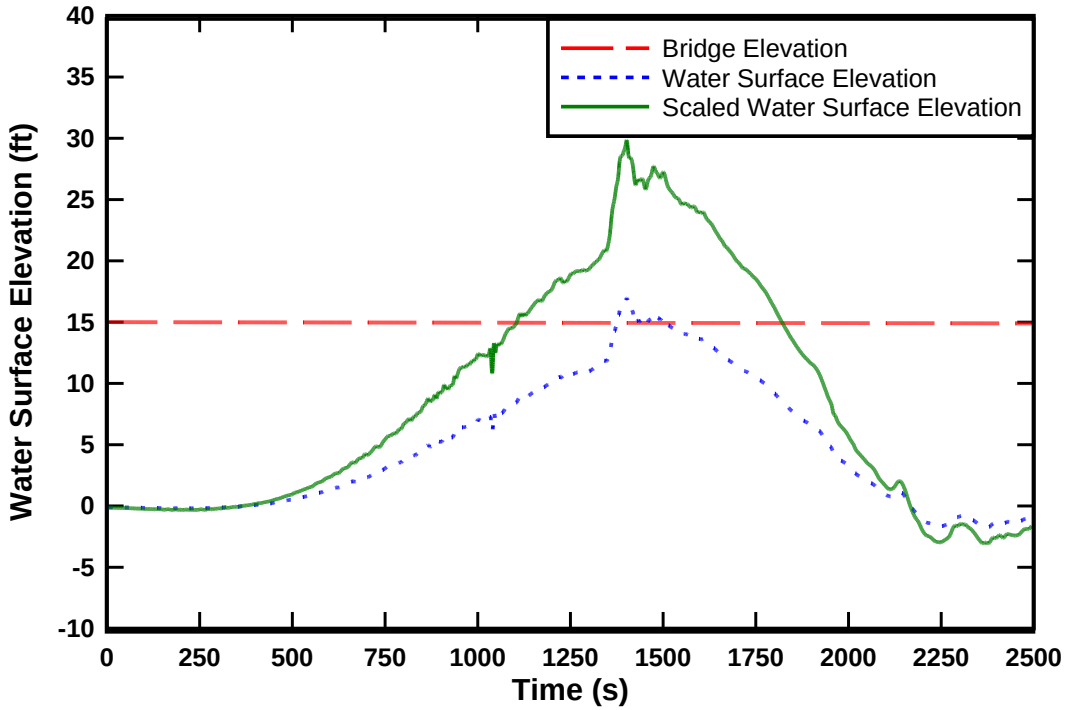

Figure A-23. Scaled tsunami water free-surface elevation compared to Mad River Slough Bridge elevation, water free-surface elevation 15 ft above bridge.

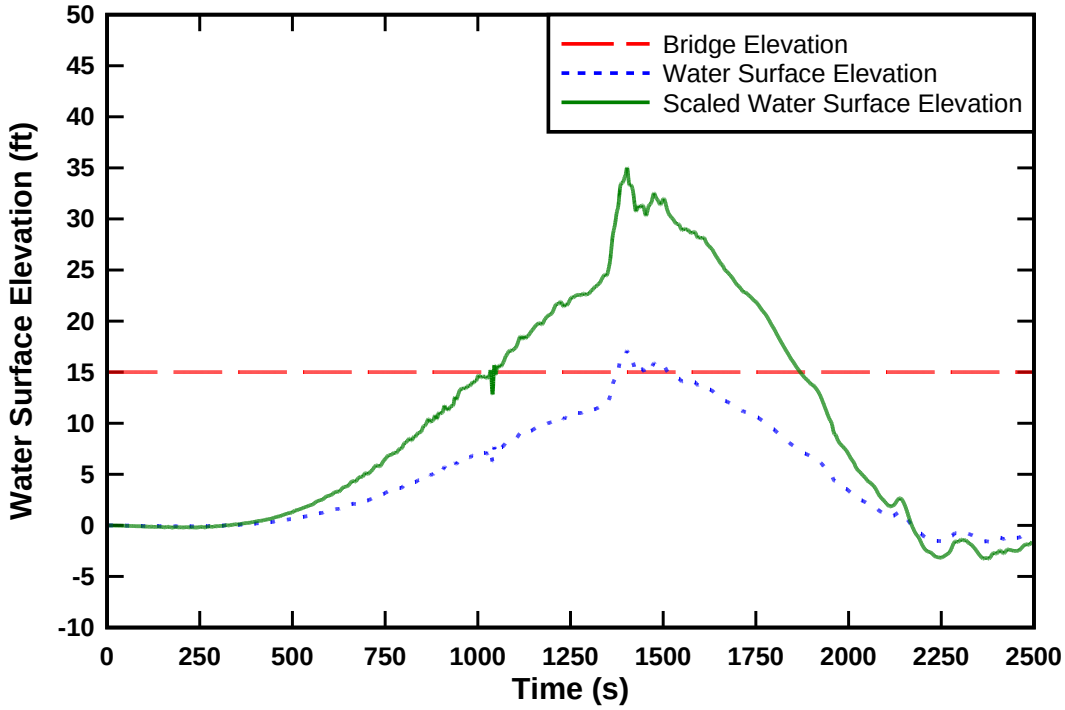

Figure A-24. Scaled tsunami water free-surface elevation compared to Mad River Slough Bridge elevation, water free-surface elevation 20 ft above bridge.

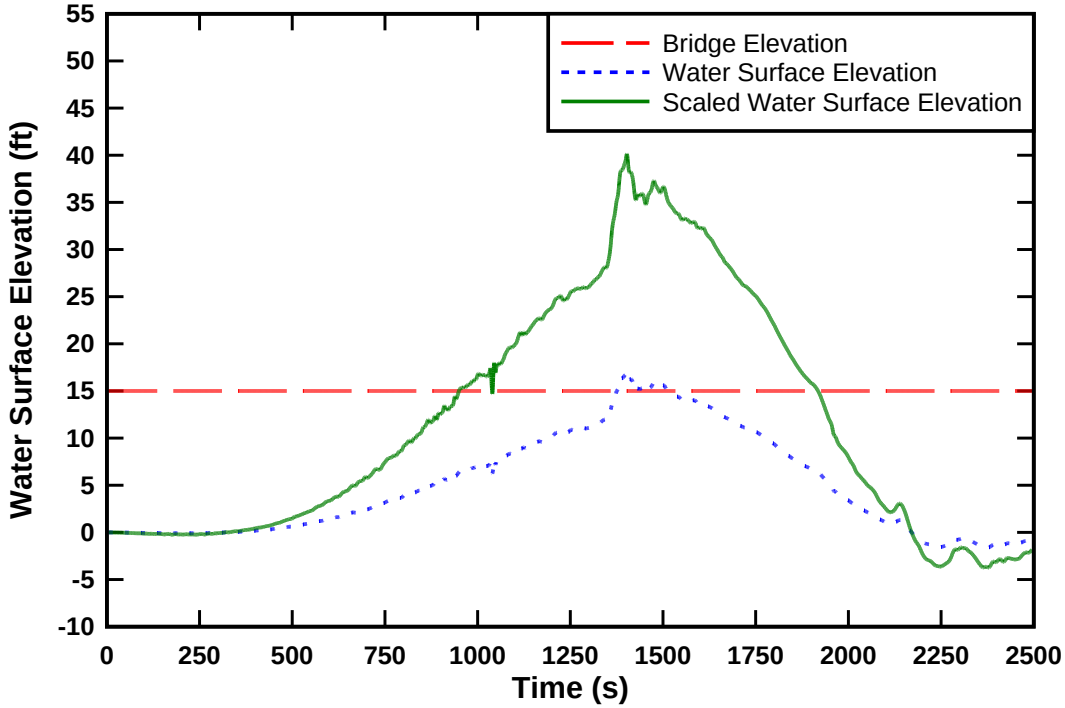

Figure A-25. Scaled tsunami water free-surface elevation compared to Mad River Slough Bridge elevation, water free-surface elevation 25 ft above bridge.

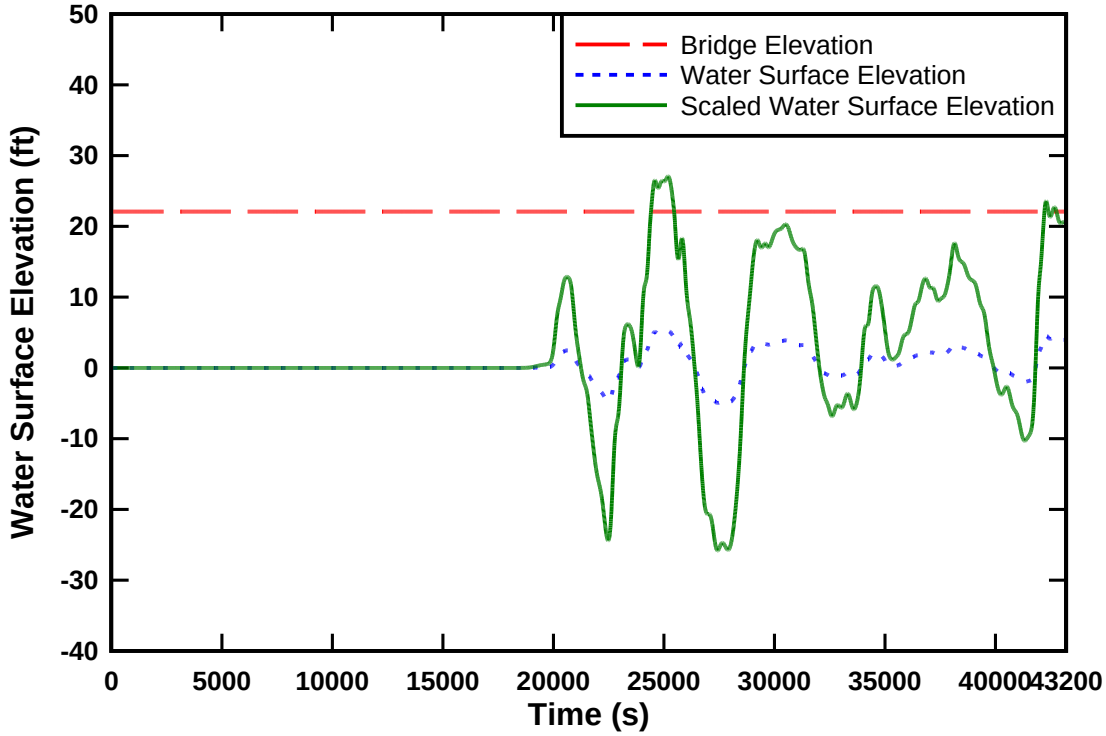

Figure A-26. Scaled tsunami water free-surface elevation compared to Salmon Creek Bridge elevation, water free-surface elevation 5 ft above bridge.

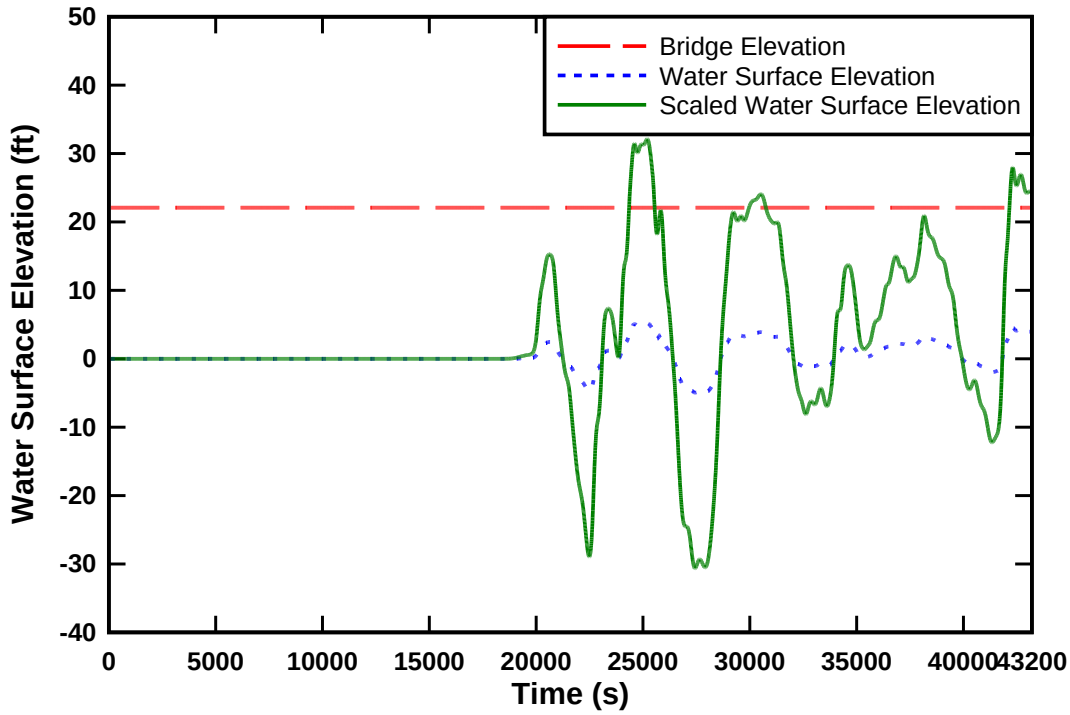

Figure A-27. Scaled tsunami water free-surface elevation compared to Salmon Creek Bridge elevation, water free-surface elevation 10 ft above bridge.

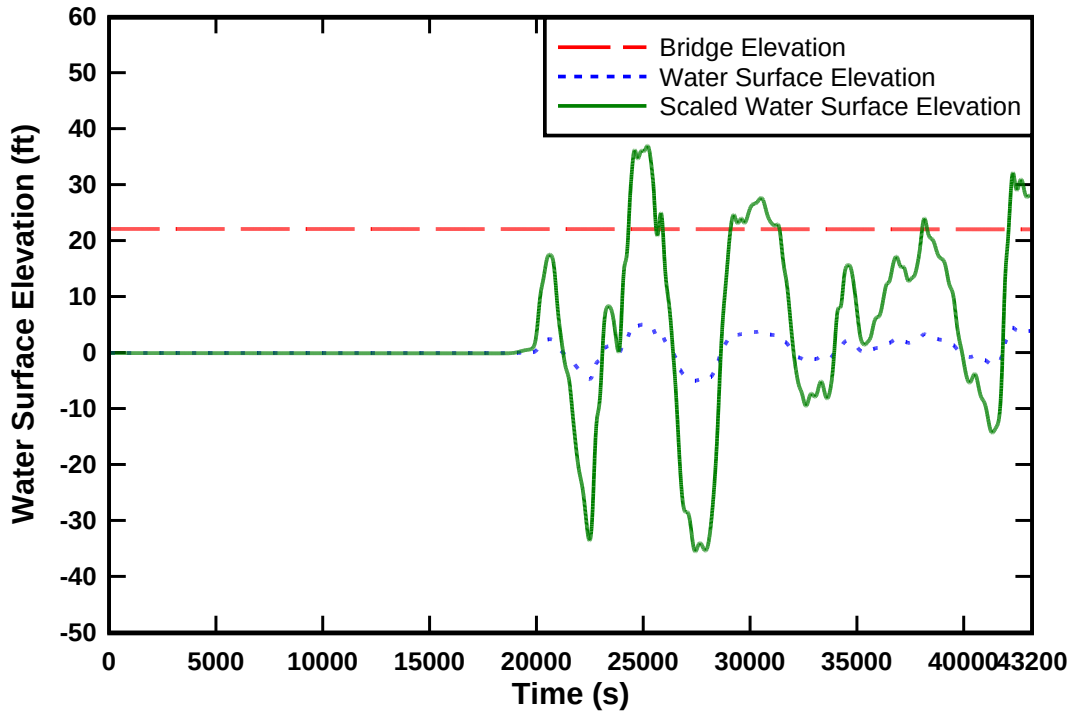

Figure A-28. Scaled tsunami water free-surface elevation compared to Salmon Creek Bridge elevation, water free-surface elevation 15 ft above bridge.

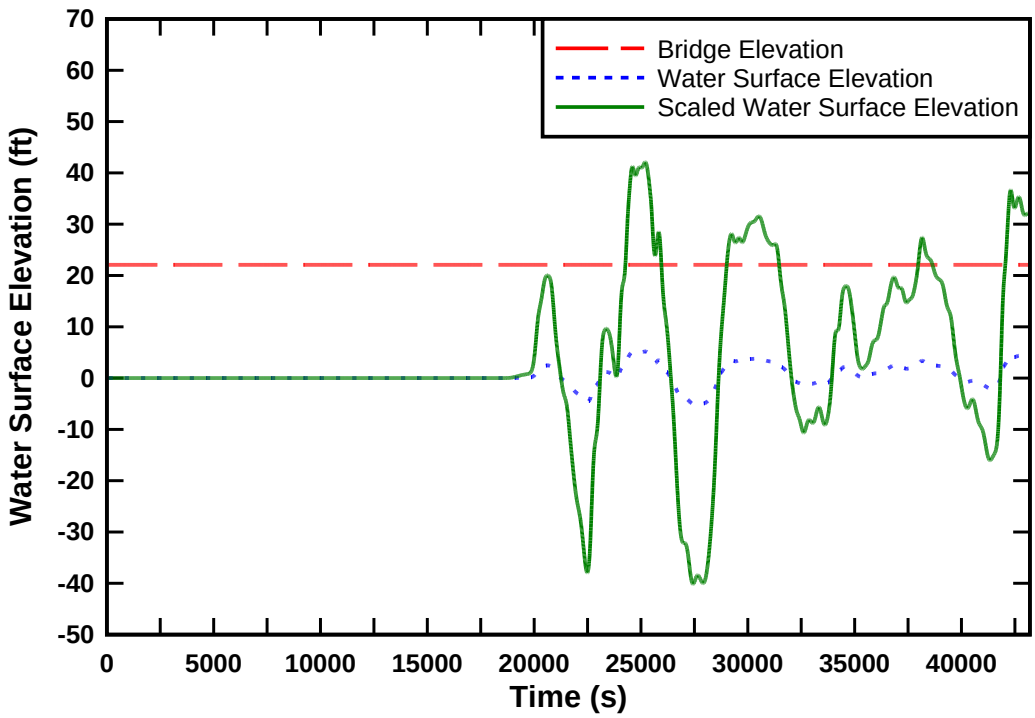

Figure A-29. Scaled tsunami water free-surface elevation compared to Salmon Creek Bridge elevation, water free-surface elevation 20 ft above bridge.

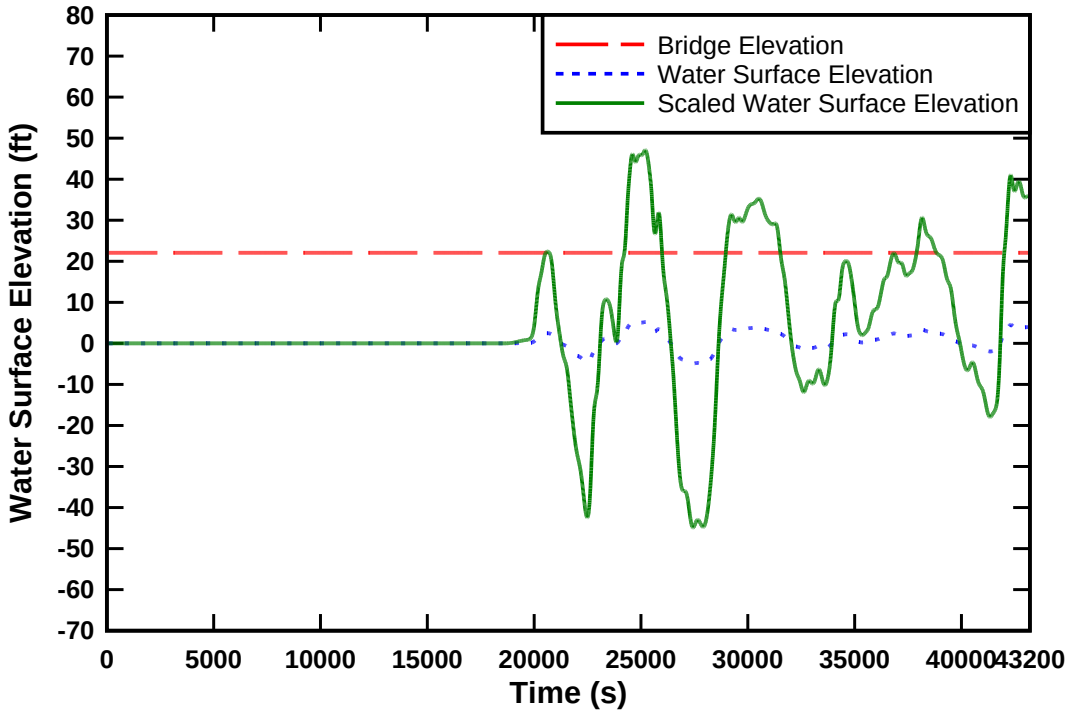

Figure A-30. Scaled tsunami water free-surface elevation compared to Salmon Creek Bridge elevation, water free-surface elevation 25 ft above bridge.

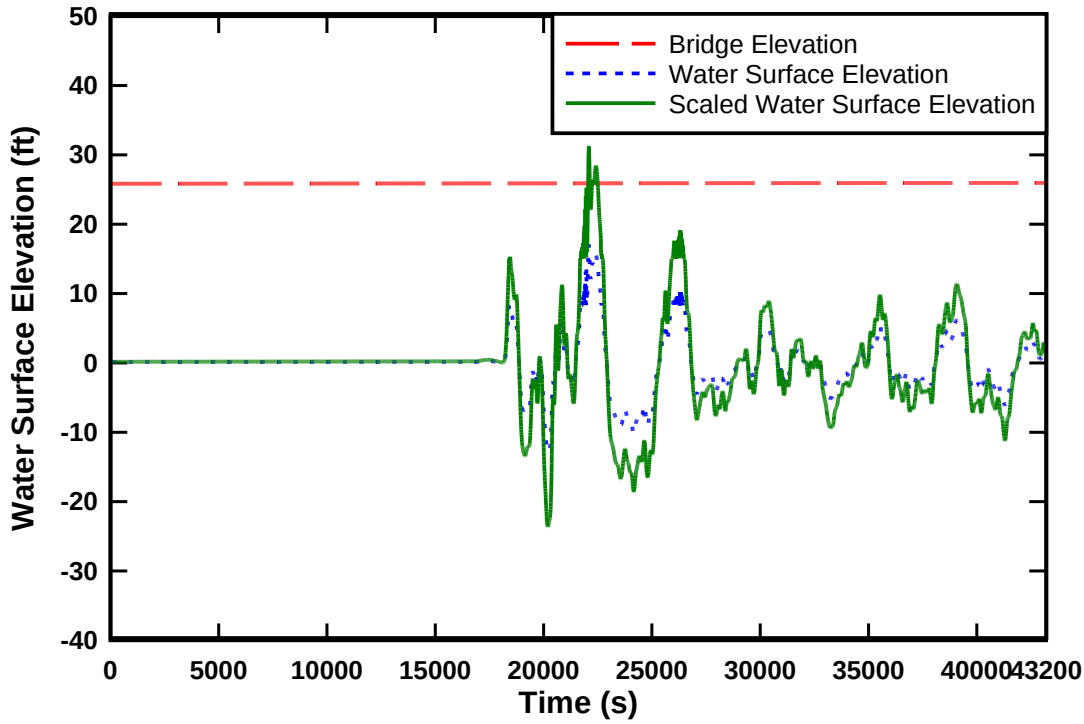

Figure A-31. Scaled tsunami water free-surface elevation compared to Salmon Old Bridge elevation, water free-surface elevation 5 ft above bridge.

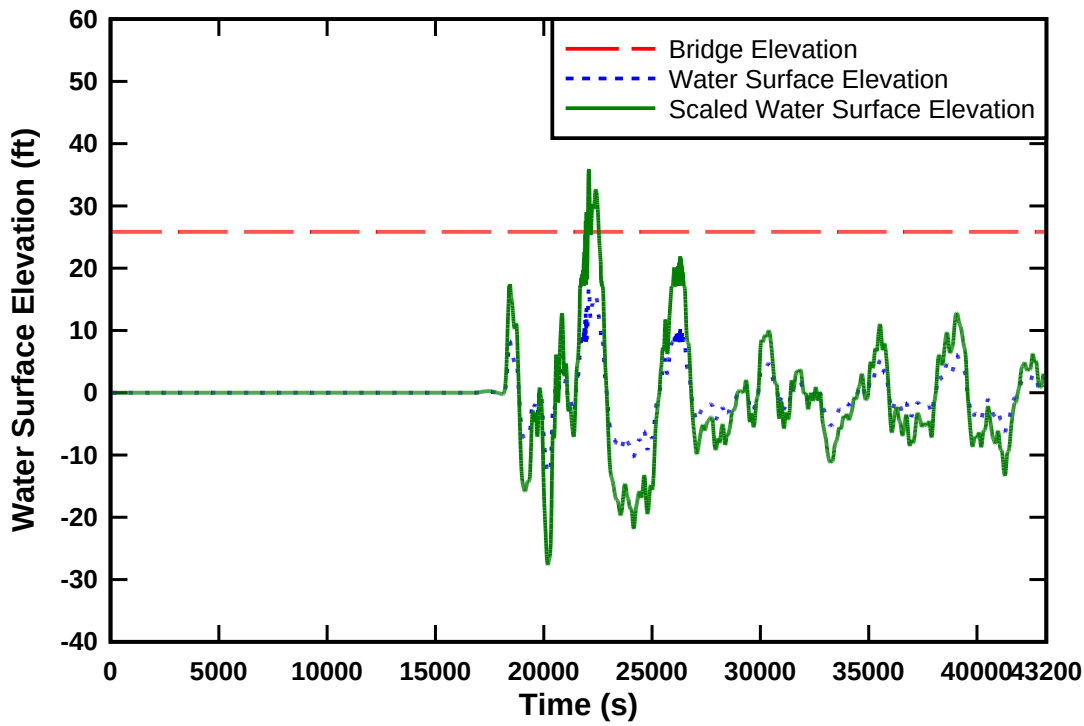

Figure A-32. Scaled tsunami water free-surface elevation compared to Salmon Old Bridge elevation, water free-surface elevation 10 ft above bridge.

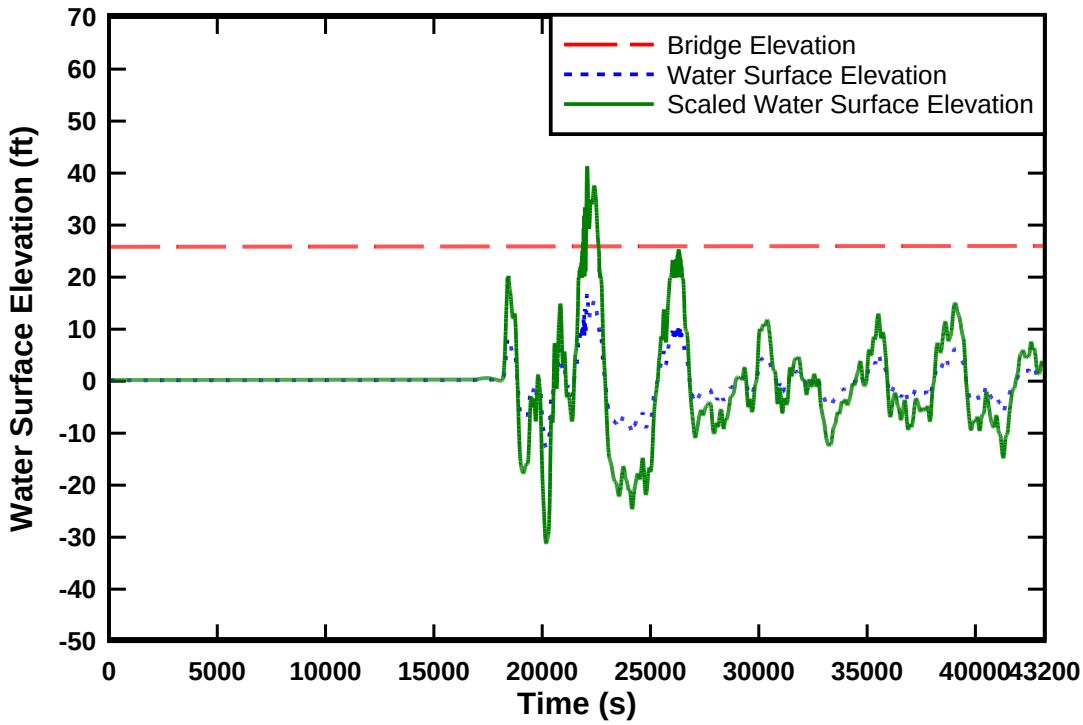

Figure A-33. Scaled tsunami water free-surface elevation compared to Salmon Old Bridge elevation, water free-surface elevation 15 ft above bridge.

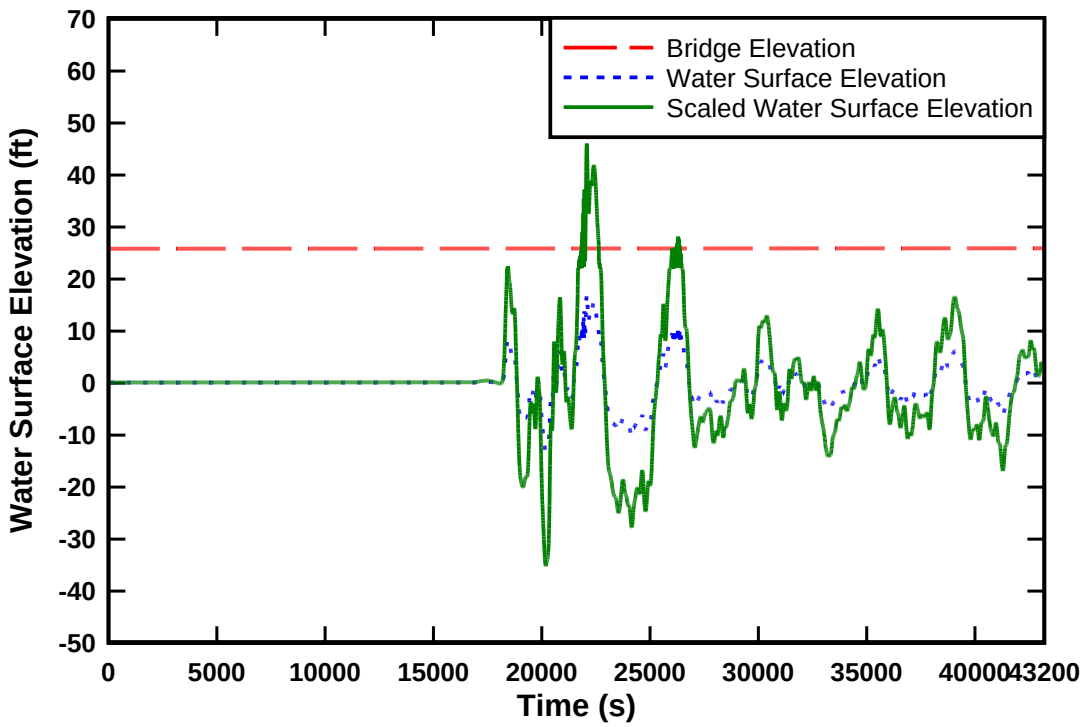

Figure A-34. Scaled tsunami water free-surface elevation compared to Salmon Old Bridge elevation, water free-surface elevation 20 ft above bridge.

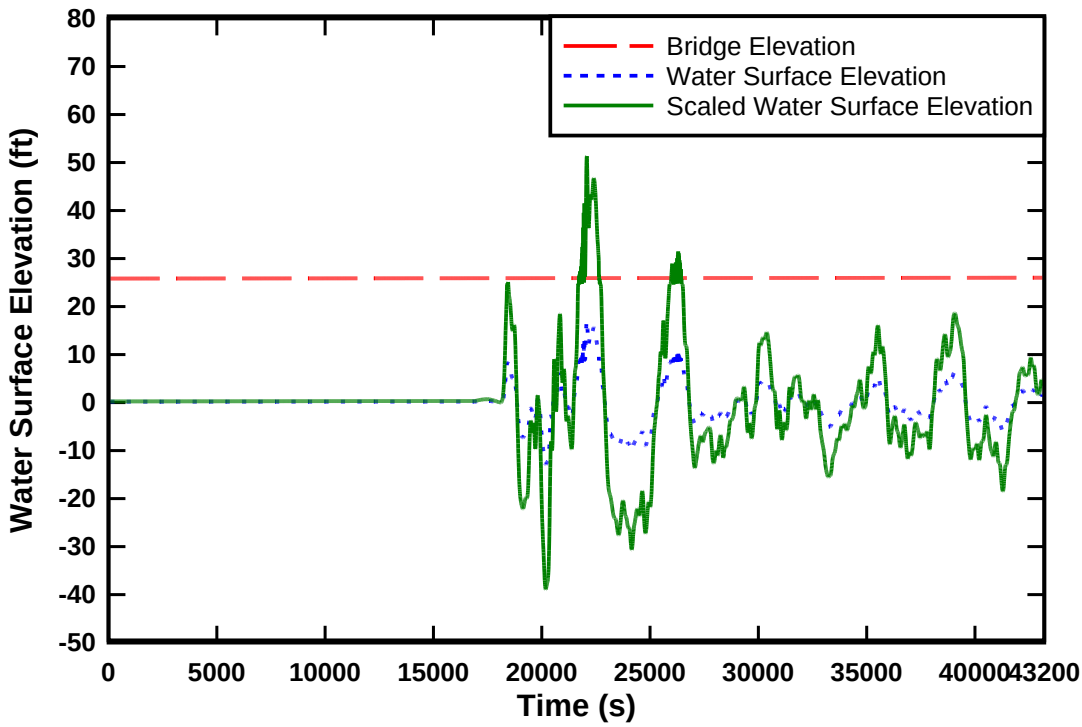

Figure A-35. Scaled tsunami water free-surface elevation compared to Salmon Old Bridge elevation, water free-surface elevation 25 ft above bridge.

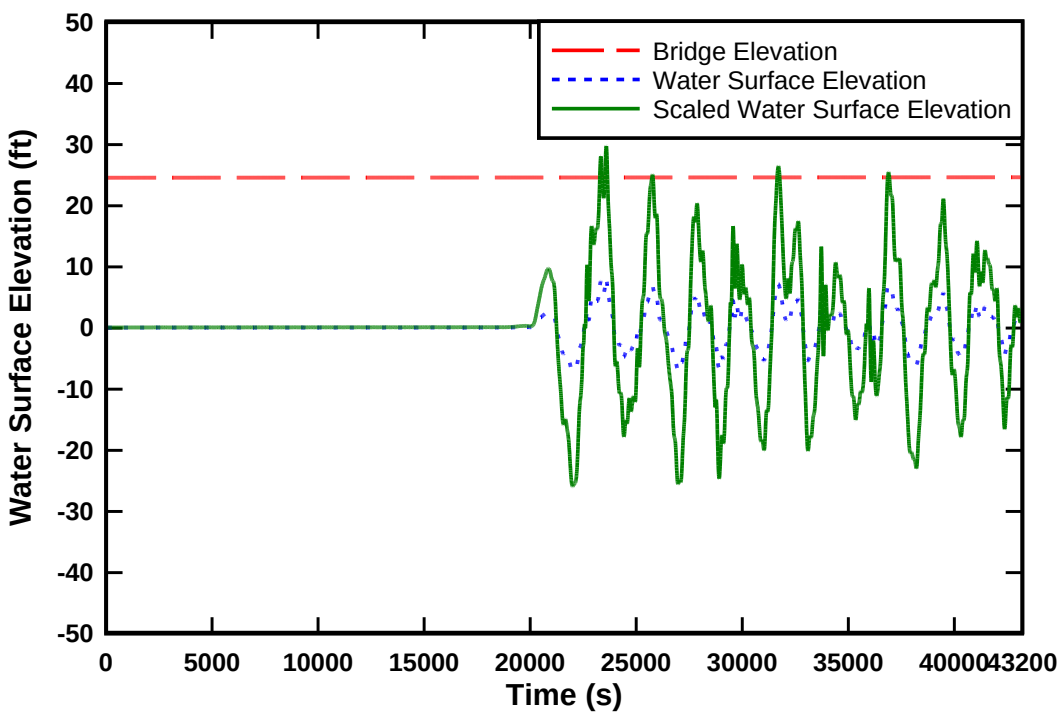

Figure A-36. Scaled tsunami water free-surface elevation compared to Malibu Lagoon Bridge elevation, water free-surface elevation 5 ft above bridge.

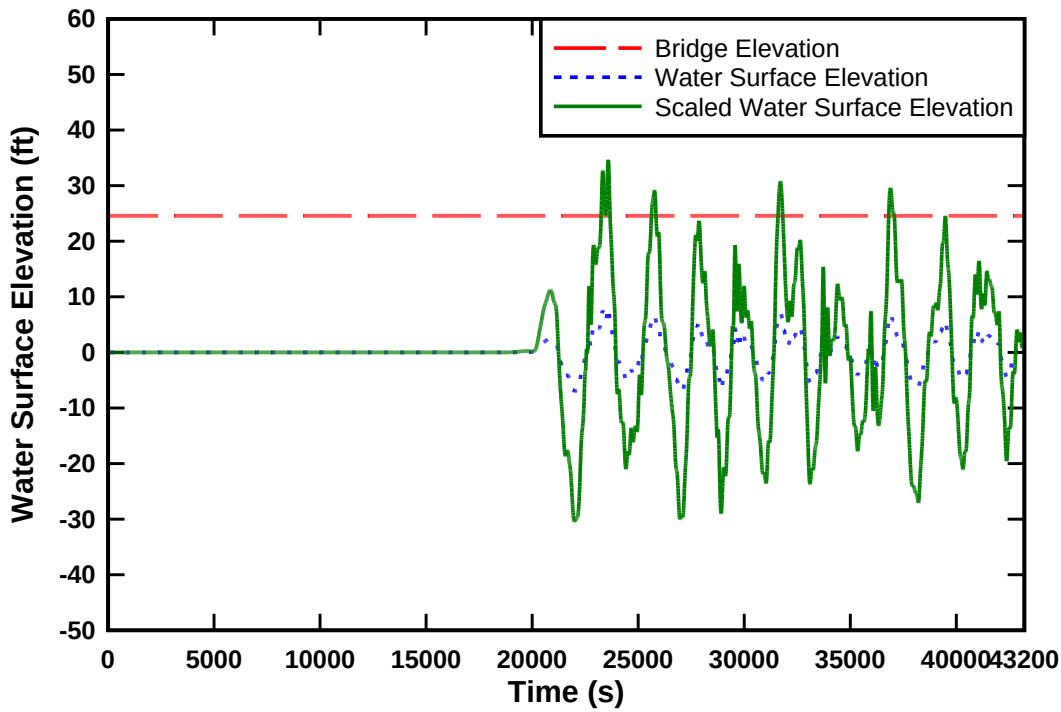

Figure A-37. Scaled tsunami water free-surface elevation compared to Malibu Lagoon Bridge elevation, water free-surface elevation 10 ft above bridge.

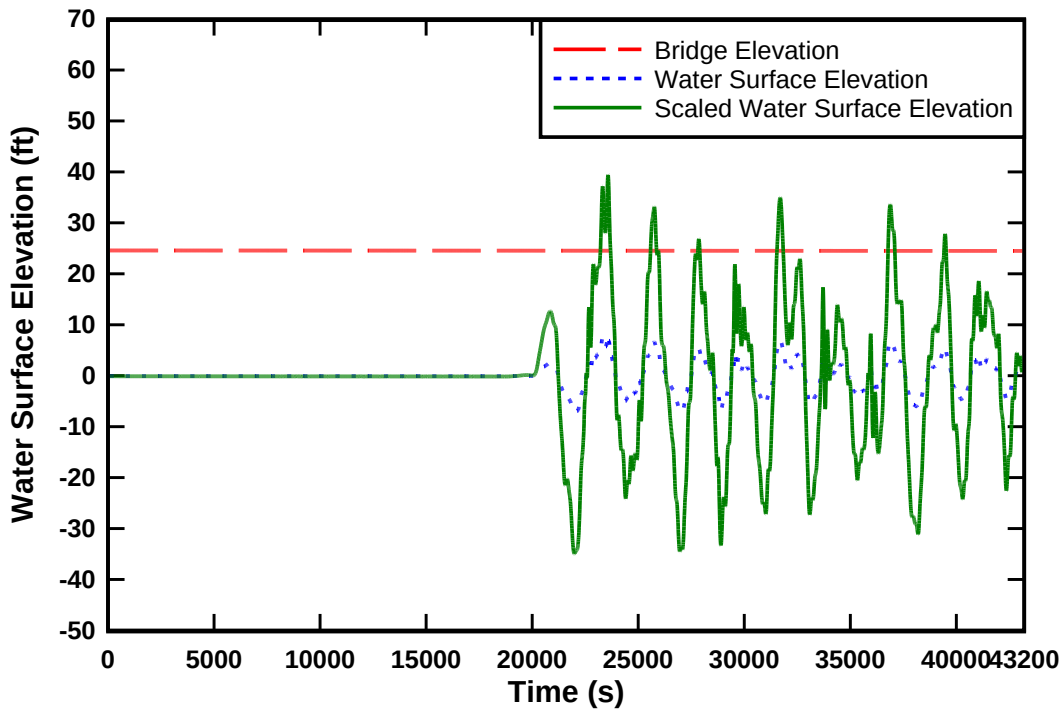

Figure A-38. Scaled tsunami water free-surface elevation compared to Malibu Lagoon Bridge elevation, water free-surface elevation 15 ft above bridge.

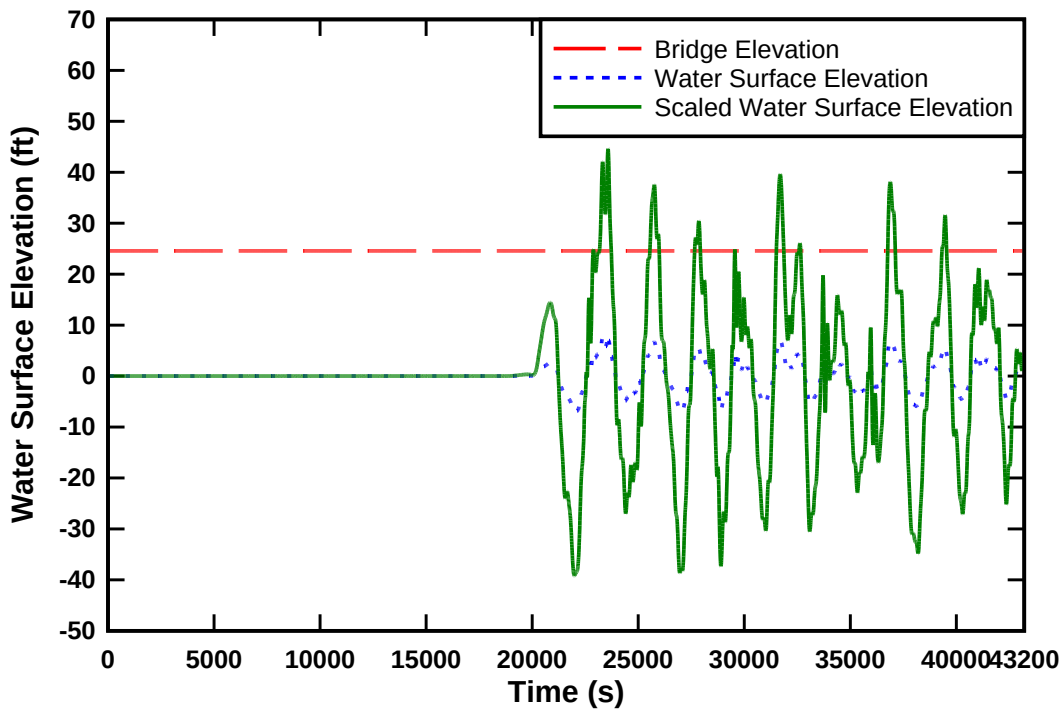

Figure A-39. Scaled tsunami water free-surface elevation compared to Malibu Lagoon Bridge elevation, water free-surface elevation 20 ft above bridge.

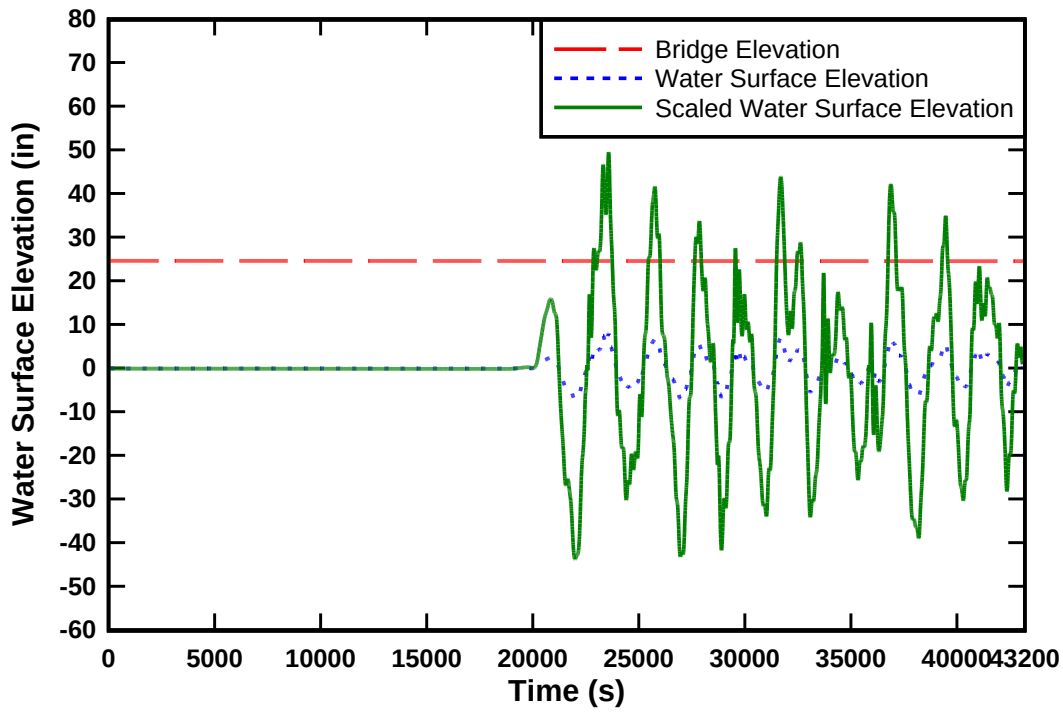

Figure A-40. Scaled tsunami water free-surface elevation compared to Malibu Lagoon Bridge elevation, water free-surface elevation 25 ft above bridge.

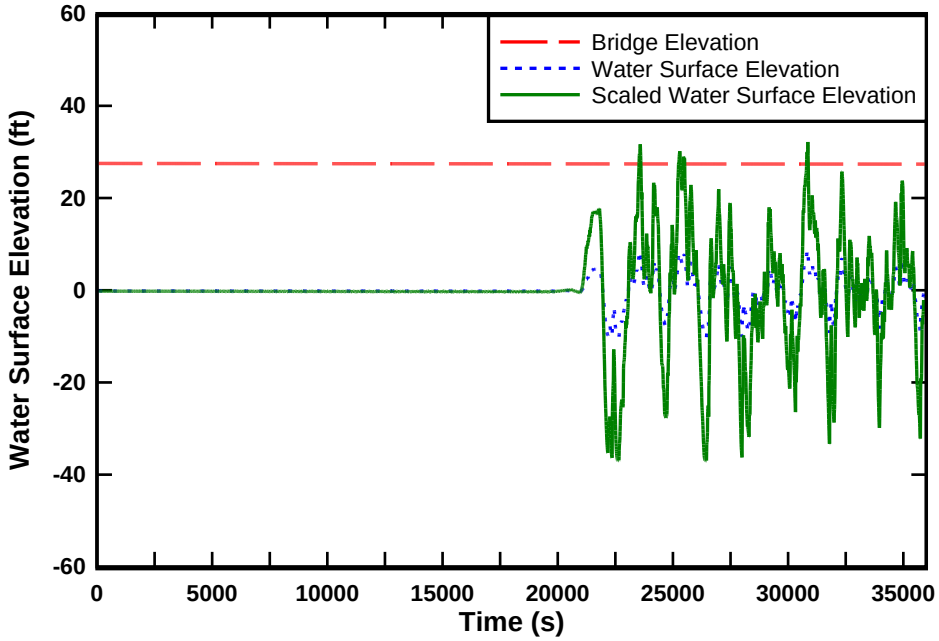

Figure A-41. Scaled tsunami water free-surface elevation compared to Agua Hedionda Lagoon Bridge elevation, water free-surface elevation 5 ft above bridge.

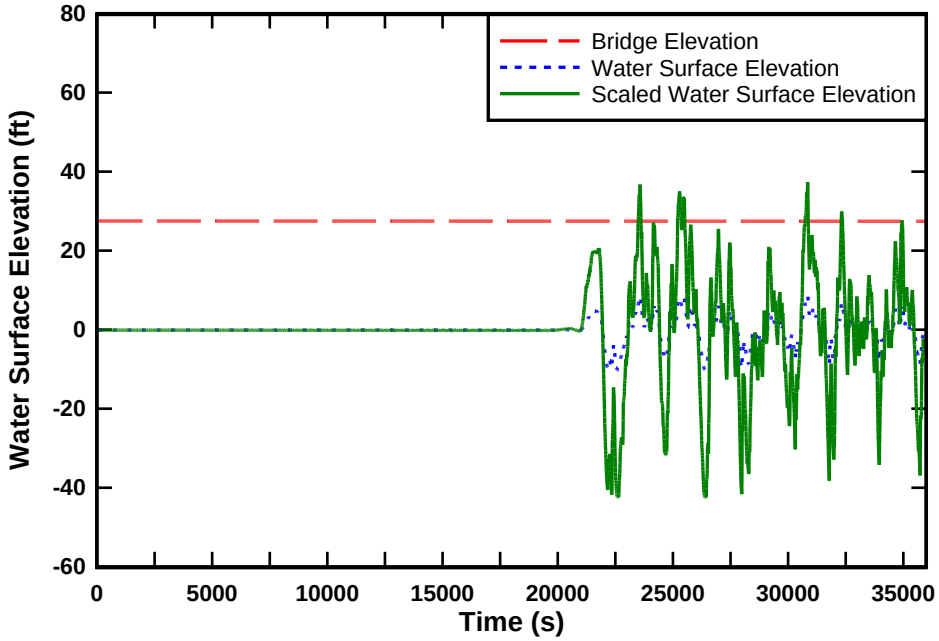

Figure A-42. Scaled tsunami water free-surface elevation compared to Agua Hedionda Lagoon Bridge elevation, water free-surface elevation 10 ft above bridge.

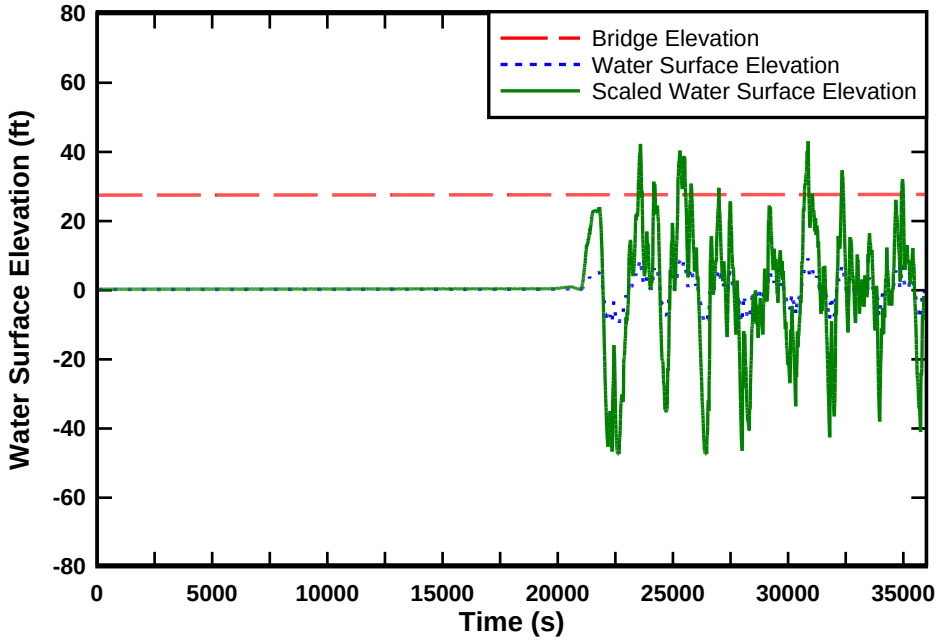

Figure A-43. Scaled tsunami water free-surface elevation compared to Agua Hedionda Lagoon Bridge elevation, water free-surface elevation 15 ft above bridge.

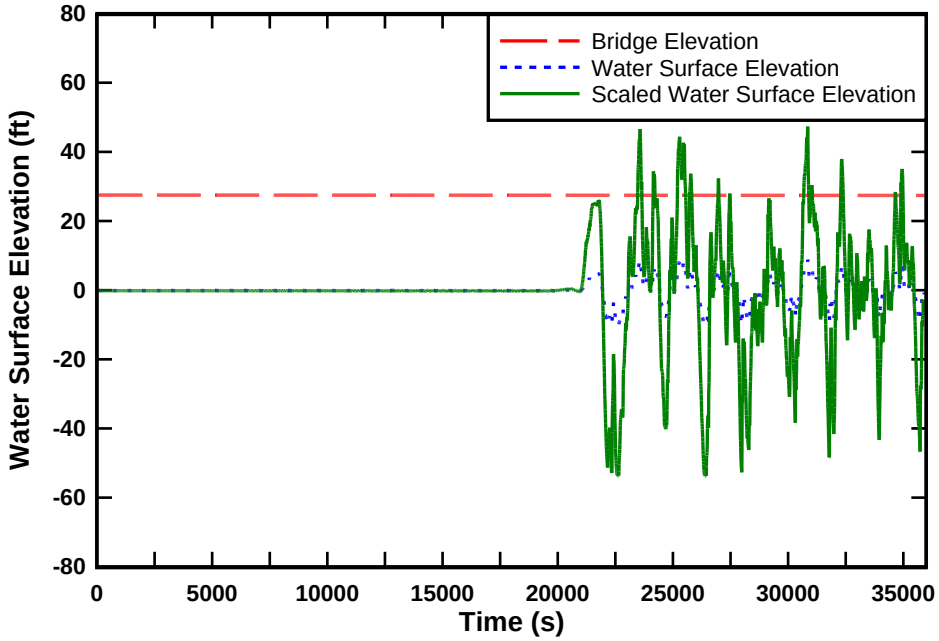

Figure A-44. Scaled tsunami water free-surface elevation compared to Agua Hedionda Lagoon Bridge elevation, water free-surface elevation 20 ft above bridge.

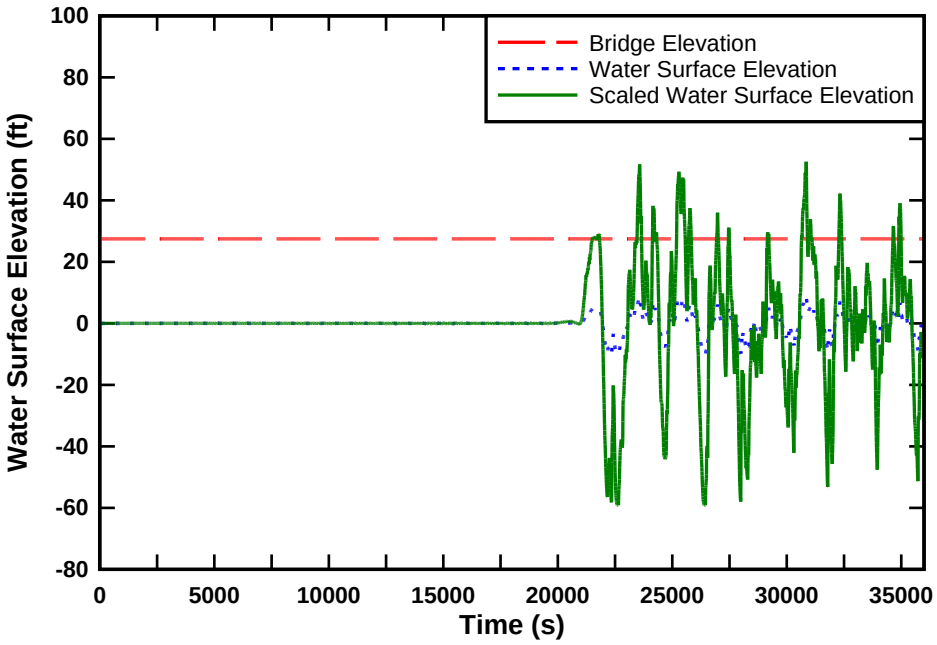

Figure A-45. Scaled tsunami water free-surface elevation compared to Agua Hedionda Lagoon Bridge elevation, water free-surface elevation 25 ft above bridge.

B. Appendix B. Time Histories of Tsunami Horizontal and Vertical Forces and Overturning Moments on Selected Bridges

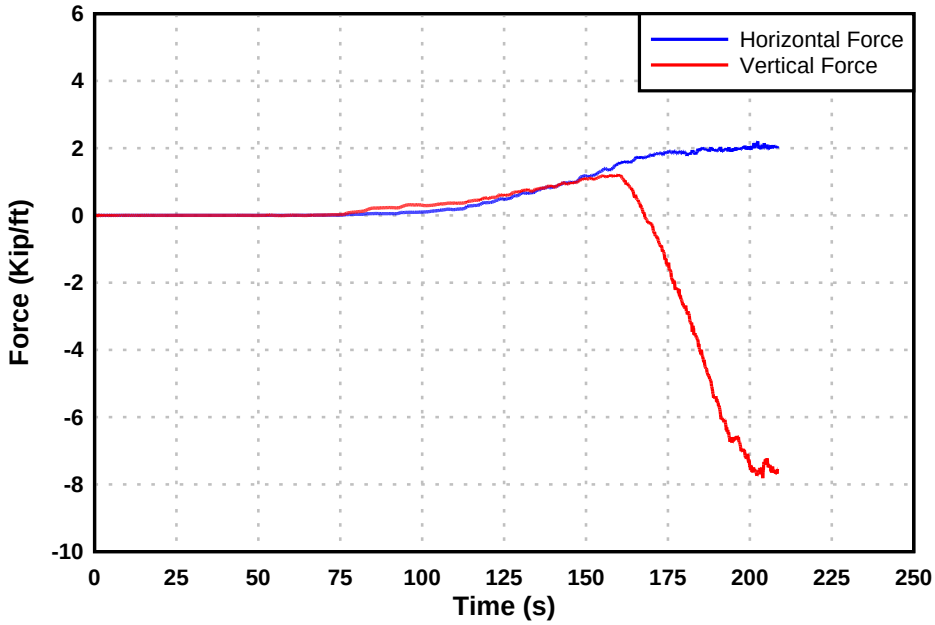

Figure B-1. Tsunami force time history on the Mad River Slough Bridge, Water surface elevation 5 ft above bridge elevation.

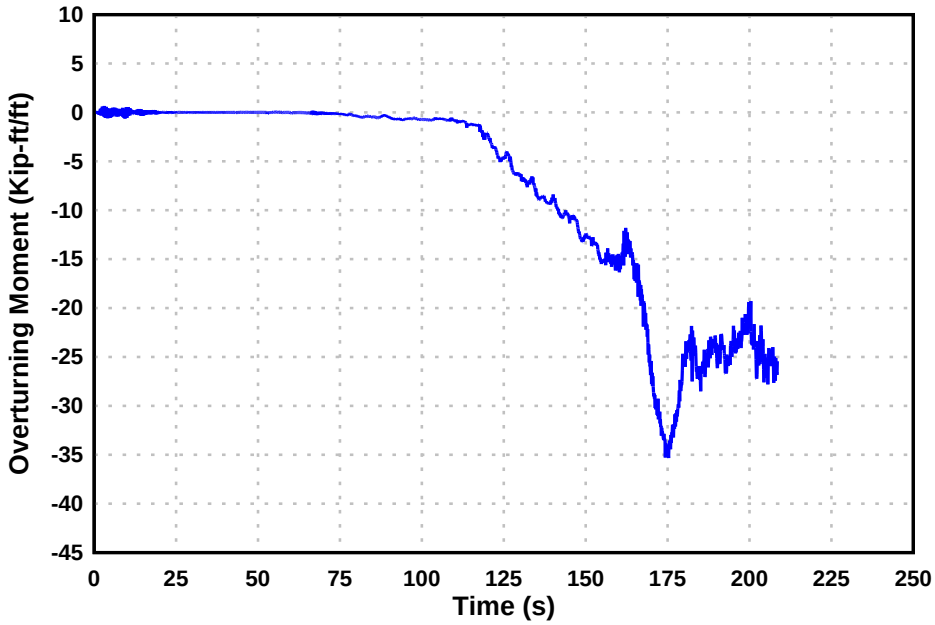

Figure B-2. Tsunami overturning moment time history on the Mad River Slough Bridge, Water surface elevation 5 ft above bridge elevation.

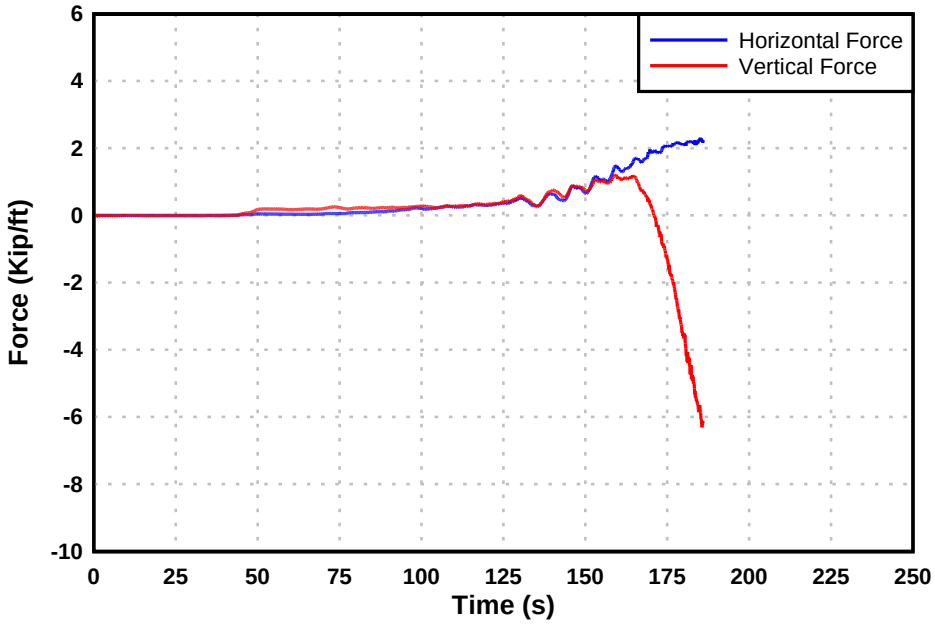

Figure B-3. Tsunami force time history on the Mad River Slough Bridge, Water surface elevation 10 ft above bridge elevation.

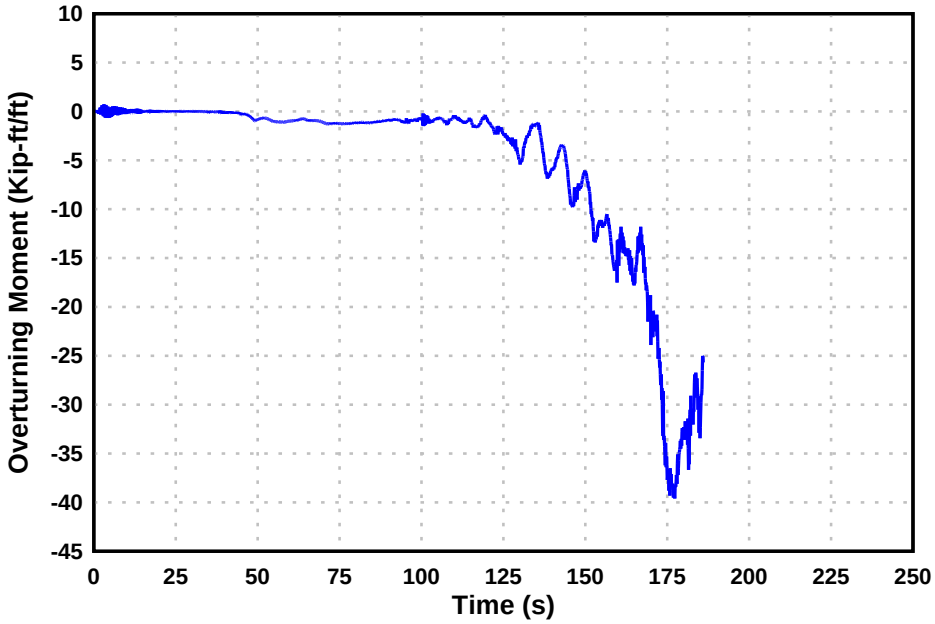

Figure B-4. Tsunami overturning moment time history on the Mad River Slough Bridge, Water surface elevation 10 ft above bridge elevation.

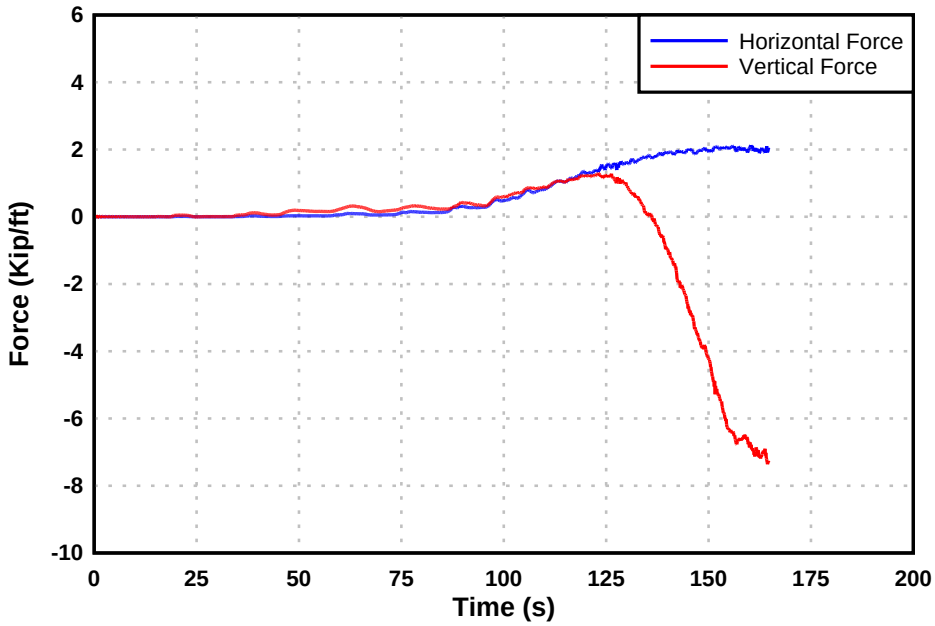

Figure B-5. Tsunami force time history on the Mad River Slough Bridge, Water surface elevation 15 ft above bridge elevation.

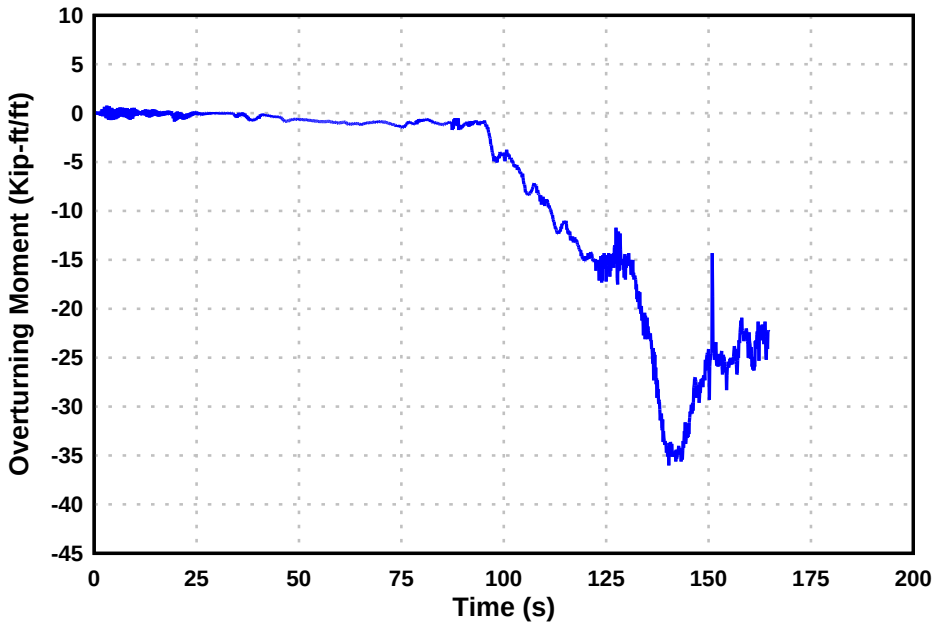

Figure B-6. Tsunami overturning moment time history on the Mad River Slough Bridge, Water surface elevation 15 ft above bridge elevation.

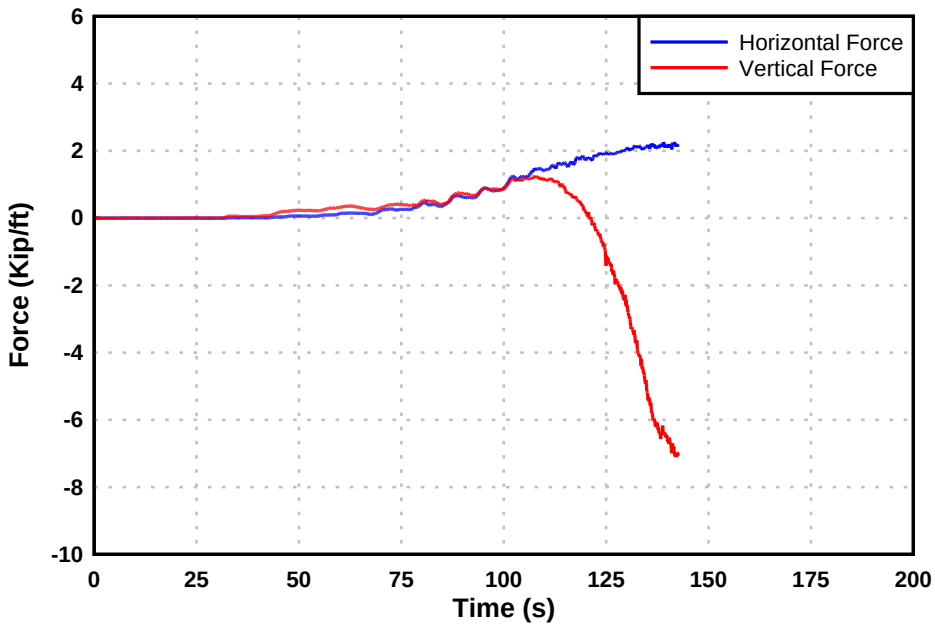

Figure B-7. Tsunami force time history on the Mad River Slough Bridge, Water surface elevation 20 ft above bridge elevation.

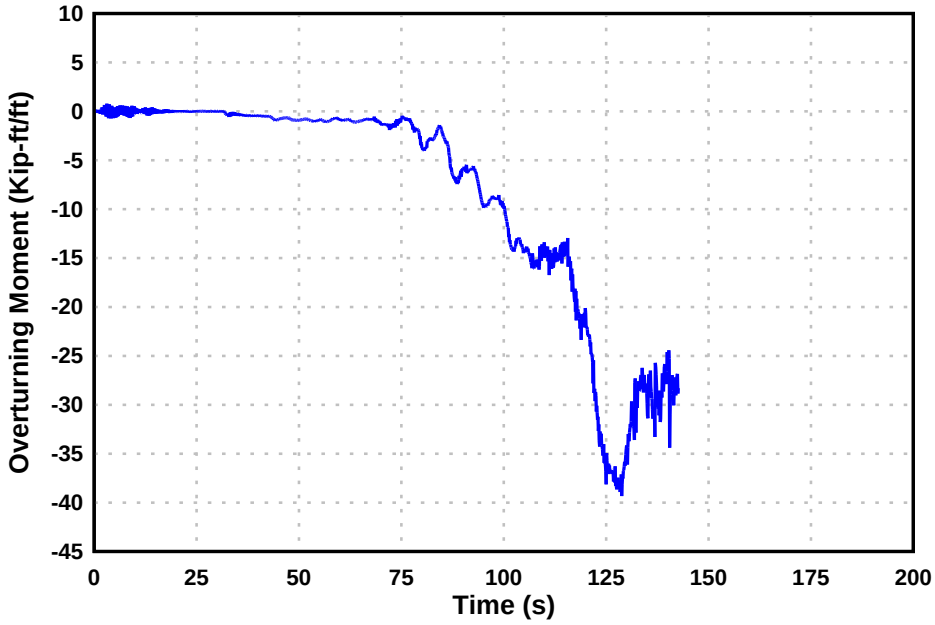

Figure B-8. Tsunami overturning moment time history on the Mad River Slough Bridge, Water surface elevation 20 ft above bridge elevation.

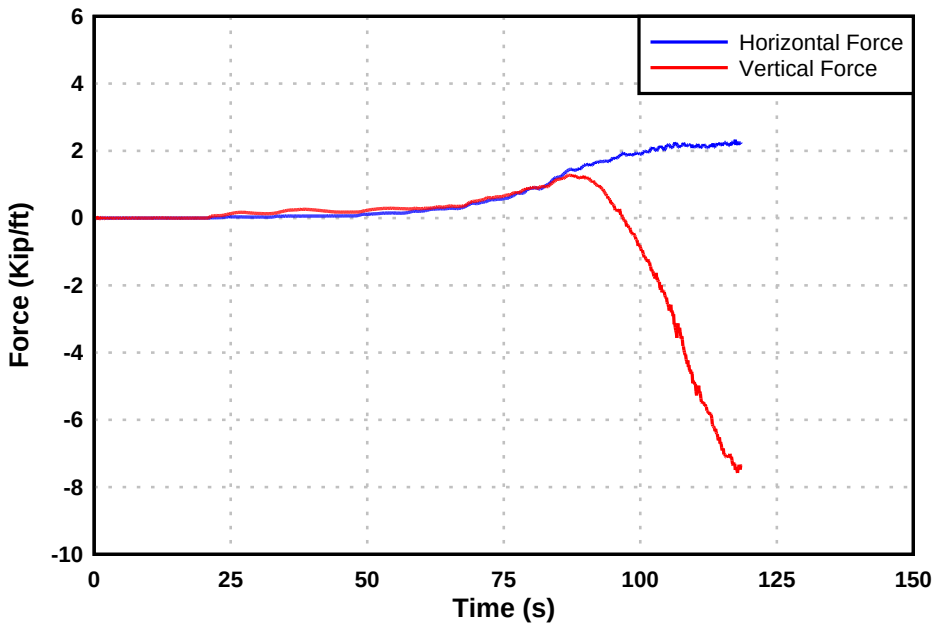

Figure B-9. Tsunami force time history on the Mad River Slough Bridge, Water surface elevation 25 ft above bridge elevation.

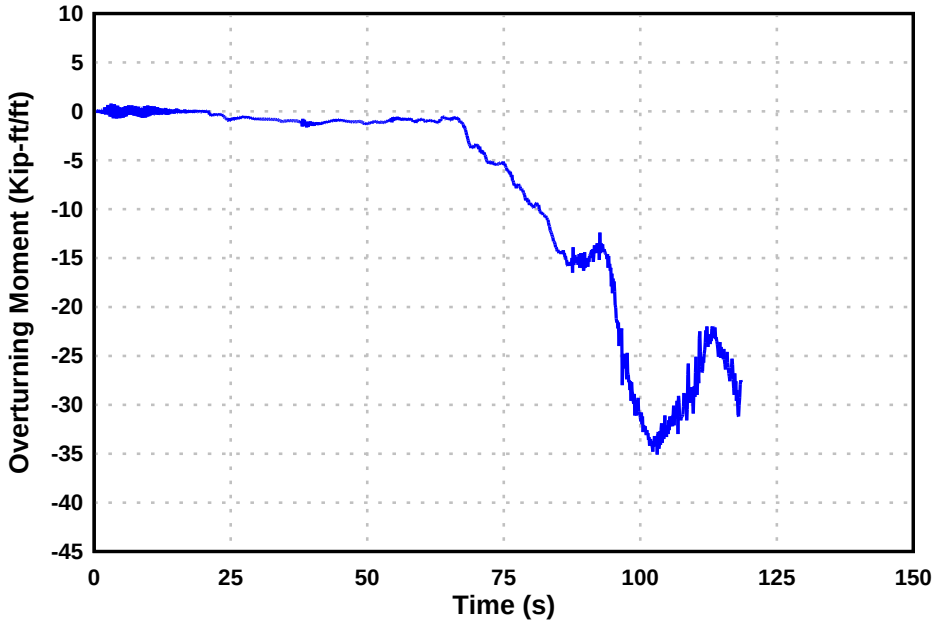

Figure B-10. Tsunami overturning moment time history on the Mad River Slough Bridge, Water surface elevation 25 ft above bridge elevation.

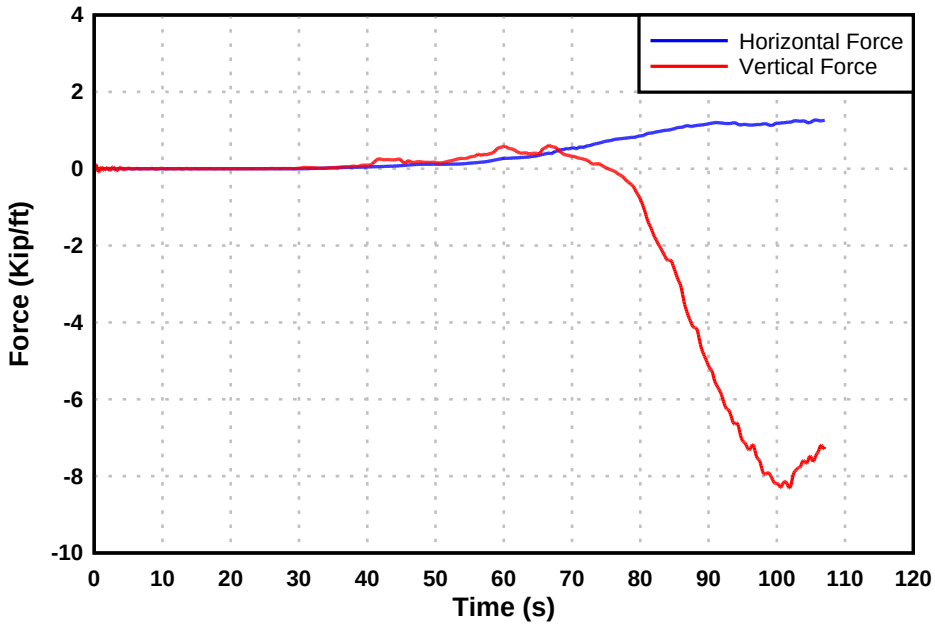

Figure B-11. Tsunami force time history on the Salmon Creek Bridge, Water surface elevation 5 ft above bridge elevation.

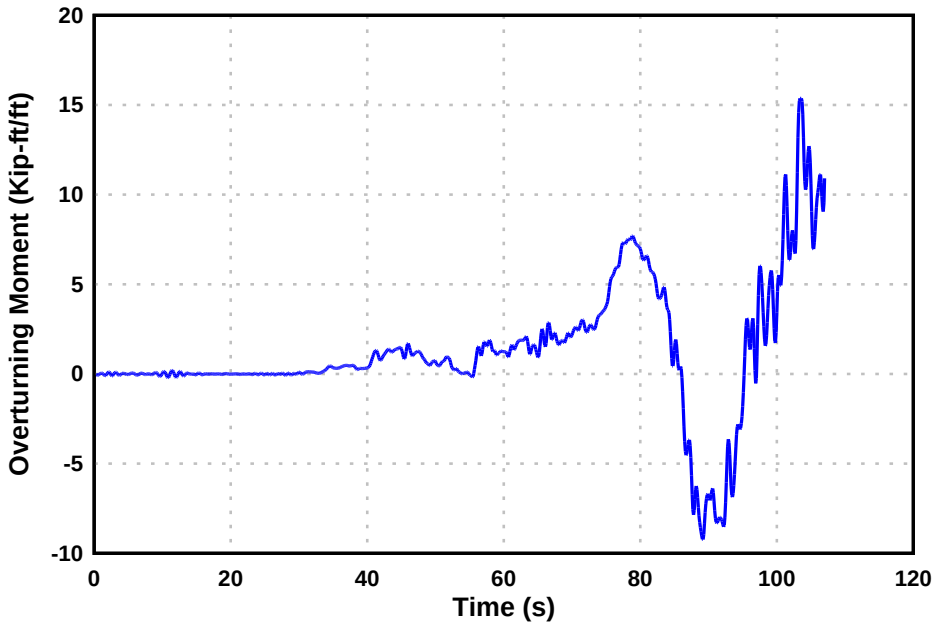

Figure B-12. Tsunami overturning moment time history on the Salmon Creek Bridge, Water surface elevation 5 ft above bridge elevation.

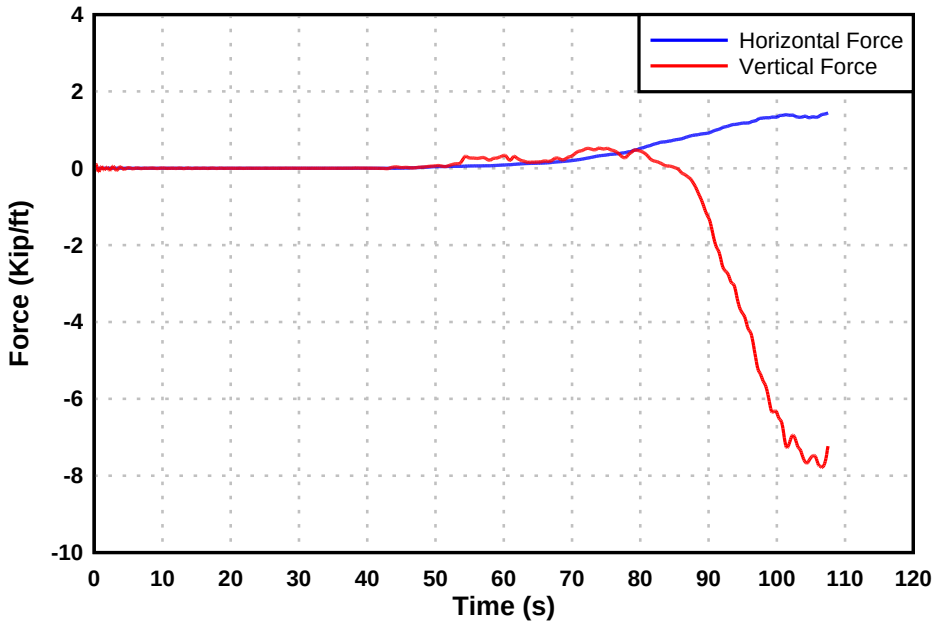

Figure B-13. Tsunami force time history on the Salmon Creek Bridge, Water surface elevation 10 ft above bridge elevation.

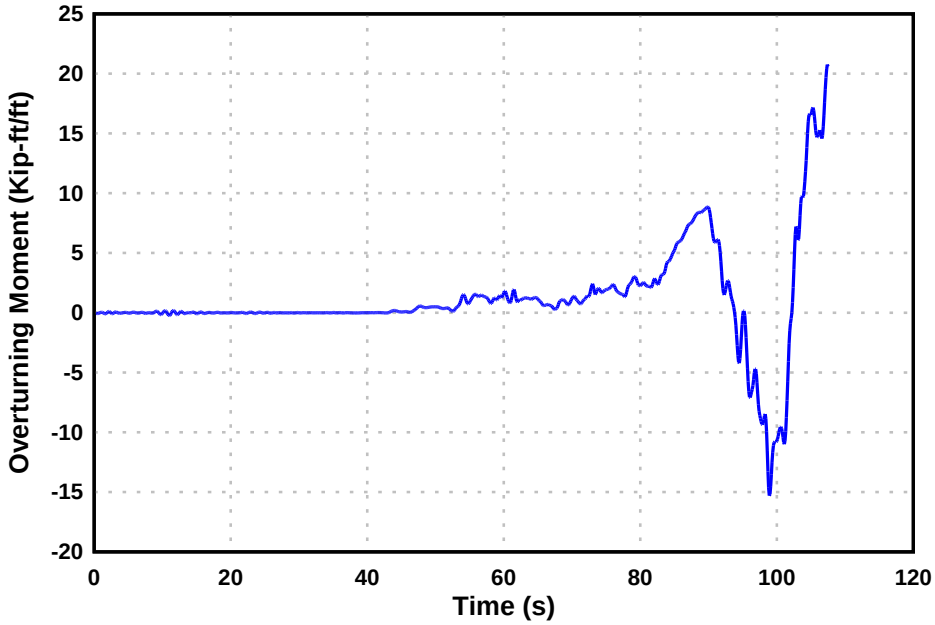

Figure B-14. Tsunami overturning moment time history on the Salmon Creek Bridge, Water surface elevation 10 ft above bridge elevation.

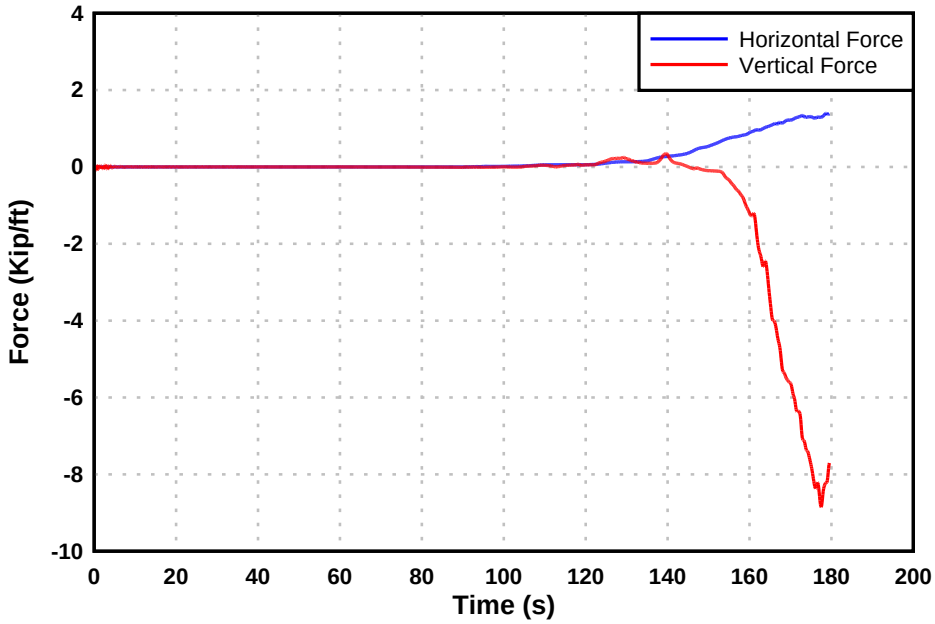

Figure B-15. Tsunami force time history on the Salmon Creek Bridge, Water surface elevation 15 ft above bridge elevation.

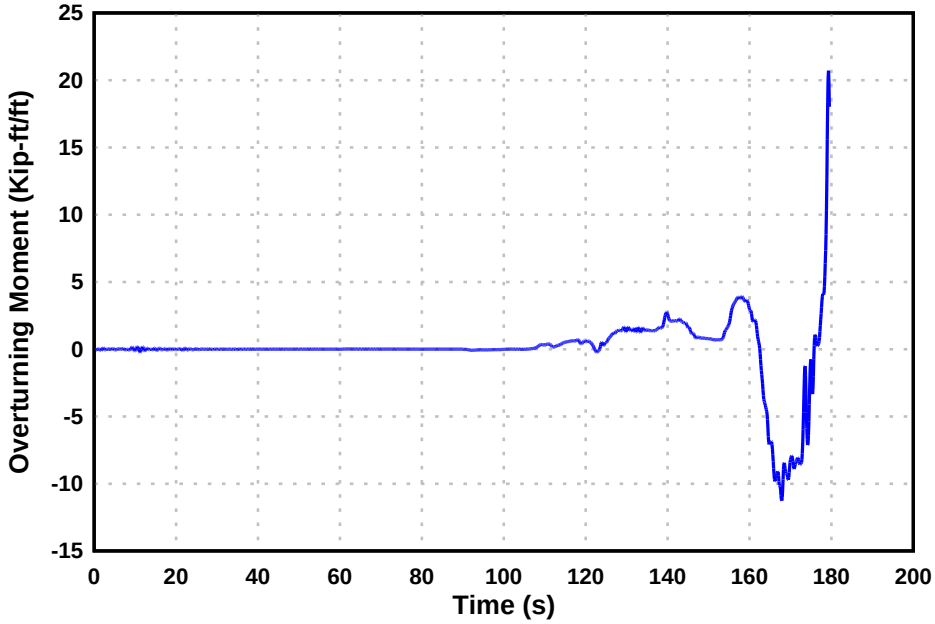

Figure B-16. Tsunami overturning moment time history on the Salmon Creek Bridge, Water surface elevation 15 ft above bridge elevation.

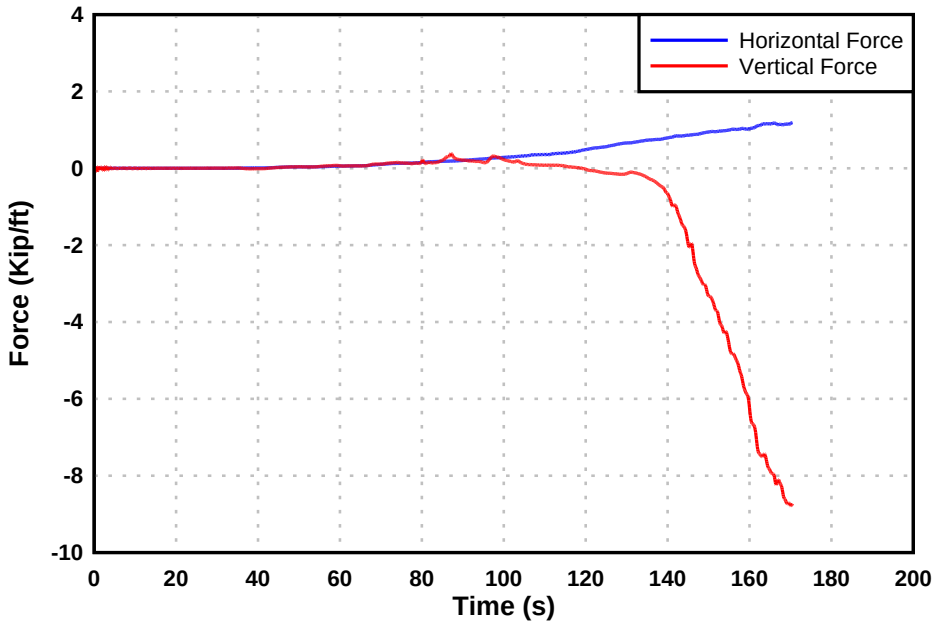

Figure B-17. Tsunami force time history on the Salmon Creek Bridge, Water surface elevation 20 ft above bridge elevation.

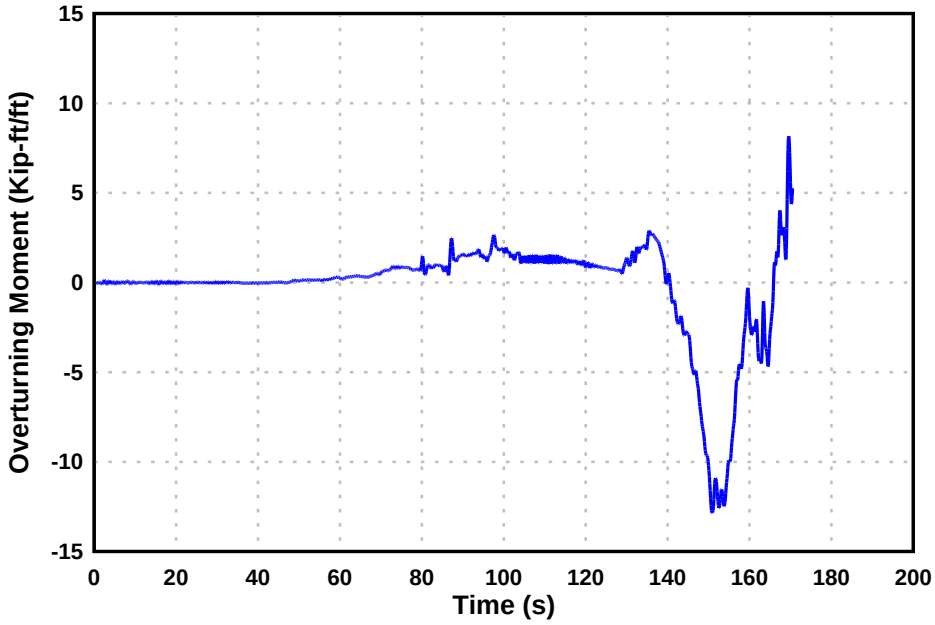

Figure B-18. Tsunami overturning moment time history on the Salmon Creek Bridge, Water surface elevation 20 ft above bridge elevation.

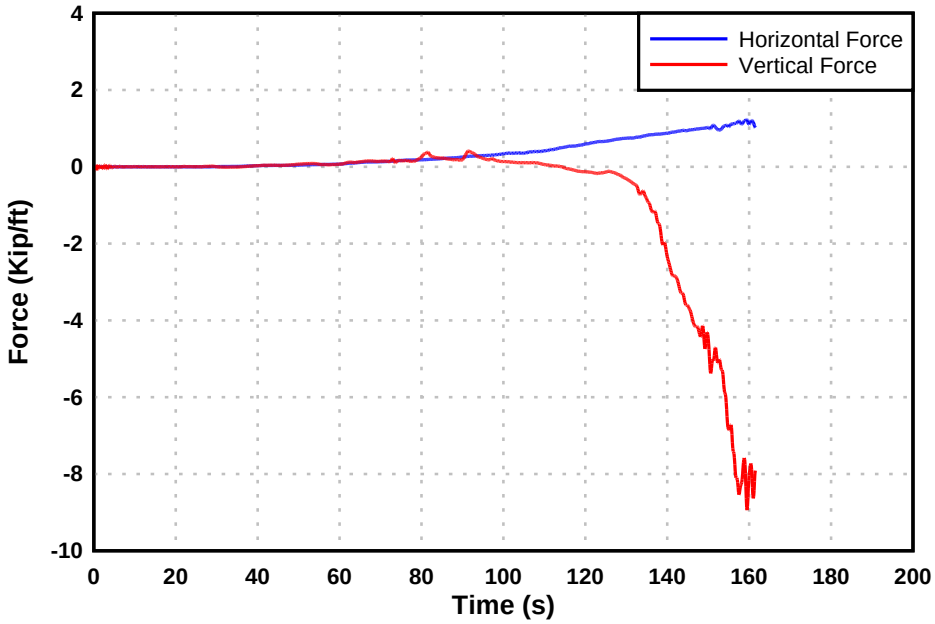

Figure B-19. Tsunami force time history on the Salmon Creek Bridge, Water surface elevation 25 ft above bridge elevation.

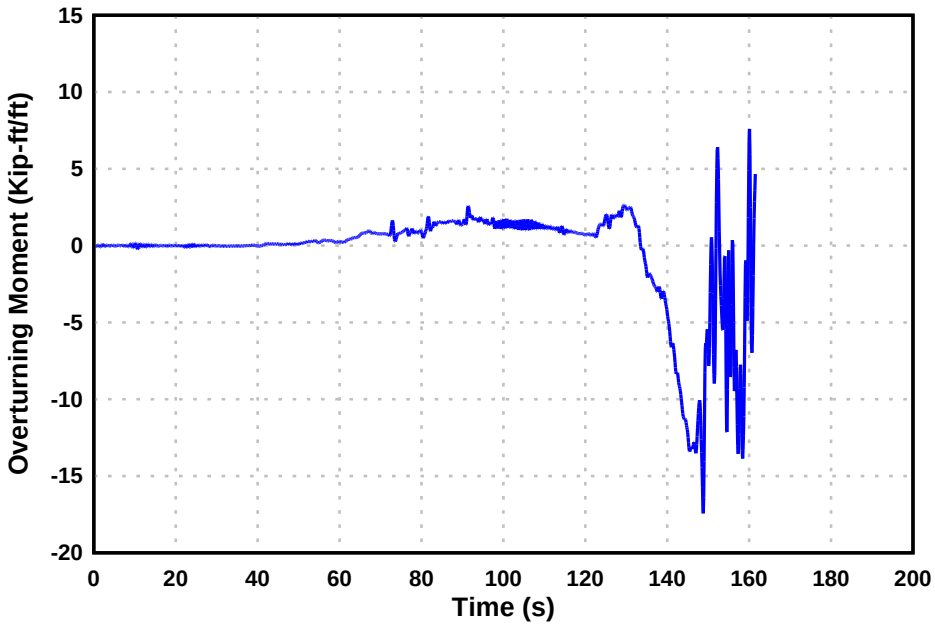

Figure B-20. Tsunami overturning moment time history on the Salmon Creek Bridge, Water surface elevation 25 ft above bridge elevation.

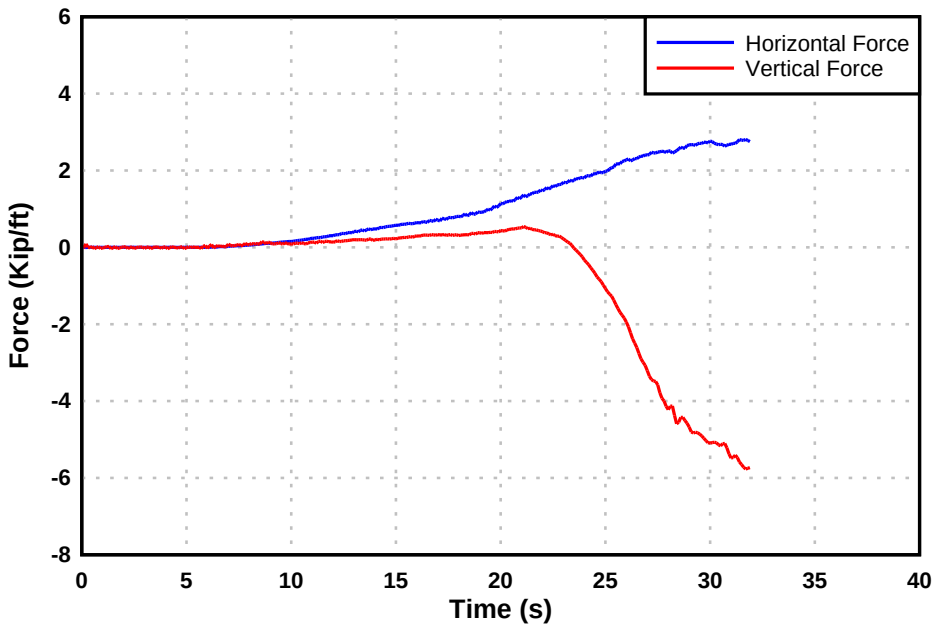

Figure B-21. Tsunami force time history on the Old Creek Bridge, Water surface elevation 5 ft above bridge elevation.

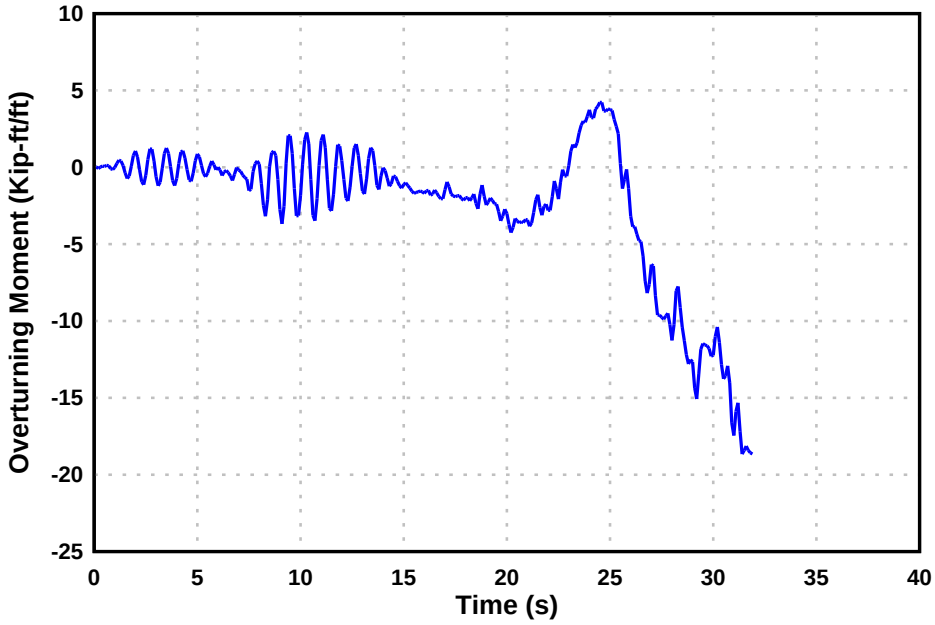

Figure B-22. Tsunami overturning moment time history on the Old Creek Bridge, Water surface elevation 5 ft above bridge elevation.

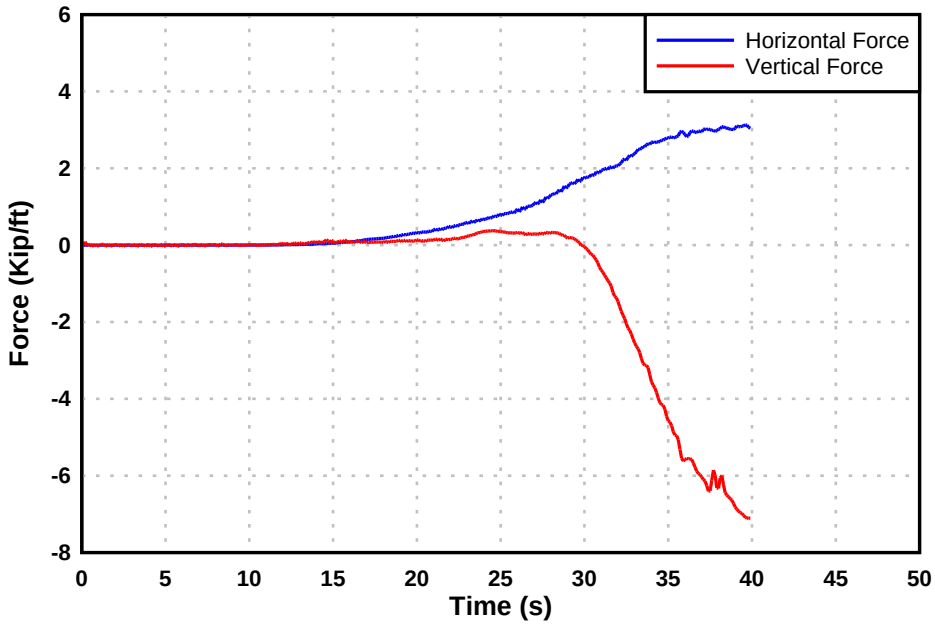

Figure B-23. Tsunami force time history on the Old Creek Bridge, Water surface elevation 10 ft above bridge elevation.

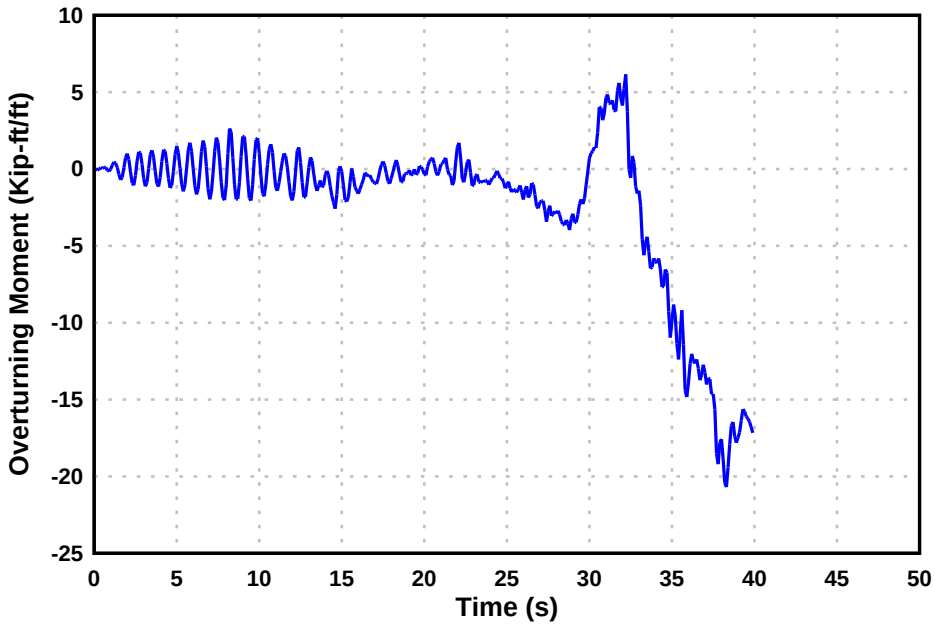

Figure B-24. Tsunami overturning moment time history on the Old Creek Bridge, Water surface elevation 10 ft above bridge elevation.

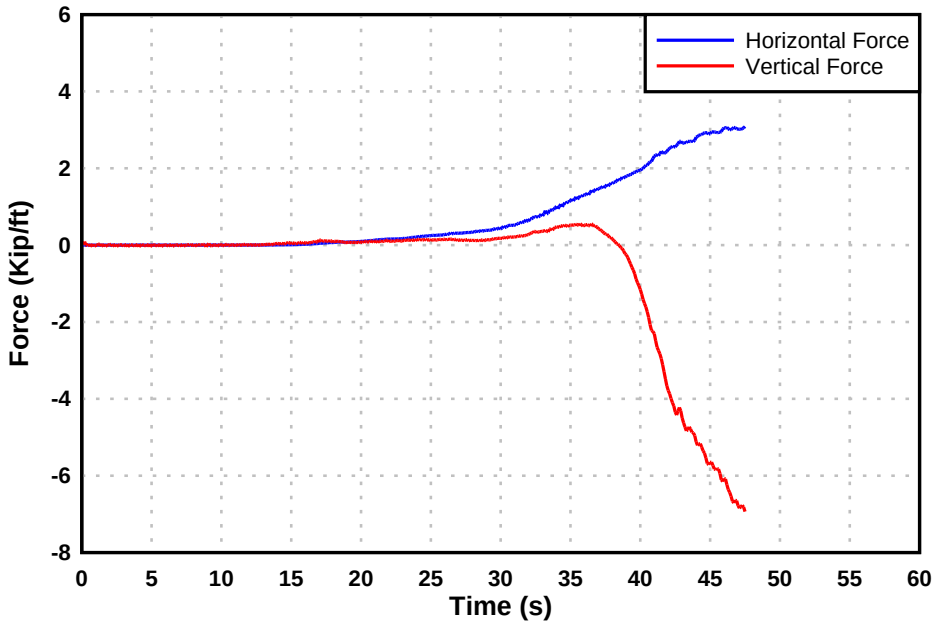

Figure B-25. Tsunami force time history on the Old Creek Bridge, Water surface elevation 15 ft above bridge elevation.

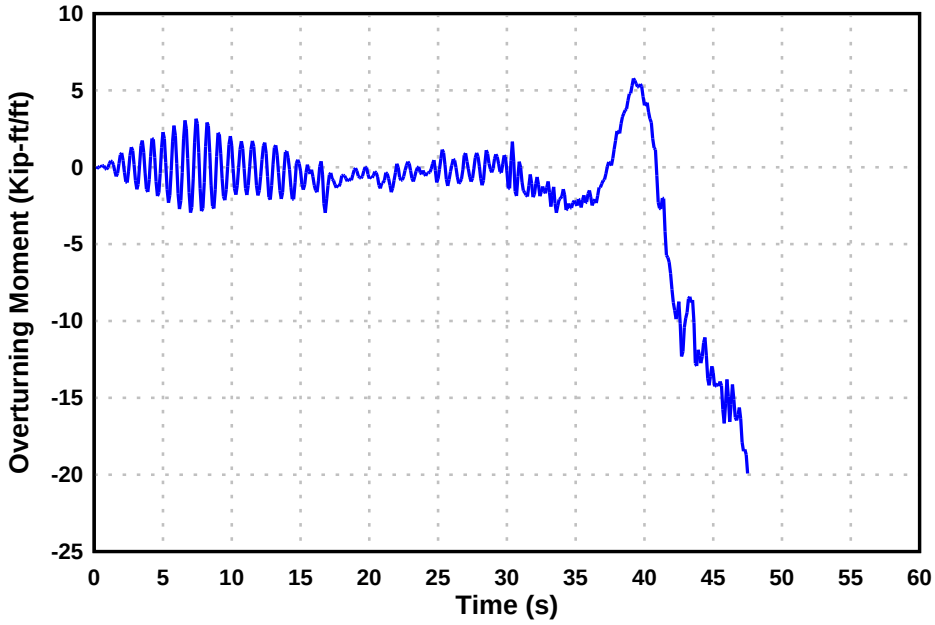

Figure B-26. Tsunami overturning moment time history on the Old Creek Bridge, Water surface elevation 15 ft above bridge elevation.

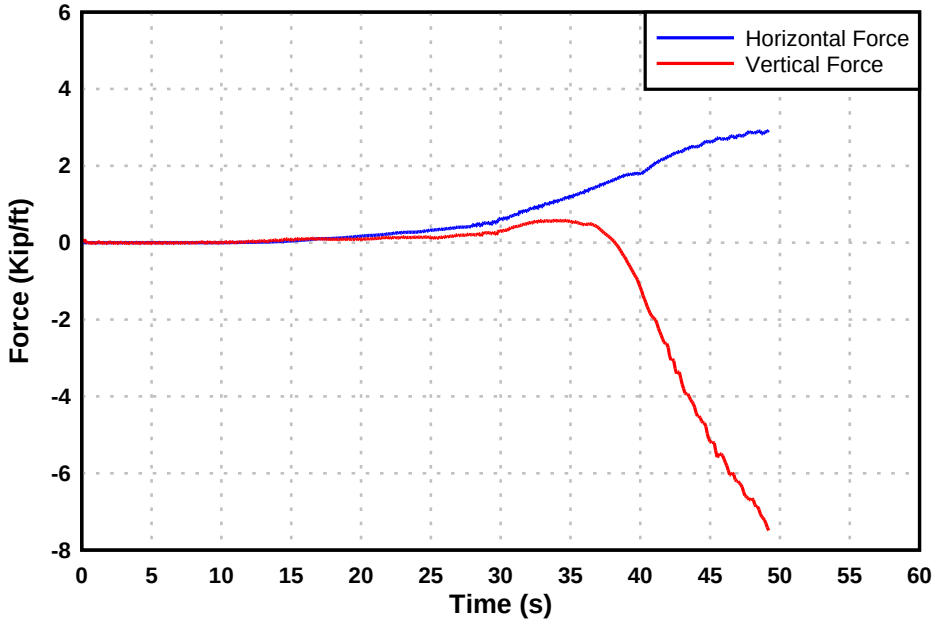

Figure B-27. Tsunami force time history on the Old Creek Bridge, Water surface elevation 20 ft above bridge elevation.

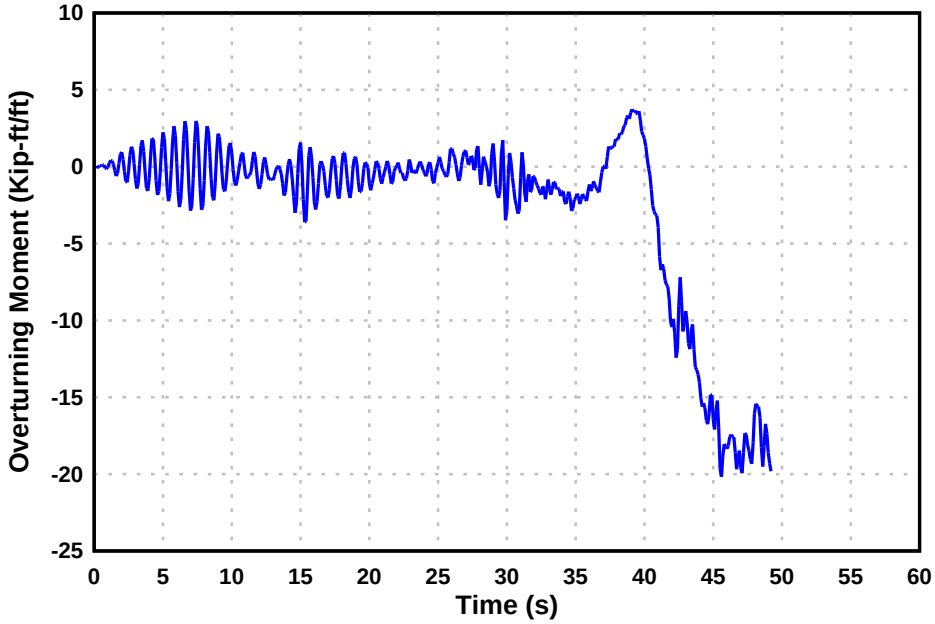

Figure B-28. Tsunami overturning moment time history on the Old Creek Bridge, Water surface elevation 20 ft above bridge elevation.

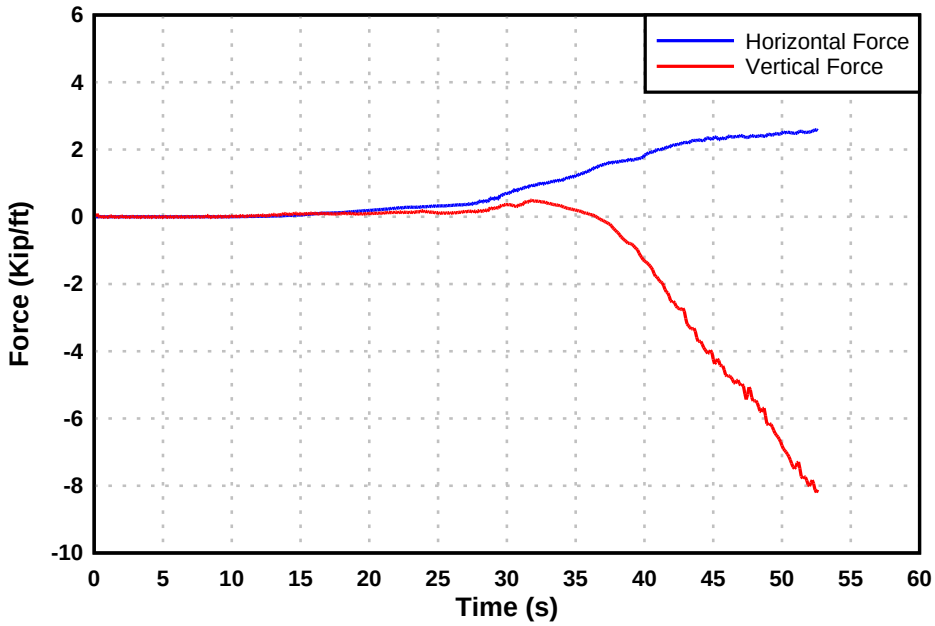

Figure B-29. Tsunami force time history on the Old Creek Bridge, Water surface elevation 25 ft above bridge elevation.

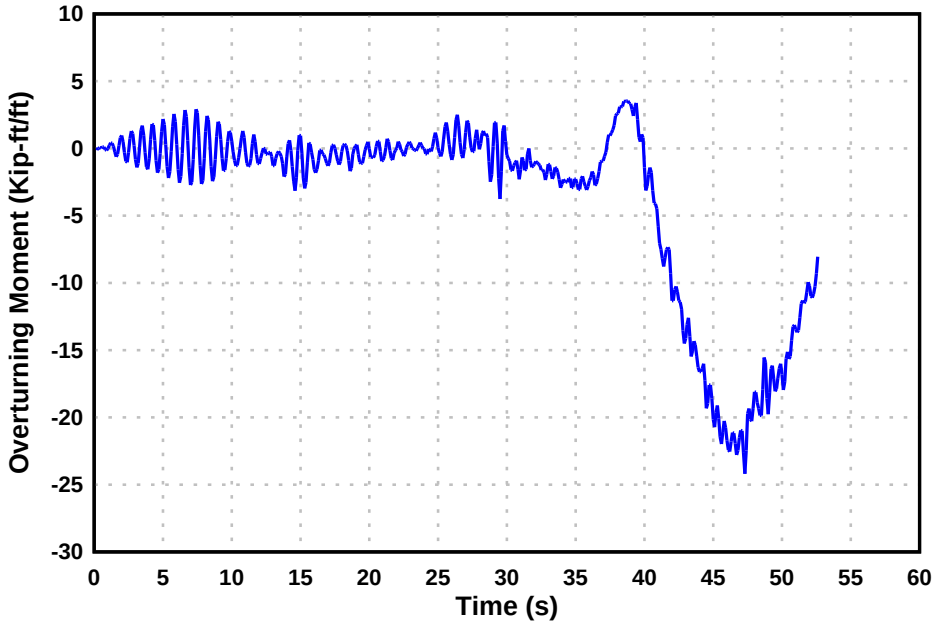

Figure B-30. Tsunami overturning moment time history on the Old Creek Bridge, Water surface elevation 25 ft above bridge elevation.

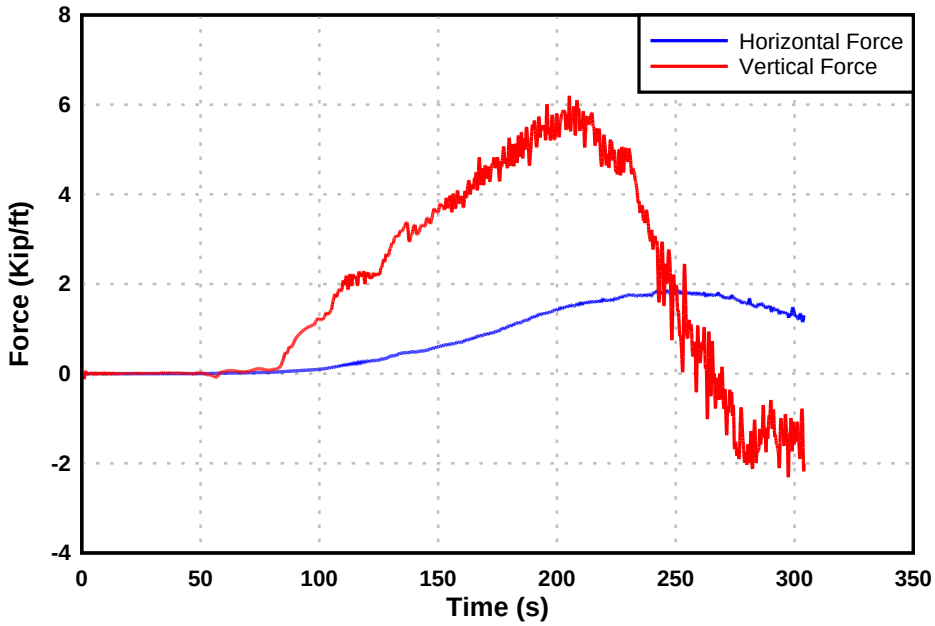

Figure B-31. Tsunami force time history on the Malibu Lagoon Bridge, Water surface elevation 5 ft above bridge elevation.

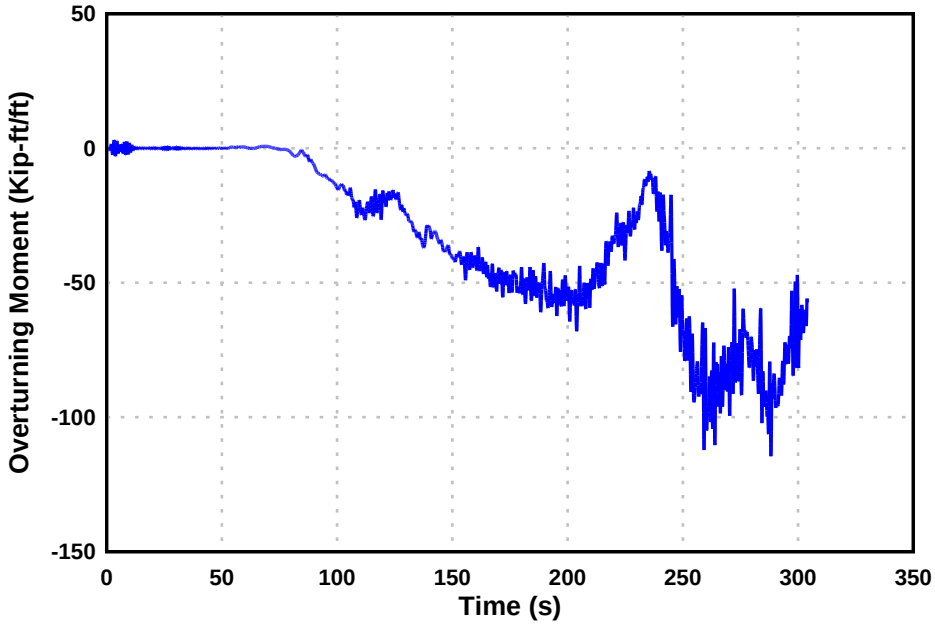

Figure B-32. Tsunami overturning moment time history on the Malibu Lagoon Bridge, Water surface elevation 5 ft above bridge elevation.

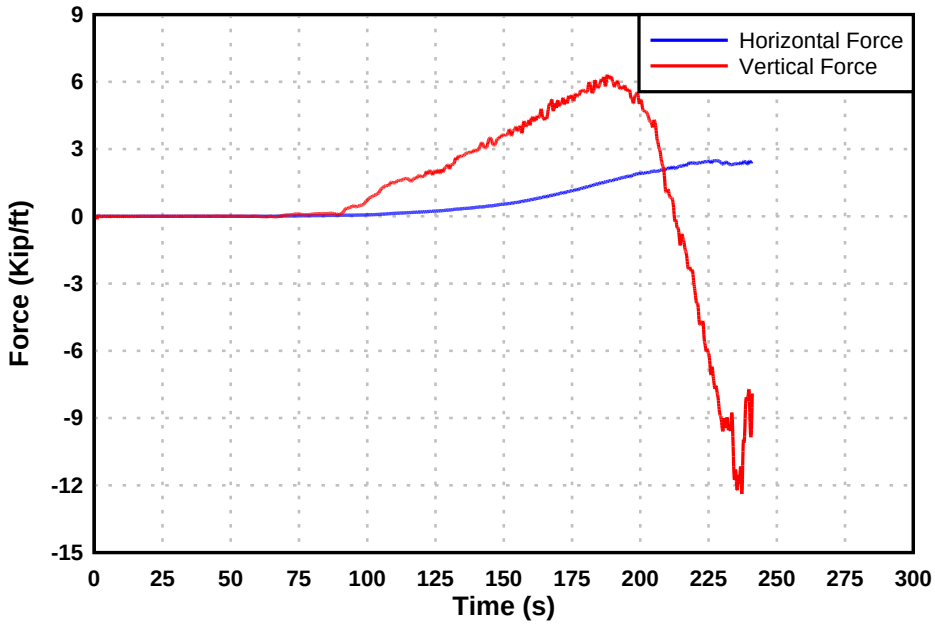

Figure B-33. Tsunami force time history on the Malibu Lagoon Bridge, Water surface elevation 10 ft above bridge elevation.

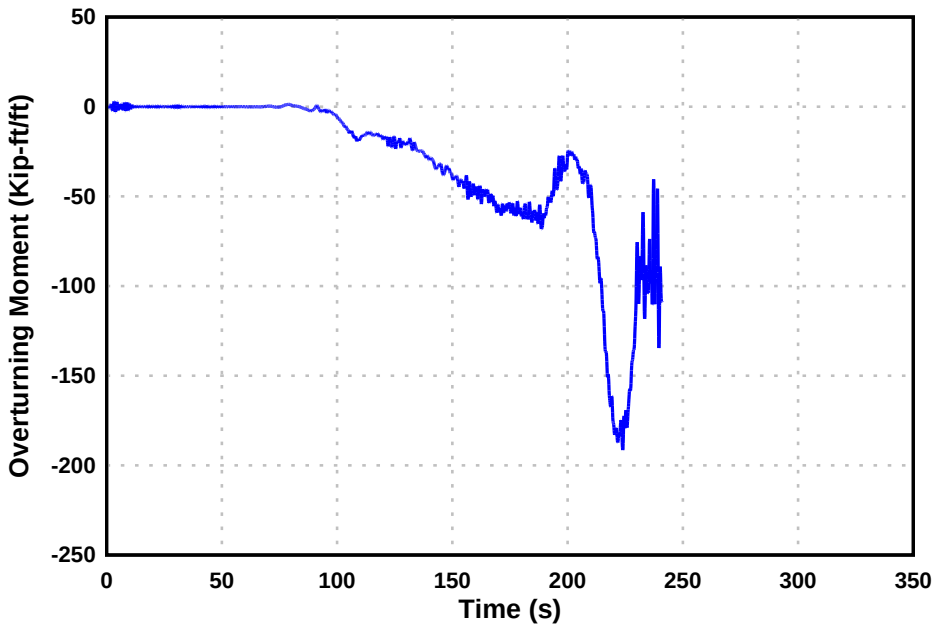

Figure B-34. Tsunami overturning moment time history on the Malibu Lagoon Bridge, Water surface elevation 10 ft above bridge elevation.

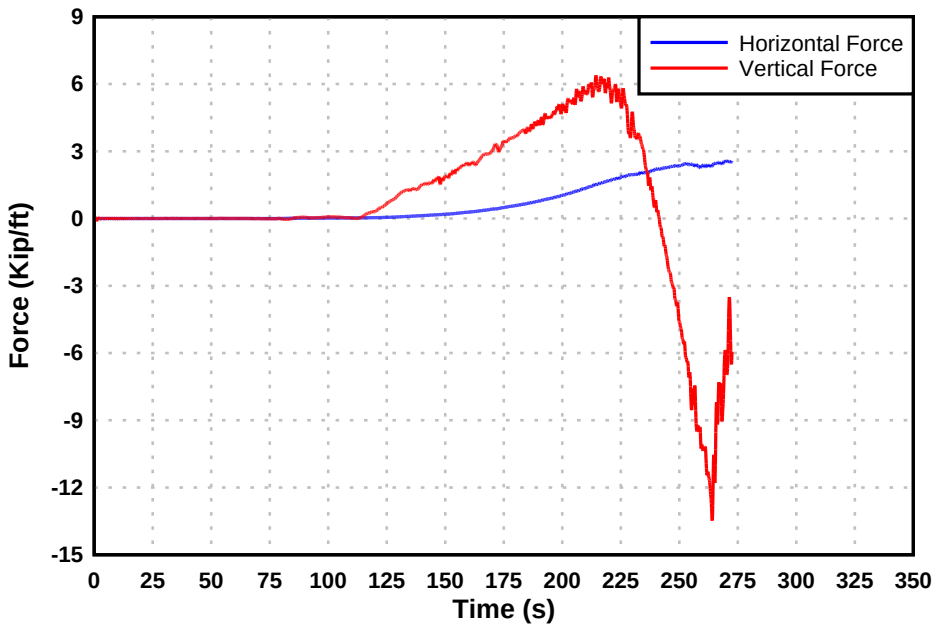

Figure B-35. Tsunami force time history on the Malibu Lagoon Bridge, Water surface elevation 15 ft above bridge elevation.

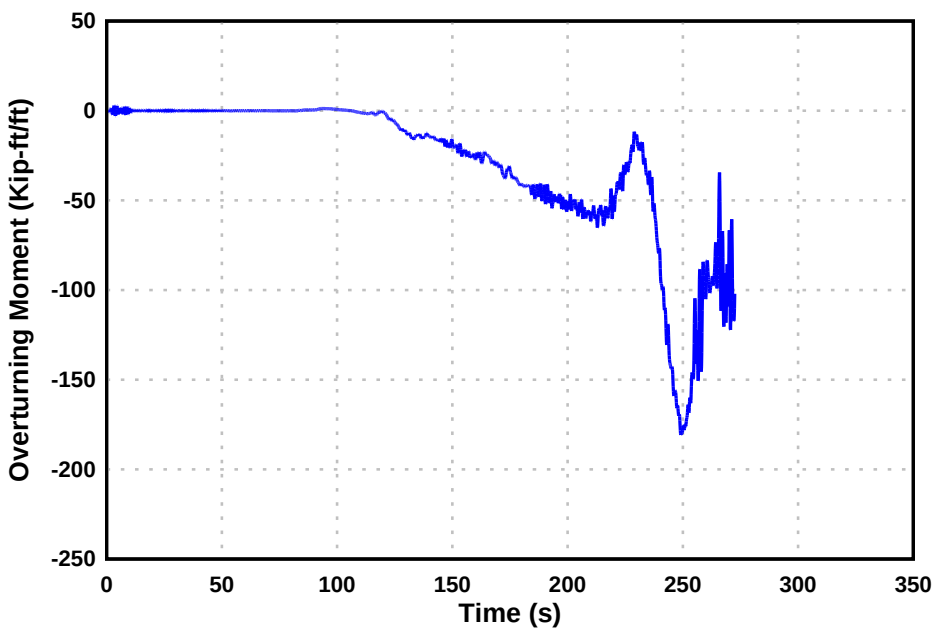

Figure B-36. Tsunami overturning moment time history on the Malibu Lagoon Bridge, Water surface elevation 15 ft above bridge elevation.

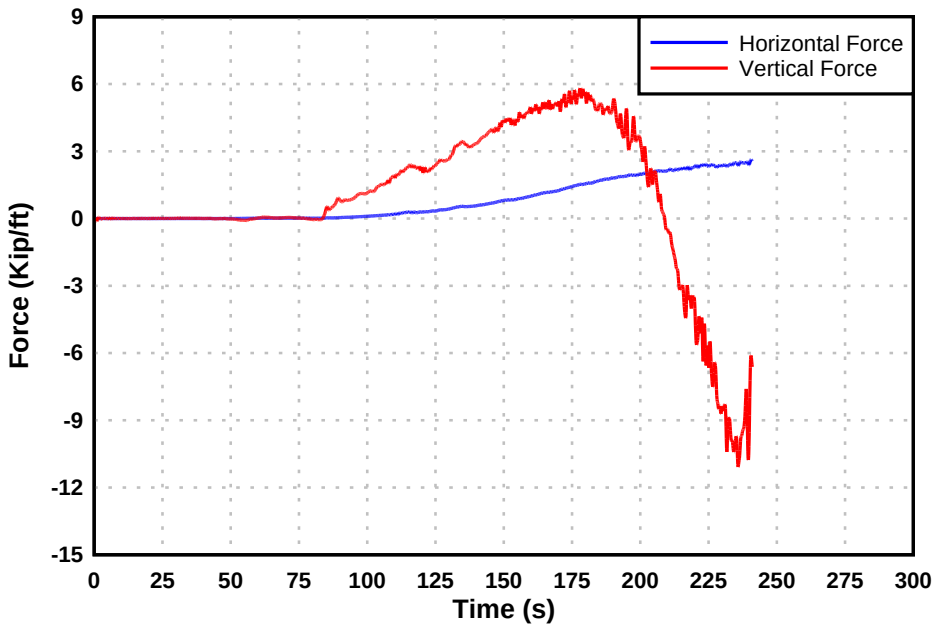

Figure B-37. Tsunami force time history on the Malibu Lagoon Bridge, Water surface elevation 20 ft above bridge elevation.

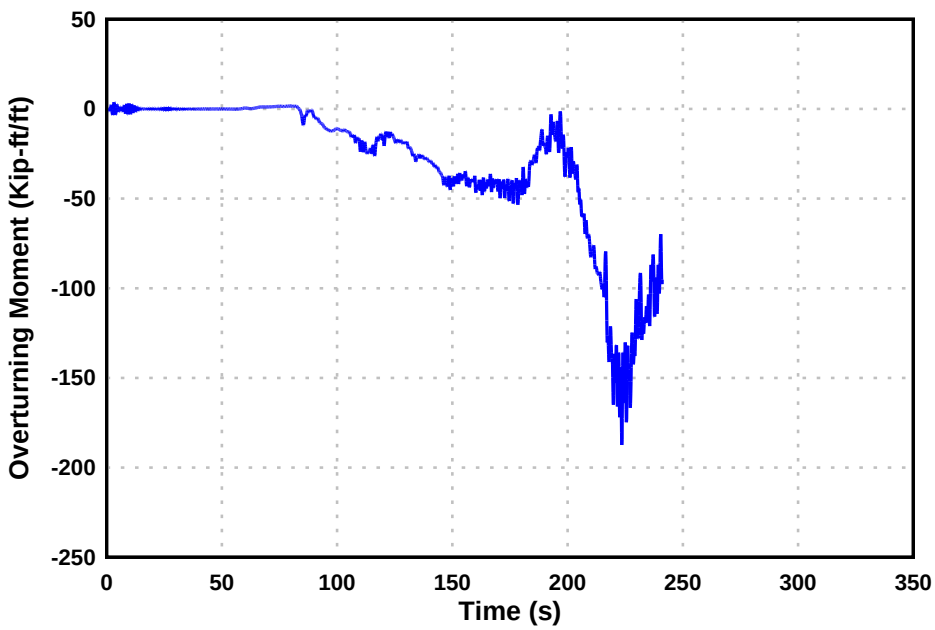

Figure B-38. Tsunami overturning moment time history on the Malibu Lagoon Bridge, Water surface elevation 20 ft above bridge elevation.

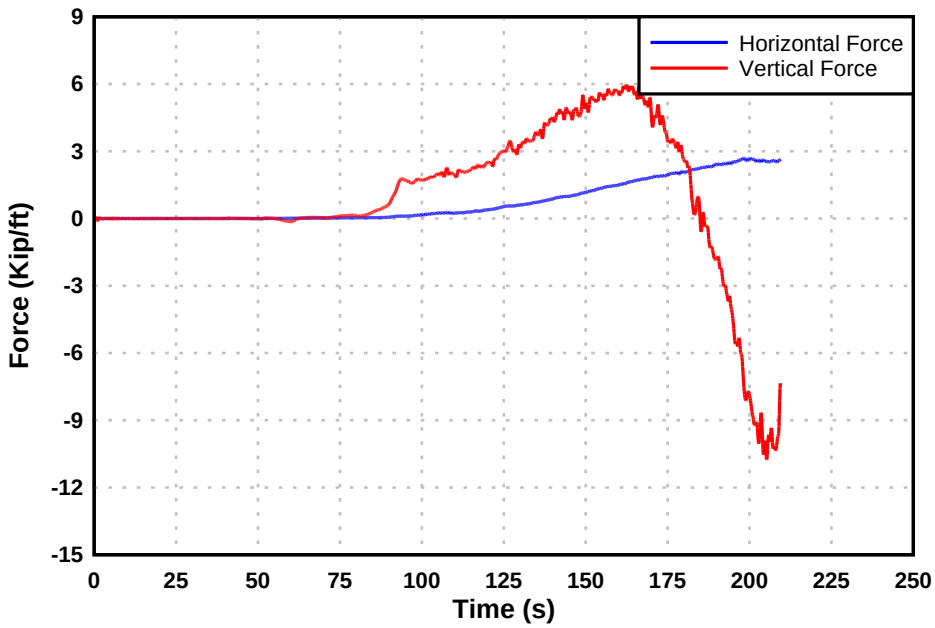

Figure B-39. Tsunami force time history on the Malibu Lagoon Bridge, Water surface elevation 25 ft above bridge elevation.

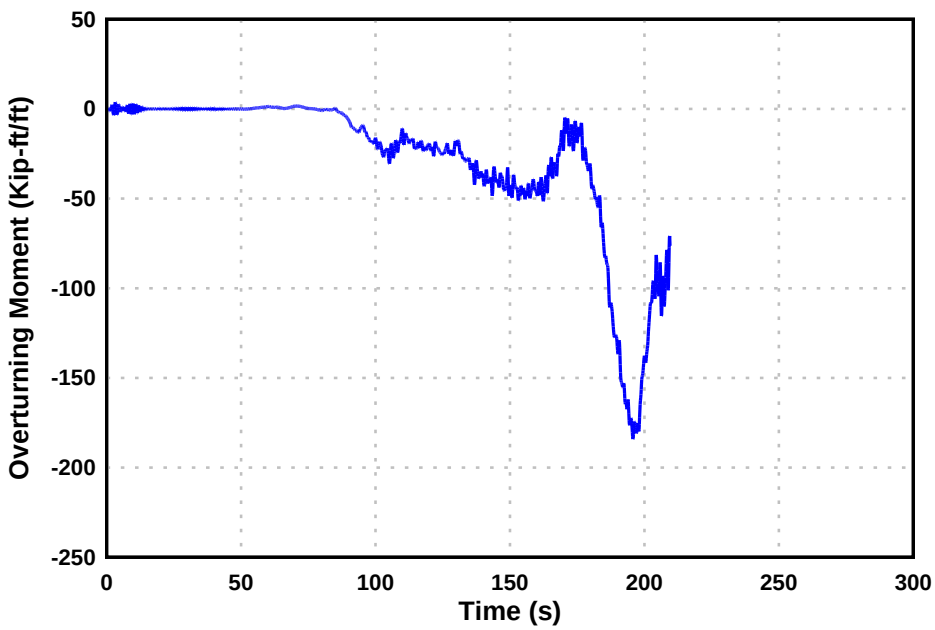

Figure B-40. Tsunami overturning moment time history on the Malibu Lagoon Bridge, Water surface elevation 25 ft above bridge elevation.

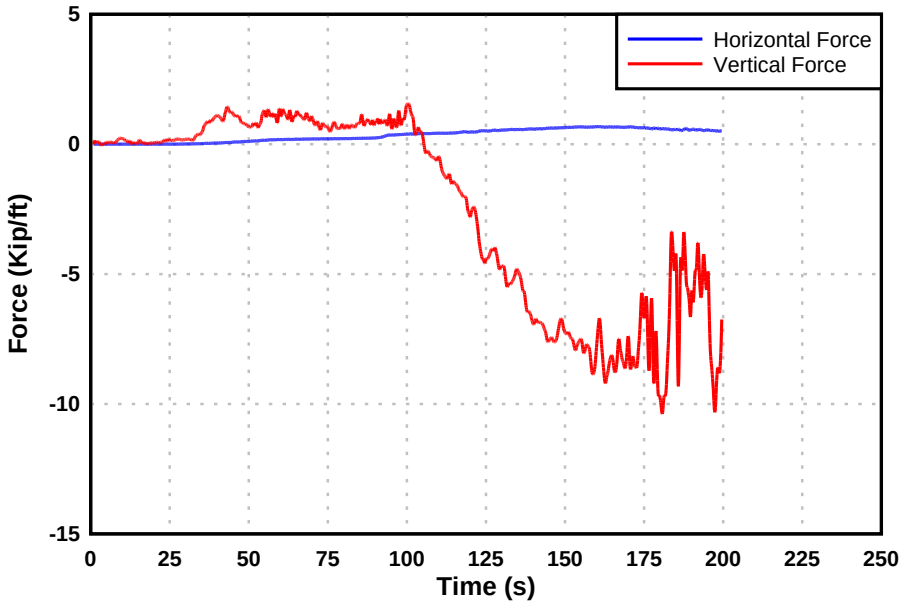

Figure B-41. Tsunami force time history on the Agua Hedionda Lagoon Bridge, Water surface elevation 5 ft above bridge elevation.

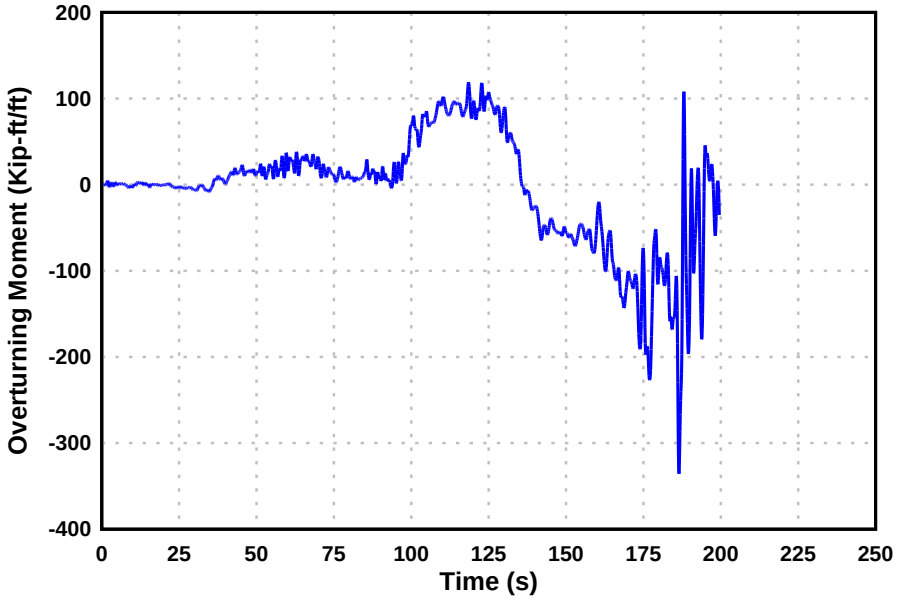

Figure B-42. Tsunami overturning moment time history on the Agua Hedionda Lagoon Bridge, Water surface elevation 5 ft above bridge elevation.

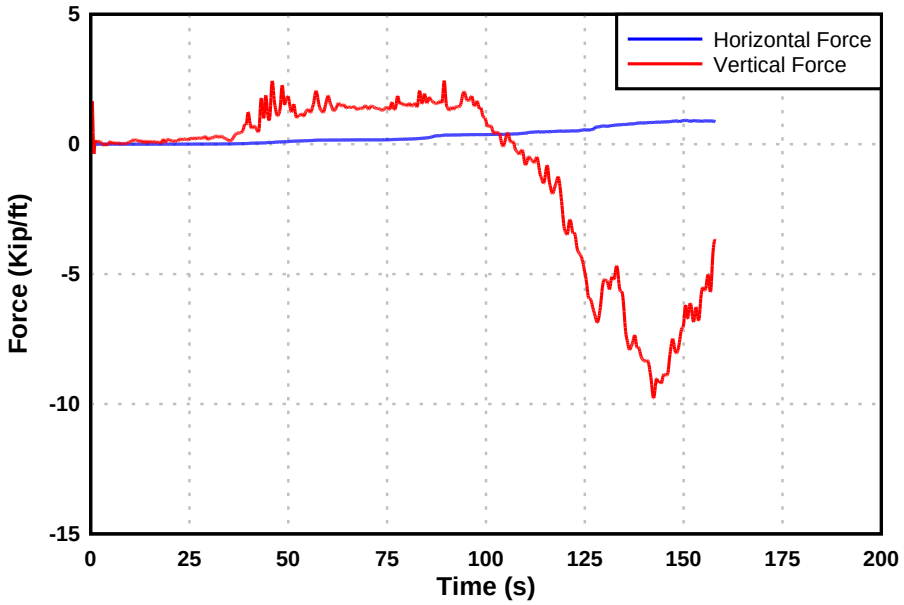

Figure B-43. Tsunami force time history on the Agua Hedionda Lagoon Bridge, Water surface elevation 10 ft above bridge elevation.

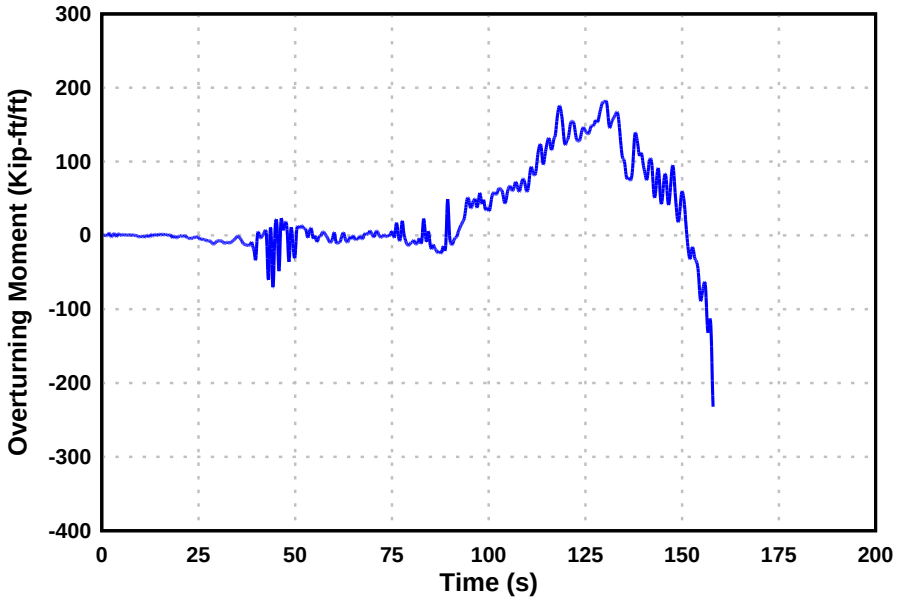

Figure B-44. Tsunami overturning moment time history on the Agua Hedionda Lagoon Bridge, Water surface elevation 10 ft above bridge elevation.

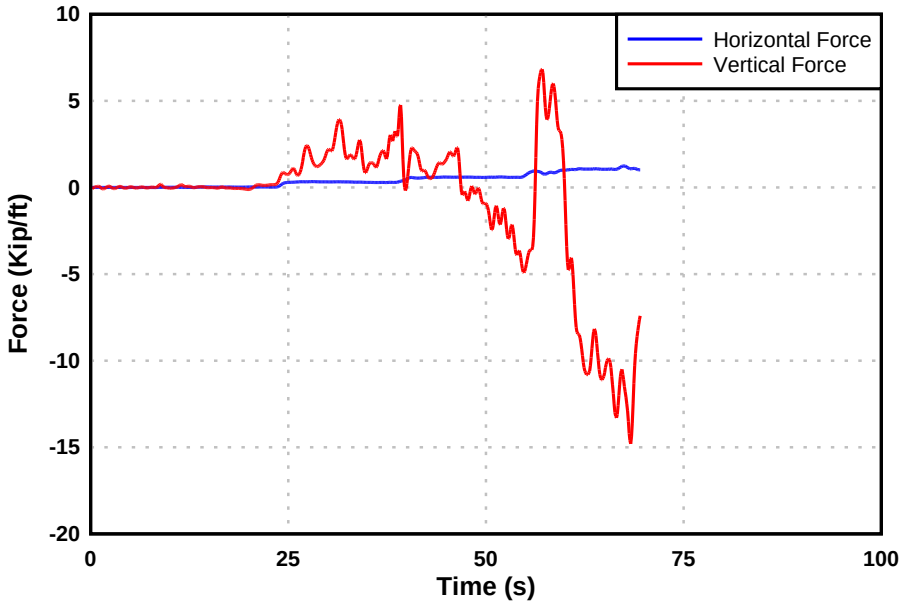

Figure B-45. Tsunami force time history on the Agua Hedionda Lagoon Bridge, Water surface elevation 15 ft above bridge elevation.

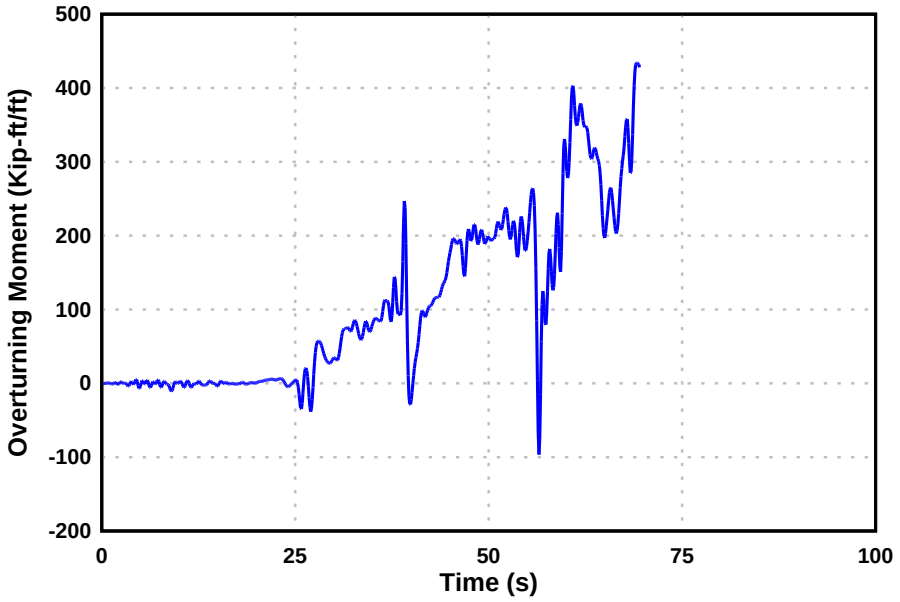

Figure B-46. Tsunami overturning moment time history on the Agua Hedionda Lagoon Bridge, Water surface elevation 15 ft above bridge elevation.

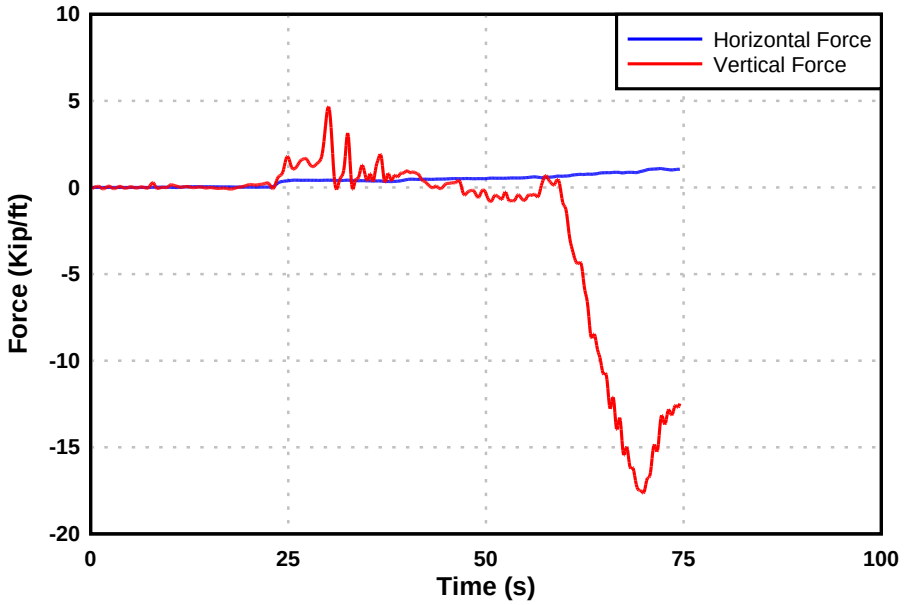

Figure B-47. Tsunami force time history on the Agua Hedionda Lagoon Bridge, Water surface elevation 20 ft above bridge elevation.

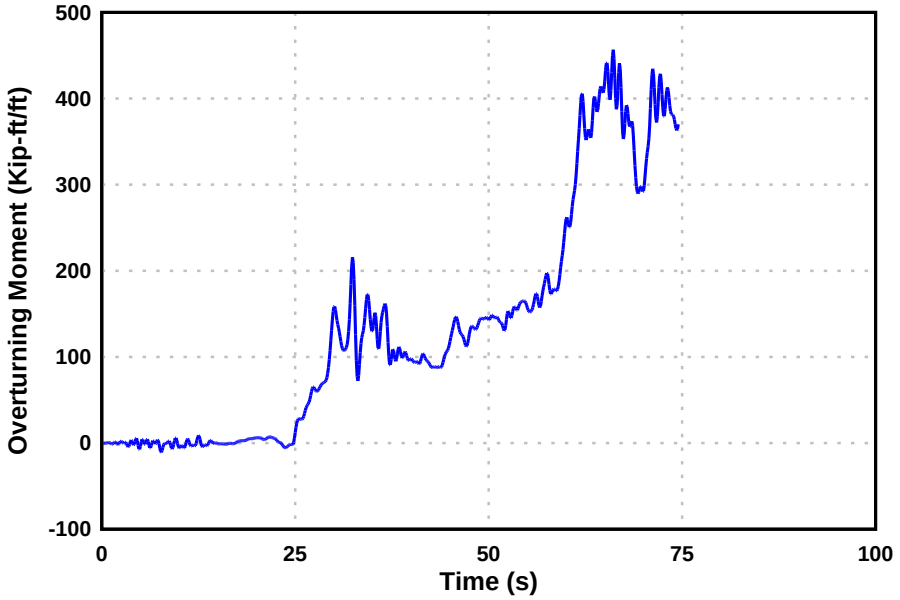

Figure B-48. Tsunami overturning moment time history on the Agua Hedionda Lagoon Bridge, Water surface elevation 20 ft above bridge elevation.

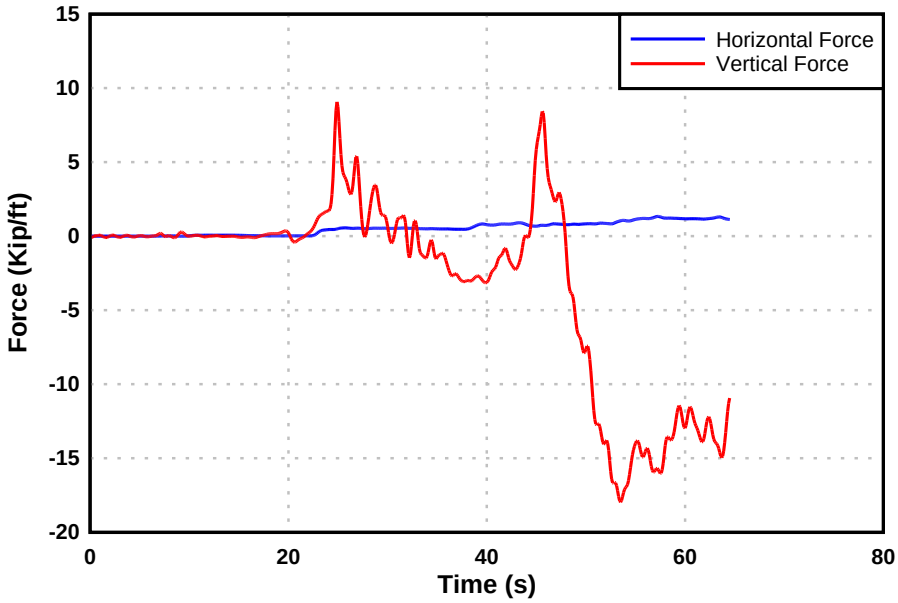

Figure B-49. Tsunami force time history on the Agua Hedionda Lagoon Bridge, Water surface elevation 25 ft above bridge elevation.

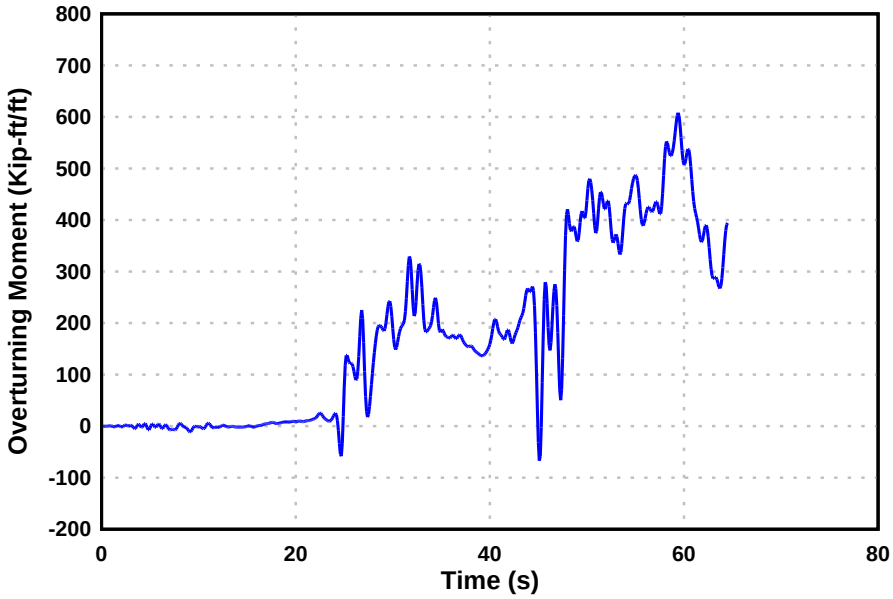

Figure B-50. Tsunami overturning moment time history on the Agua Hedionda Lagoon Bridge, Water surface elevation 25 ft above bridge elevation.

Table B-1. Tsunami Forces and Moments on Mad River Slough Bridge

Tsunami Scenario (Water free-surface elevation/time period)	Horizontal Force (Kip/ft)	Vertical Downward Force (Kip/ft)	Uplift Force (Kip/ft)	Positive Overturning Moment (Kip-ft/ft)	Negative Overturning Moment (Kip-ft/ft)
5-I	2.21	-7.82	1.22	0.66	-35.34
5-V	1.13	-0.05			-4.42
5-HV-HV^2	1.02		2.13		-7.32
10-I	2.32	-6.29	1.22	0.74	-39.59
10-V	1.37		0.75		-2.97
10-HV-HV^2	1.10		3.65		-7.01
15-I	2.13	-7.36	1.30	0.77	-35.97
15-V	1.35		4.44		-15.82
15-HV-HV^2	1.13		5.51		-9.86
20-I	2.26	-7.10	1.25	0.79	-39.34
20-V	1.51		4.93		-11.96
20-HV-HV^2	1.12		6.96		-0.95
25-I	2.33	-7.58	1.30	0.79	-35.09
25-V	1.57		6.30		-4.35
25-HV-HV^2	1.13		7.60		-1.57

I: Initial impact time period

V: Maximum tsunami flow velocity time period

HV: Maximum tsunami mass flux time period

HV^2: Maximum tsunami momentum flux time period

For example, 20-HV-HV^2 means the tsunami scenario where the tsunami water free-surface elevation is 20 ft above the bridge and maximum tsunami mass flux and momentum flux occur.

Table B-2. Maximum Tsunami Forces and Moments on Mad River Slough Bridge

Tsunami Scenario (Water free-surface elevation/time period)	Horizontal Force (Kip/ft)	Vertical Downward Force (Kip/ft)	Uplift Force (Kip/ft)	Positive Overturning Moment (Kip-ft/ft)	Negative Overturning Moment (Kip-ft/ft)
5	2.21	-7.82	2.13	0.66	-35.34
10	2.32	-6.29	3.65	0.74	-39.59
15	2.13	-7.36	5.51	0.77	-35.97
20	2.26	-7.1	6.96	0.79	-39.34
25	2.33	-7.58	7.60	0.79	-35.09

Table B-3. Tsunami Forces and Moments on Salmon Creek Bridge

Tsunami Scenario (Water free-surface elevation/time period)	Horizontal Force (Kip/ft)	Vertical Downward Force (Kip/ft)	Uplift Force (Kip/ft)	Positive Overturning Moment (Kip-ft/ft)	Negative Overturning Moment (Kip-ft/ft)
5	1.27	-8.31	0.61	15.37	-9.23
10	1.44	-7.79	0.53	20.77	-15.29
15-I	1.4	-8.85	0.35	20.7	-11.27
15-V	0.35		3.39	7.05	
15-HV	0.31		4.51	3.03	
15-HV^2	0.32		4.49	5.2	
20-I	1.19	-8.79	0.38	8.15	-12.85
20-V	0.38		4.38	5.09	
20-HV	0.32		5.24	4.95	
20-HV^2	0.35		5.21	5.65	
25-I	1.23	-8.94	0.42	7.59	-17.43
25-V	0.40		4.83	3.29	
25-HV	0.32		6.03	7.59	
25-HV^2	0.37		5.73	6.71	

Table B-4. Maximum Tsunami Forces and Moments on Salmon Creek Bridge

Tsunami Scenario (Water free-surface elevation/time period)	Horizontal Force (Kip/ft)	Vertical Downward Force (Kip/ft)	Uplift Force (Kip/ft)	Positive Overturning Moment (Kip-ft/ft)	Negative Overturning Moment (Kip-ft/ft)
5	1.27	-8.31	0.61	15.37	-9.23
10	1.44	-7.79	0.53	20.77	-15.29
15	1.40	-8.85	4.51	20.7	-11.27
20	1.19	-8.79	5.24	8.15	-12.85
25	1.23	-8.94	6.03	7.59	-17.43

Table B-5. Tsunami Forces and Moments on Old Creek Bridge

Tsunami Scenario (Water free-surface elevation/time period)	Horizontal Force (Kip/ft)	Vertical Downward Force (Kip/ft)	Uplift Force (Kip/ft)	Positive Overturning Moment (Kip-ft/ft)	Negative Overturning Moment (Kip-ft/ft)
5	2.81	-5.77	0.54	4.22	-18.66
10-I-V	3.13	-7.11	0.38	6.16	-20.69
10-HV	0.36		1.86		-1.30
10-HV^2	0.45		1.17		-1.66
15-I	3.09	-6.94	0.56	5.78	-19.92
15-V	0.53		0.77		-0.78
15-HV	0.37		2.24		-1.96
15-HV^2	0.44		1.93		-1.64
20-I	2.93	-7.49	0.60	3.73	-20.18
20-V	0.55		1.50		-1.00
20-HV	0.38		2.58		-0.9
20-HV^2	0.46		2.14		-2.29
25-I	2.59	-8.20	0.49	3.54	-24.19
25-V	0.59		1.68		-2.67
25-HV	0.41		3.01		-0.43
25-HV^2	0.47		2.69		-0.91

Table B-6. Maximum Tsunami Forces and Moments on Old Creek Bridge

Tsunami Scenario	Horizontal Force (Kip/ft)	Vertical Downward	Uplift Force (Kip/ft)	Positive Overturning	Negative Overturning

(Water free-surface elevation/time period)		Force (Kip/ft)		Moment (Kip-ft/ft)	Moment (Kip-ft/ft)
5	2.81	-5.77	0.54	4.22	-18.66
10	3.13	-7.11	1.86	6.16	-20.69
15	3.09	-6.94	2.24	5.78	-19.92
20	2.93	-7.49	2.58	3.73	-20.18
25	2.59	-8.20	3.01	3.54	-24.19

Table B-7. Tsunami Forces and Moments on Malibu Lagoon Bridge

Tsunami Scenario	Horizontal Force (Kip/ft)	Vertical Downward	Uplift Force (Kip/ft)	Positive Overturning	Negative Overturning

(Water free-surface elevation/time period)		Force (Kip/ft)		Moment (Kip-ft/ft)	Moment (Kip-ft/ft)
5	1.87	-2.31	6.20	3.06	-114.52
10-I-V	2.49	-12.39	6.32	2.95	-191.47
10-HV	0.15		20.53		-1.22
10-HV^2	0.17		20.43		-0.12
15-I	2.58	-13.47	6.39	2.84	-180.77
15-V	0.19		20.5		-0.93
15-HV	0.19		20.44		-3.71
15-HV^2	0.18		20.76		-2.6
20-I-V	2.62	-11.08	5.81	3.74	-187.4
20-HV	0.18		20.88		-4.98
20-HV^2	0.19		20.77		-5.19
25-I-V	2.69	-10.75	5.97	3.75	-184.11
25-HV	0.19		20.71		-5.28
25-HV^2	0.21		20.75		-5.89

Table B-8. Maximum Tsunami Forces and Moments on Malibu Lagoon Bridge

Tsunami Scenario	Horizontal Force (Kip/ft)	Vertical Downward	Uplift Force (Kip/ft)	Positive Overturning	Negative Overturning

(Water free-surface elevation/time period)		Force (Kip/ft)		Moment (Kip-ft/ft)	Moment (Kip-ft/ft)
5	1.87	-2.31	6.20	3.06	-114.52
10	2.49	-12.39	20.53	2.95	-191.47
15	2.58	-13.47	20.76	2.84	-180.77
20	2.62	-11.08	20.88	3.74	-187.4
25	2.69	-10.75	20.75	3.75	-184.11

Table B-9. Tsunami Forces and Moments on Agua Hedionda Lagoon Bridge

Tsunami Scenario (Water free-surface elevation/time period)	Horizontal Force (Kip/ft)	Vertical Downward Force (Kip/ft)	Uplift Force (Kip/ft)	Positive Overturning Moment (Kip-ft/ft)	Negative Overturning Moment (Kip-ft/ft)
5-I	0.68	-10.38	1.56	118.88	-335.58
5-V-HV-HV^2	0.09		14.34	15.00	
10-I	0.92	-9.77	2.44	182.61	-231.92
10-V-HV-HV^2	0.29		10.51	19.78	
15-I-V-HV^2	1.25	-14.75	6.83	434.21	-96.38
15-HV	0.32		13.35		-11.62
20-I-V-HV^2	1.10	-17.65	4.67	456.67	-10.70
20-HV	0.33		14.01	7.11	
25-I-V-HV^2	1.34	-17.95	9.08	608.07	-66.9
25-HV	0.76	-0.16		140.18	

Table B-10. Maximum Tsunami Forces and Moments on Agua Hedionda Lagoon Bridge

Tsunami Scenario	Horizontal Force (Kip/ft)	Vertical Downward	Uplift Force (Kip/ft)	Positive Overturning	Negative Overturning

(Water free-surface elevation/time period)		Force (Kip/ft)		Moment (Kip-ft/ft)	Moment (Kip-ft/ft)
5	0.68	-10.38	14.34	118.88	-335.58
10	0.92	-9.77	10.51	182.61	-231.92
15	1.25	-14.75	13.35	434.21	-97.38
20	1.10	-17.65	14.01	465.67	-10.70
25	1.34	-17.95	9.08	608.07	-66.9

C. Appendix C. Load Estimation Procedure Input and Results

The results of the load estimation procedure explained in Section 9 of the report and the corresponding representative input values used in proposed equations are provided here. These input values are presented for all tsunami scenarios studied in this study. The following tables provide two sets of information. The first includes bridge geometry information and the second contains tsunami flow field data. The empirical coefficients are those presented in Tables 2 and 3 in Section 9. The density of water is 64 lb/ft^3 (or 0.002 Kip-s^2/ft^4) and acceleration of gravity is 32.17 ft/s^2. Definition of all the following parameters is provided in Section 9.

Table C-1. Estimation of Maximum Tsunami Forces on Mad River Slough Bridge from Proposed Design Procedure

Tsunami Scenario (Water free-surface elevation/time period)	Horizontal Force (Kip/ft)	Vertical Downward Force (Kip/ft)	Uplift Force (Kip/ft)
5	2.71	8.20	4.50
10	2.74	8.23	4.93
15	2.69	8.18	5.41
20	2.72	8.21	5.89
25	2.80	8.29	6.34

Table C-2. Estimation of Maximum Tsunami Forces on Salmon Creek Bridge from Proposed Design Procedure

Tsunami Scenario (Water free-surface elevation/time period)	Horizontal Force (Kip/ft)	Vertical Downward Force (Kip/ft)	Uplift Force (Kip/ft)
5	1.58	4.20	
10	1.63	4.26	
15	1.63	4.27	5.15
20	1.56	4.18	5.31
25	1.58	4.21	5.46

Table C-3. Estimation of Maximum Tsunami Forces on Old Creek Bridge from Proposed

Design Procedure

Tsunami Scenario (Water free-surface elevation/time period)	Horizontal Force (Kip/ft)	Vertical Downward Force (Kip/ft)	Uplift Force (Kip/ft)
5	2.13	4.73	
10	2.14	4.74	3.34
15	2.20	4.78	3.49
20	2.22	4.79	3.62
25	2.08	4.66	3.78

Table C-4. Estimation of Maximum Tsunami Forces on Malibu Lagoon Bridge from Proposed Design Procedure

Tsunami Scenario (Water free-surface elevation/time period)	Horizontal Force (Kip/ft)	Vertical Downward Force (Kip/ft)	Uplift Force (Kip/ft)
5	2.96	17.41	
10	3.02	17.46	16.90
15	3.04	17.48	17.06
20	3.15	17.57	17.19
25	3.15	17.57	17.33

Table C-5. Estimation of Maximum Tsunami Forces on Agua Hedionda Lagoon Bridge from Proposed Design Procedure

Tsunami Scenario (Water free-surface elevation/time period)	Horizontal Force (Kip/ft)	Vertical Downward Force (Kip/ft)	Uplift Force (Kip/ft)
5	0.54	13.46	14.53
10	0.70	13.62	19.54
15	0.90	13.80	20.50
20	1.07	13.96	21.35
25	1.06	13.95	

Table C-6. Mad River Slough Bridge Geometry

, ft	8.7
, ft	3.08
, ft	0.58
, ft	2.68
, ft	43.5
, ft	6.34
V, ft³	53.8
	10.7

Table C-7. Tsunami Flow Field at Mad River Slough Bridge

Tsunami Scenario (Water free-surface elevation/time period)	*, ft*	*, ft*	*v, ft/s*
5-I	17.7	9.0	5.17
5-HV-HV[2]	20.2	11.5	7.42
10-I	17.7	9.0	5.42
10-HV-HV[2]	25.1	16.4	8.25
15-I	17.7	9.0	5
15-HV-HV[2]	30.1	21.4	9.08
20-I	17.7	9.0	5.25
20-HV-HV[2]	35	26.3	9.83
25-I	17.7	9.0	5.83
25-HV-HV[2]	40.1	31.4	10.5

Table C-8. Salmon Creek Bridge Geometry

, ft	15.8
, ft	0
, ft	1.75
, ft	2.68
, ft	43.5
, ft	4.43
V, ft³	81
	10.7

Table C-9. Tsunami Flow Field at Salmon Creek Bridge

Tsunami Scenario (Water free-surface elevation/time period)	*, ft*	*, ft*	*v, ft/s*
5	22.9	7.1	4.68
10	22.9	7.1	5.27
15-I	22.9	7.1	5.32
15-HV	26.5	10.7	5.83
20-I	22.9	7.1	4.47
20-HV	30.1	14.3	6.25
25-I	22.9	7.1	4.75
25-HV	33.7	17.9	6.58

Table C-10. Old Creek Bridge Geometry

, ft	18.5

, ft	3.65
, ft	0.56
, ft	1.67
, ft	39.7
, ft	5.89
V, ft³	47.7
	6.68

Table C-11. Tsunami Flow Field at Old Creek Bridge

Tsunami Scenario (Water free-surface elevation/time period)	*, ft*	*, ft*	*v, ft/s*
5	26.1	7.6	5.75
10-I-V	26.1	7.6	5.83
10-HV	31.7	13.2	5.67
15-I	26.1	7.6	6.25
15-HV	36.2	17.7	6.08
20-I	26.1	7.6	6.42
20-HV	40.5	22	6.42
25-I	26.1	7.6	5.39
25-HV	42.3	23.8	7.17

Table C-12. Malibu Lagoon Bridge Geometry

, ft	16.3
, ft	0

, ft	4.05
, ft	2.90
, ft	88
, ft	6.94
V, ft³	325
	11.6

Table C-13. Tsunami Flow Field at Malibu Lagoon Bridge

Tsunami Scenario (Water free-surface elevation/time period)	*, ft*	*, ft*	*v, ft/s*
5	26.1	9.8	3.11
10-I-V	26.1	9.8	3.72
10-HV	28.6	12.3	3.42
15-I	26.1	9.8	3.93
15-HV[2]	31.3	15.0	3.75
20-I-V	26.1	9.8	4.83
20-HV[2]	35.2	18.9	4.0
25-I-V	26.1	9.8	4.83
25-HV[2]	39.2	22.9	4.25

Table C-14. Agua Hedionda Lagoon Bridge Geometry

, ft	23.6
, ft	0
, ft	1.58

, ft	1.25
, ft	158
, ft	2.83
V, ft³	251
	5

Table C-15. Tsunami Flow Field at Agua Hedionda Lagoon Bridge

Tsunami Scenario (Water free-surface elevation/time period)	*, ft*	*, ft*	*v, ft/s*
5-I	27.7	4.1	3.14
5-V-HV-HV^2	28.4	4.8	4.16
10-I	27.7	4.1	6.23
10-V-HV-HV^2	29.3	5.7	7.67
15-I-V-HV^2	27.7	4.1	8.62
15-HV	33.1	9.5	8.17
20-I-V-HV^2	27.7	4.1	10.2
20-HV	37	13.4	6.58
25-I-V-HV^2	27.7	4.1	10.1

D. Appendix D. Screen Captures of CFD Simulations

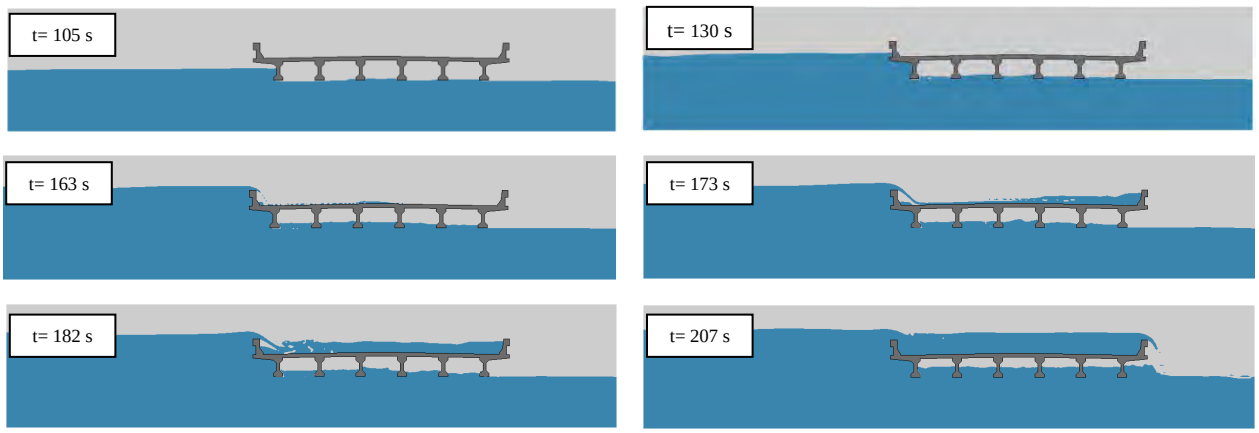

Figure D-1. Screen captures of Mad River Slough Bridge, Water surface elevation 5 ft above bridge elevation, Initial impact time period.

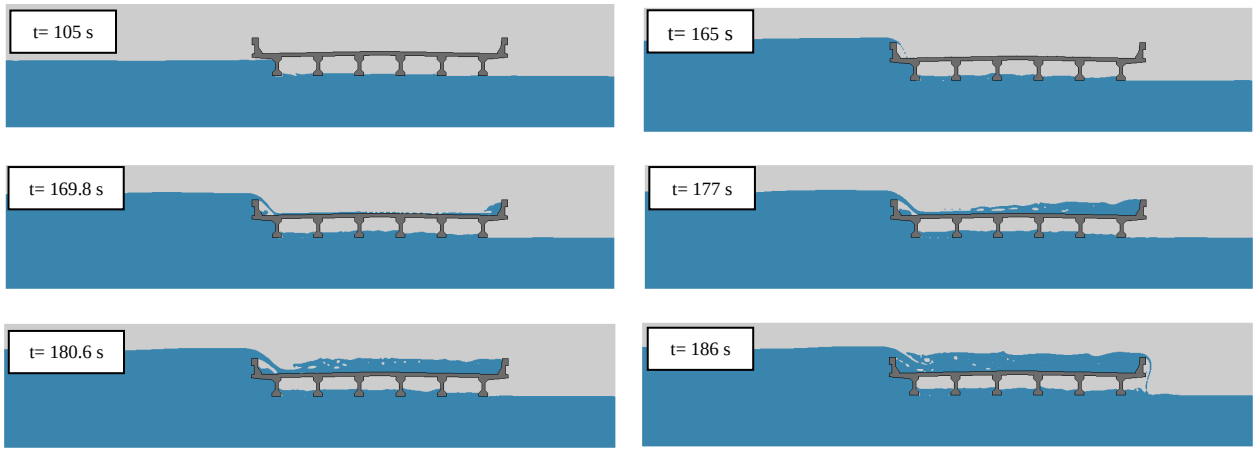

Figure D-2. Screen captures of Mad River Slough Bridge, Water surface elevation 10 ft above bridge elevation, Initial impact time period.

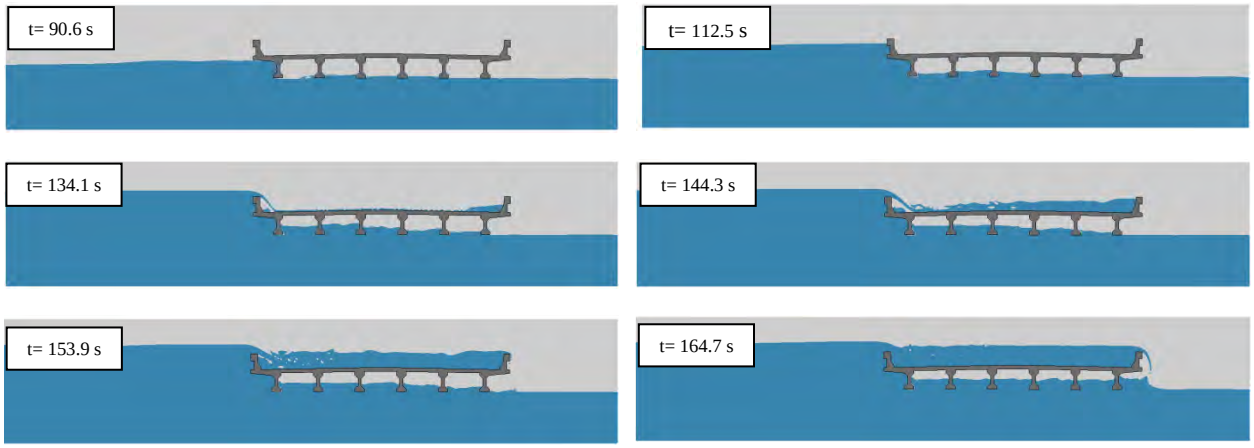

Figure D-3. Screen captures of Mad River Slough Bridge, Water surface elevation 15 ft above bridge elevation, Initial impact time period.

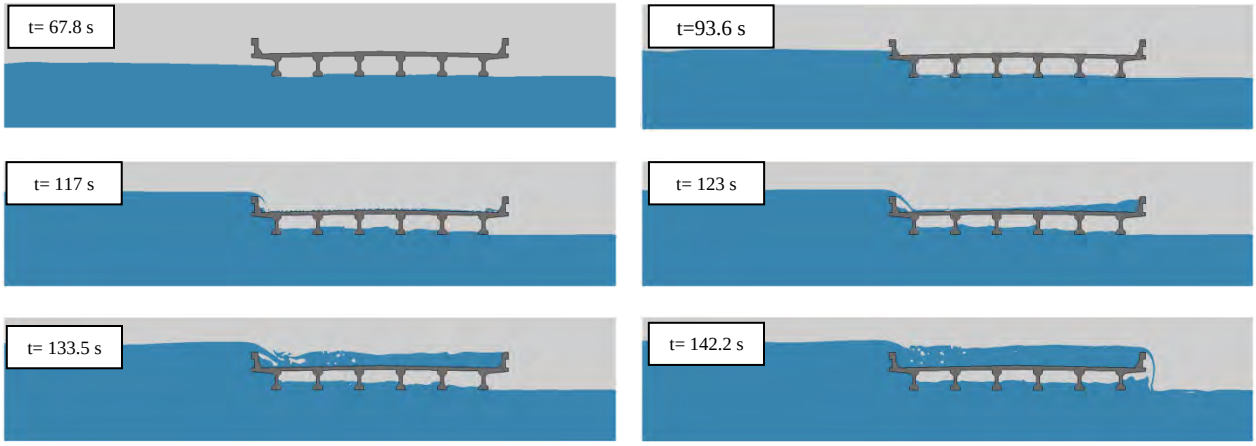

Figure D-4. Screen captures of Mad River Slough Bridge, Water surface elevation 20 ft above bridge elevation, Initial impact time period.

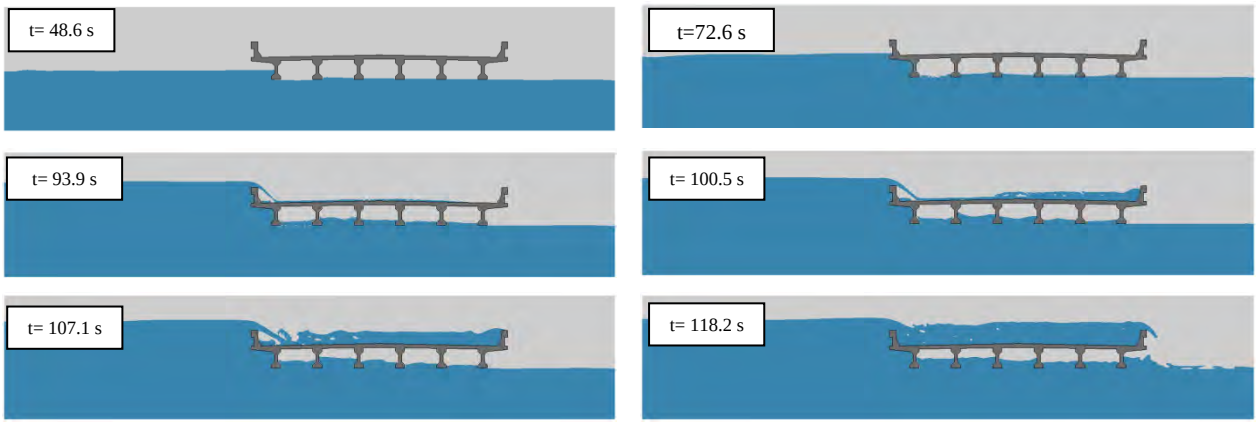

Figure D-5. Screen captures of Mad River Slough Bridge, Water surface elevation 25 ft above bridge elevation, Initial impact time period.

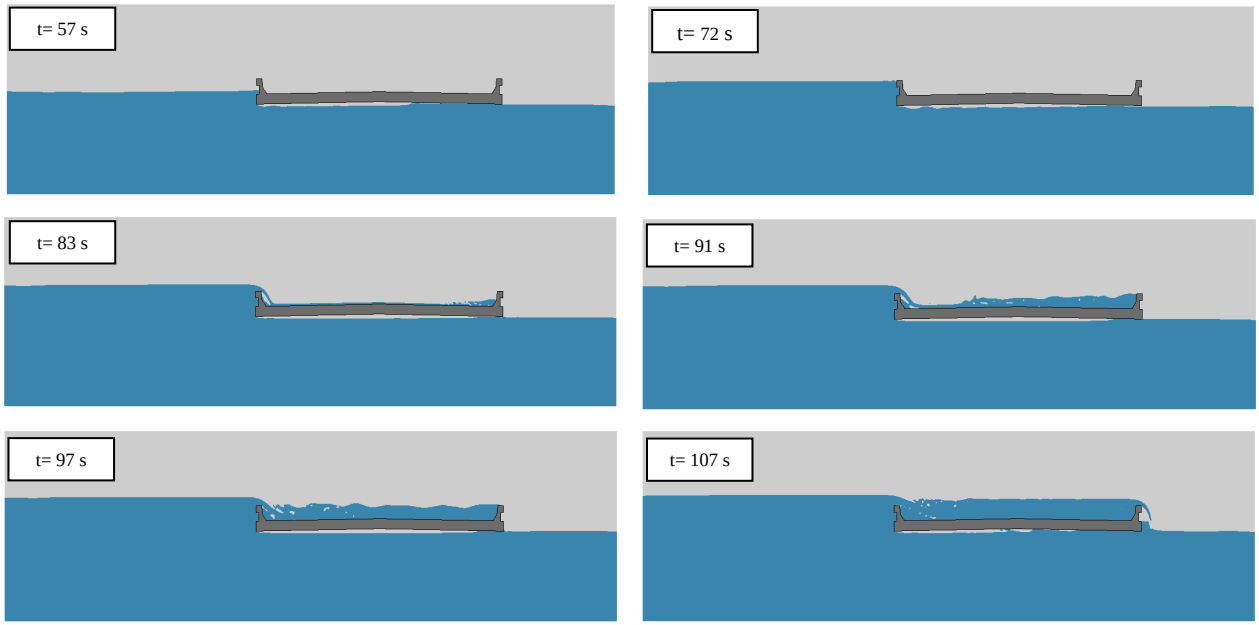

Figure D-6. Screen captures of Salmon Creek Bridge, Water surface elevation 5 ft above bridge elevation, Initial impact time period.

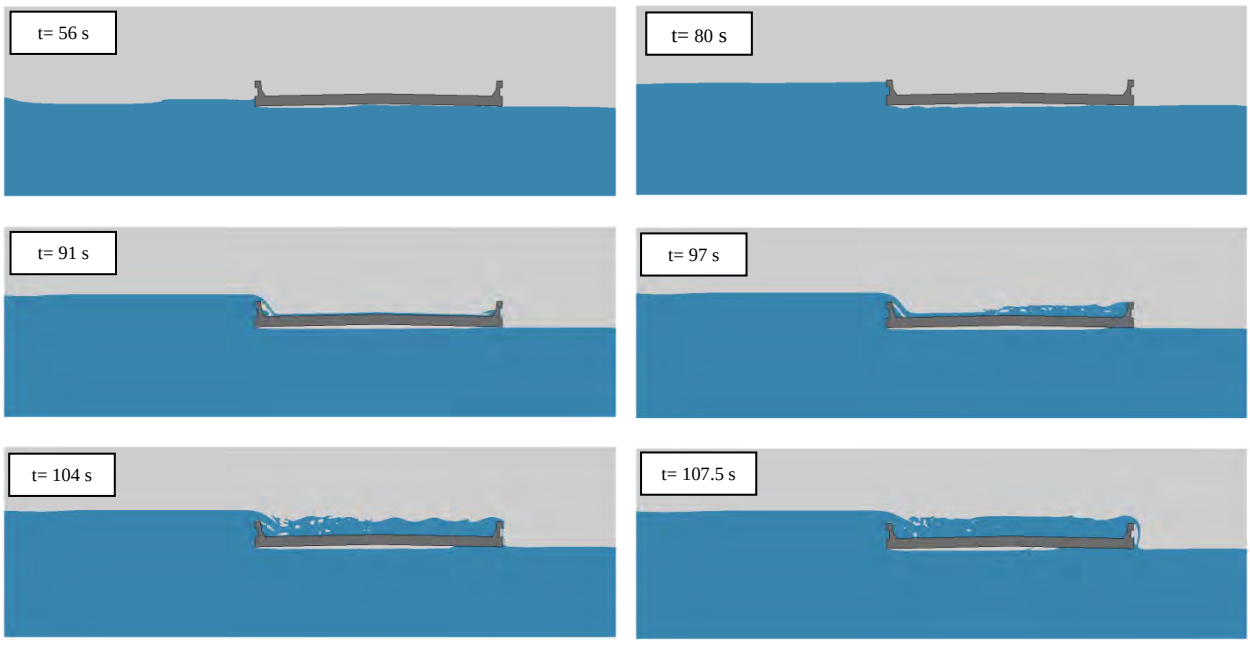

Figure D-7. Screen captures of Salmon Creek Bridge, Water surface elevation 10 ft above bridge elevation, Initial impact time period.

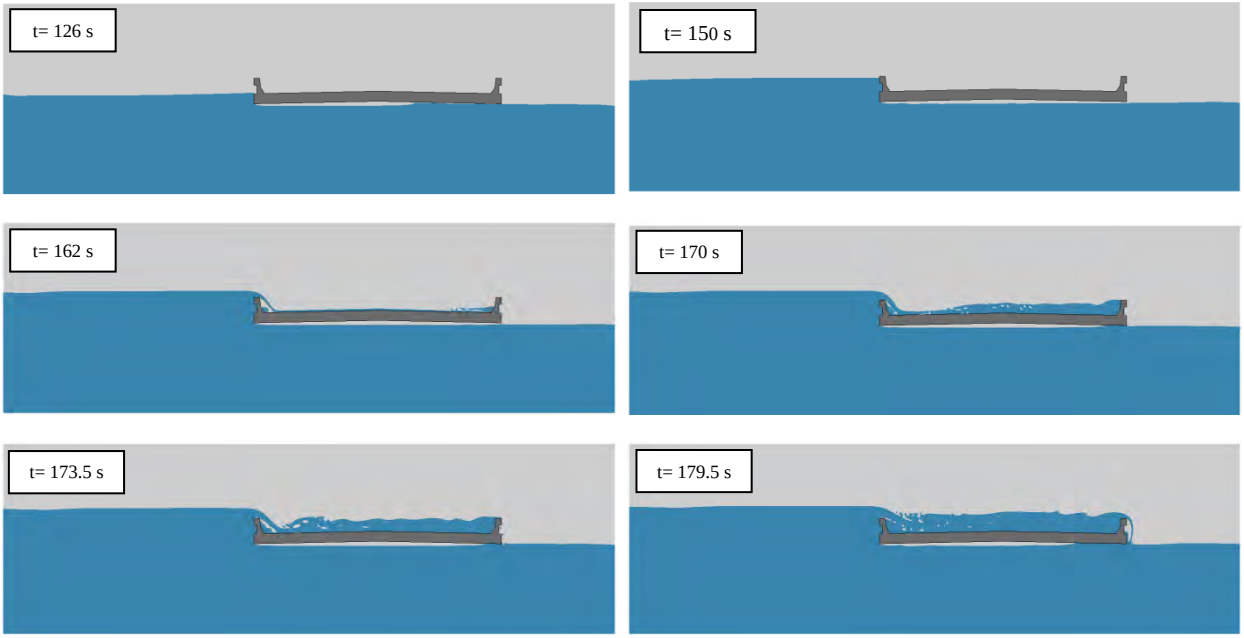

Figure D-8. Screen captures of Salmon Creek Bridge, Water surface elevation 15 ft above bridge elevation, Initial impact time period.

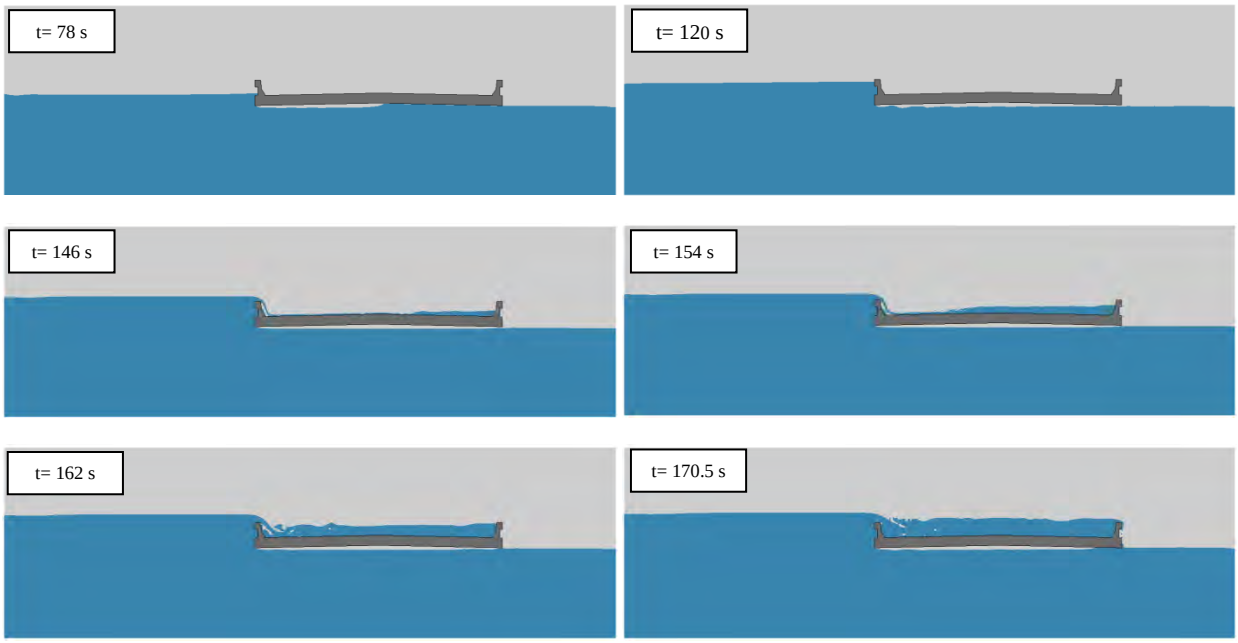

Figure D-9. Screen captures of Salmon Creek Bridge, Water surface elevation 20 ft above bridge elevation, Initial impact time period.

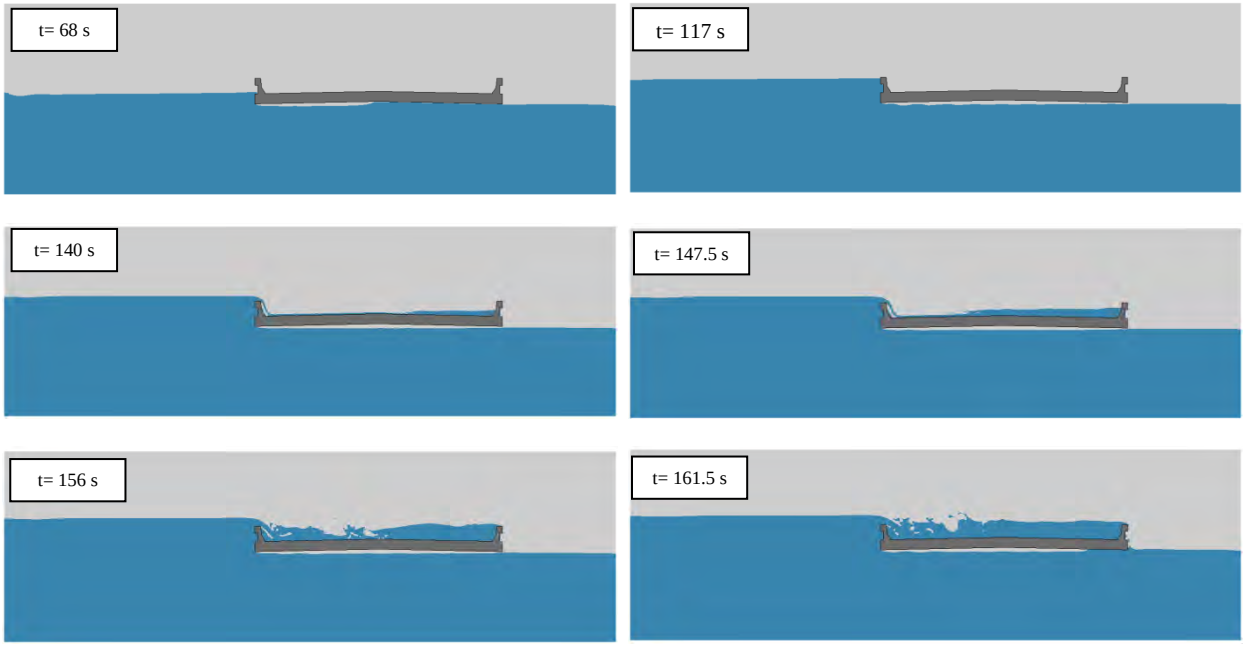

Figure D-10. Screen captures of Salmon Creek Bridge, Water surface elevation 25 ft above bridge elevation, Initial impact time period.

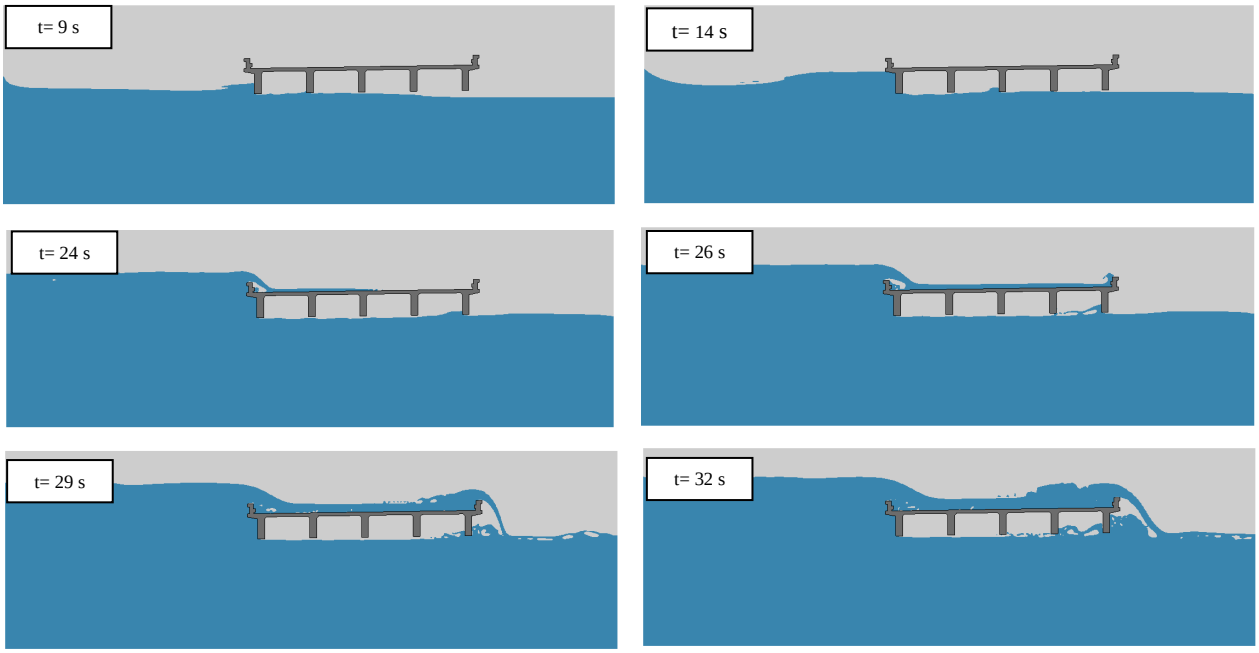

Figure D-11. Screen captures of Old Creek Bridge, Water surface elevation 5 ft above bridge elevation, Initial impact time period.

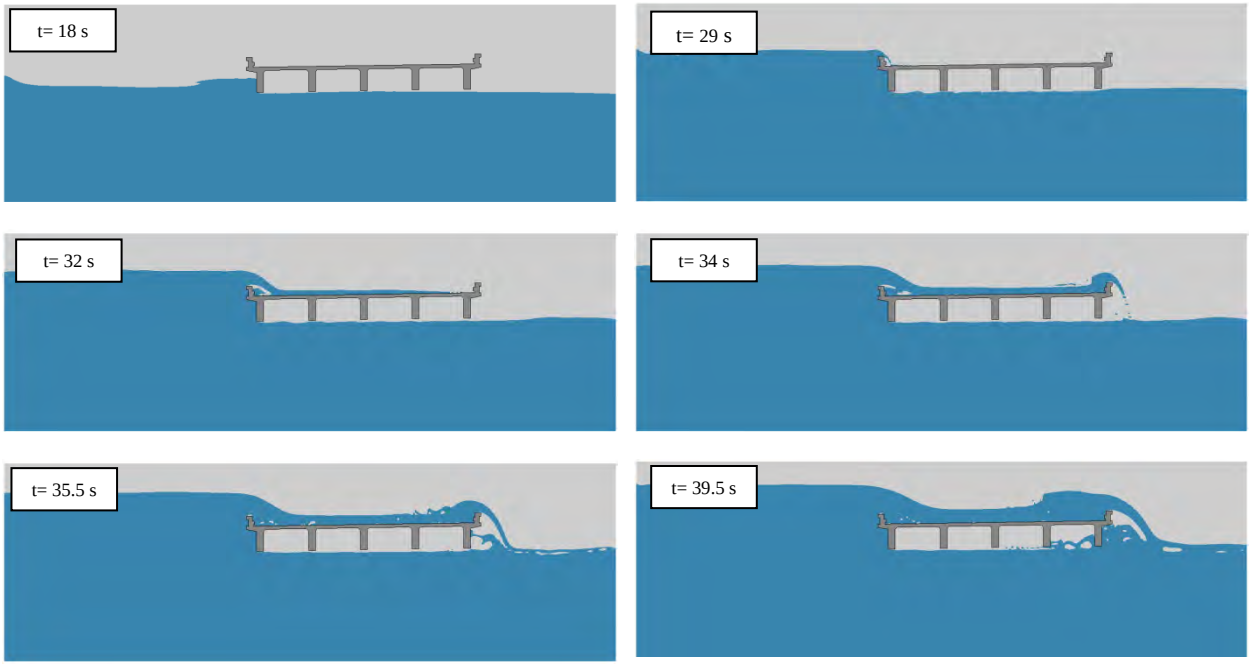

Figure D-12. Screen captures of Old Creek Bridge, Water surface elevation 10 ft above bridge elevation, Initial impact time period.

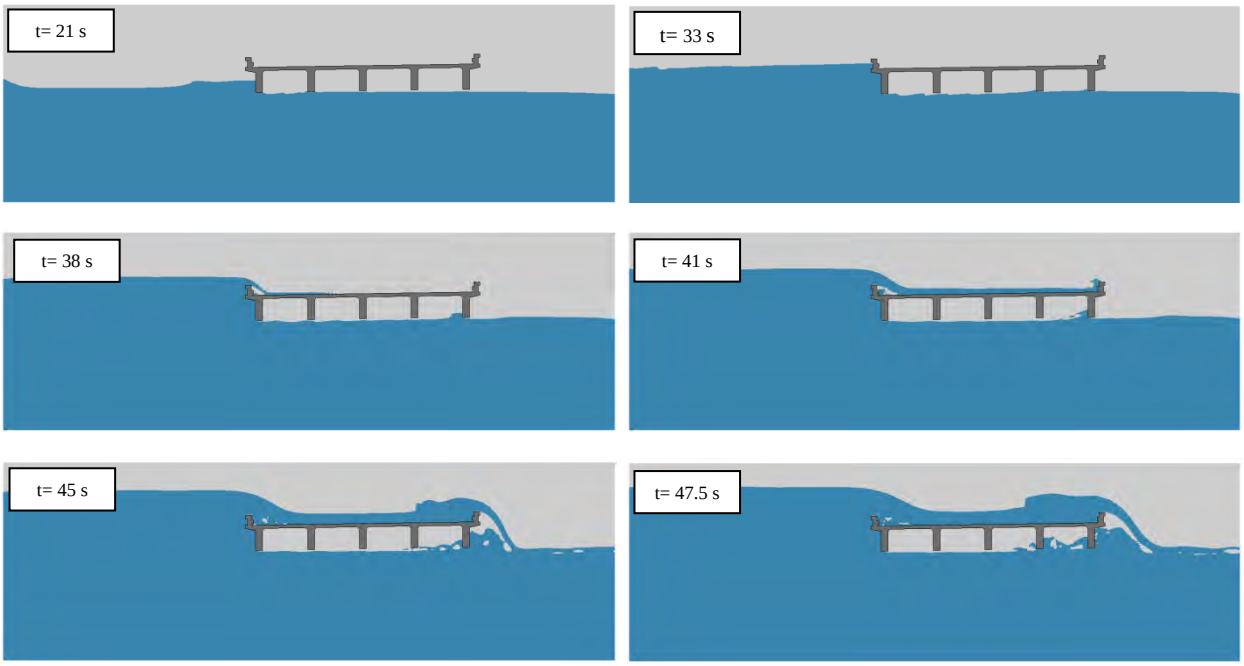

Figure D-13. Screen captures of Old Creek Bridge, Water surface elevation 15 ft above bridge elevation, Initial impact time period.

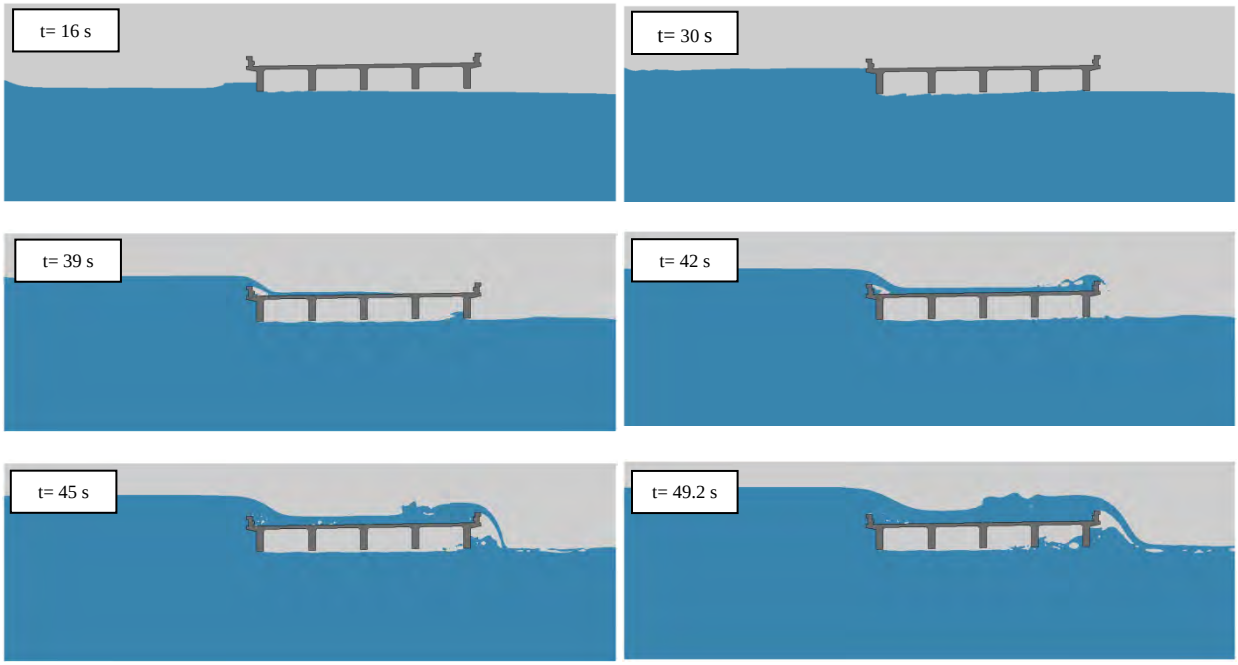

Figure D-14. Screen captures of Old Creek Bridge, Water surface elevation 20 ft above bridge elevation, Initial impact time period.

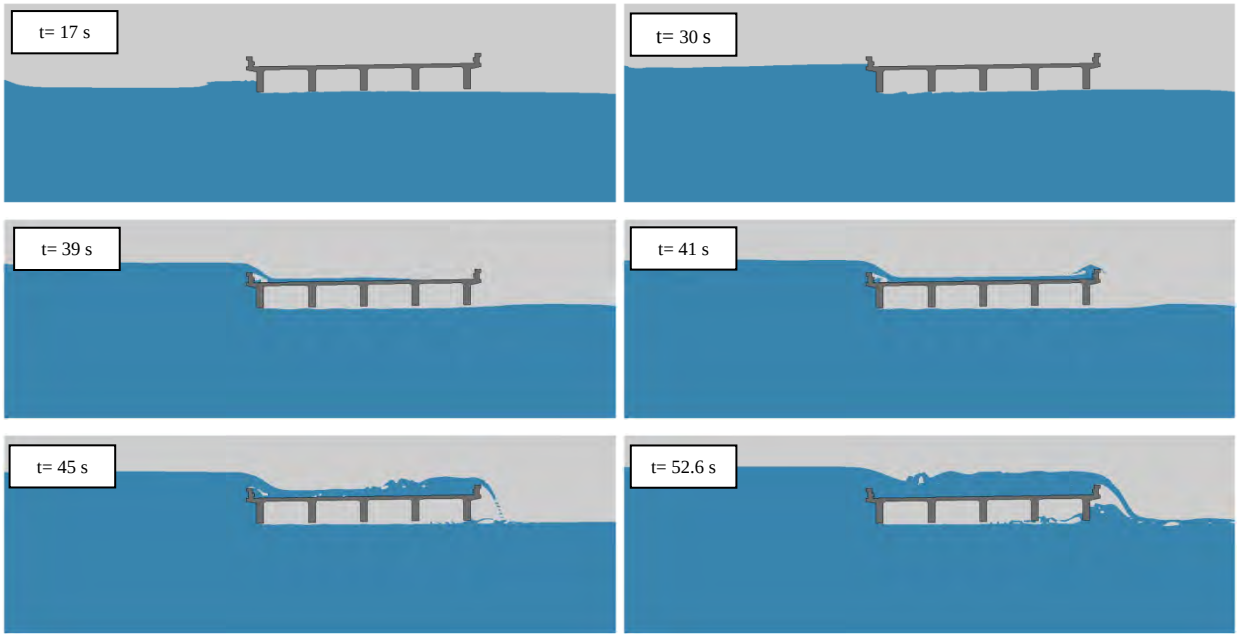

Figure D-15. Screen captures of Old Creek Bridge, Water surface elevation 25 ft above bridge elevation, Initial impact time period.

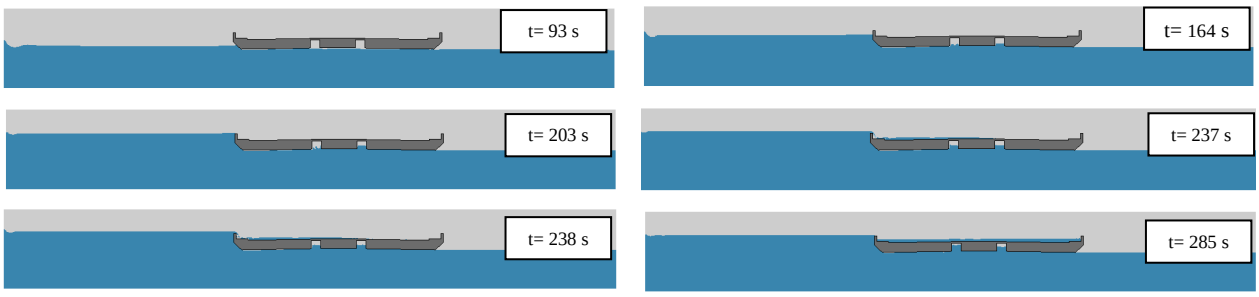

Figure D-16. Screen captures of Malibu Lagoon Bridge, Water surface elevation 5 ft above bridge elevation, Initial impact time period.

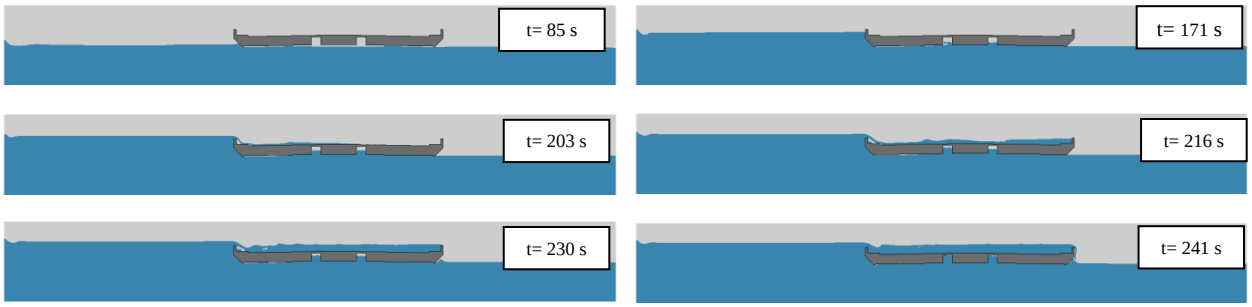

Figure D-17. Screen captures of Malibu Lagoon Bridge, Water surface elevation 10 ft above bridge elevation, Initial impact time period.

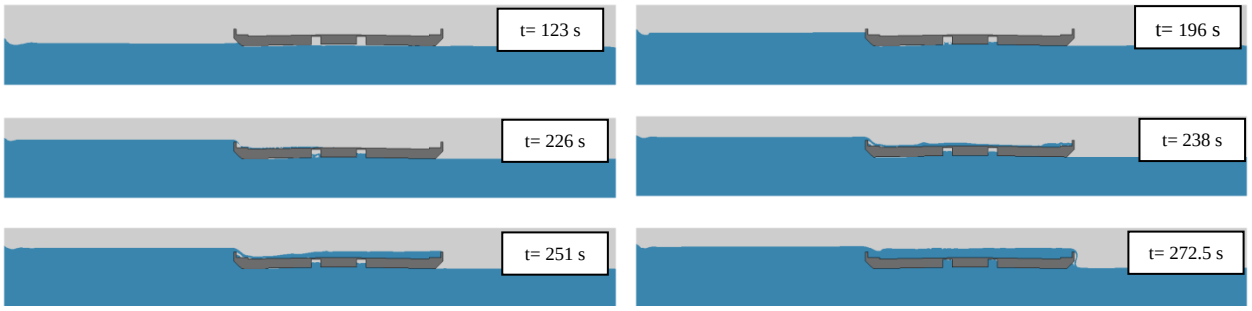

Figure D-18. Screen captures of Malibu Lagoon Bridge, Water surface elevation 15 ft above bridge elevation, Initial impact time period.

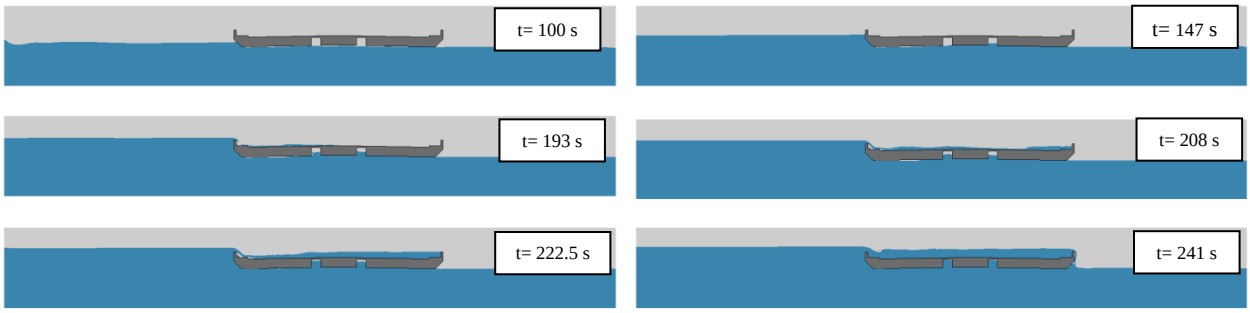

Figure D-19. Screen captures of Malibu Lagoon Bridge, Water surface elevation 20 ft above bridge elevation, Initial impact time period.

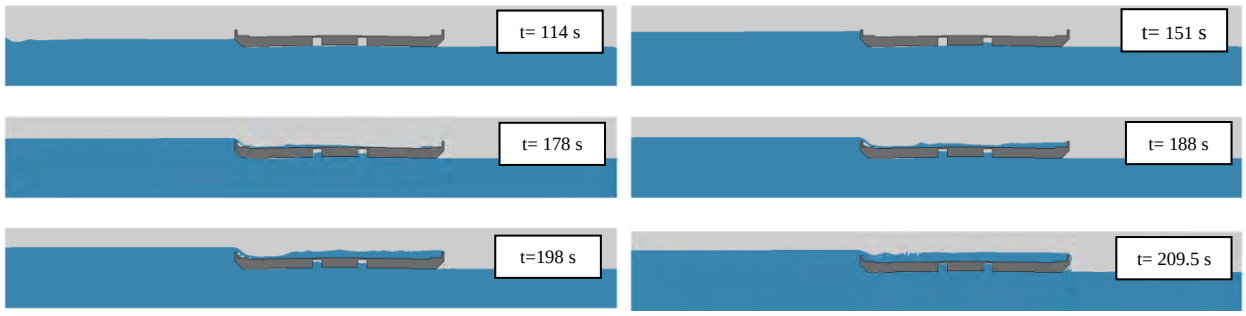

Figure D-20. Screen captures of Malibu Lagoon Bridge, Water surface elevation 25 ft above bridge elevation, Initial impact time period.

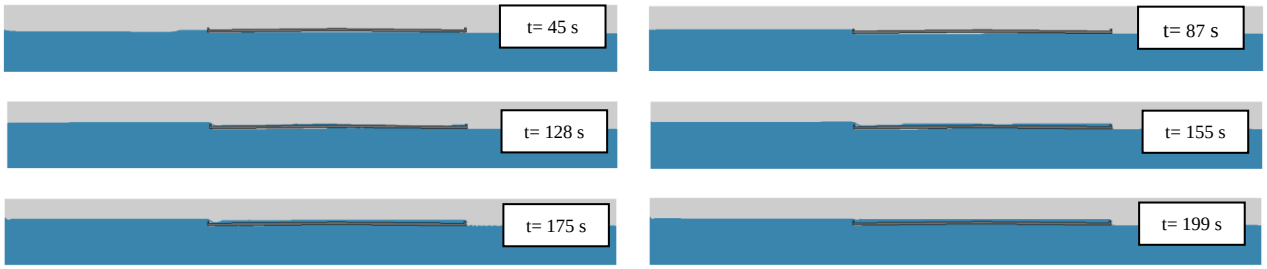

Figure D-21. Screen captures of Agua Hedionda Lagoon Bridge, Water surface elevation 5 ft above bridge elevation, Initial impact time period.

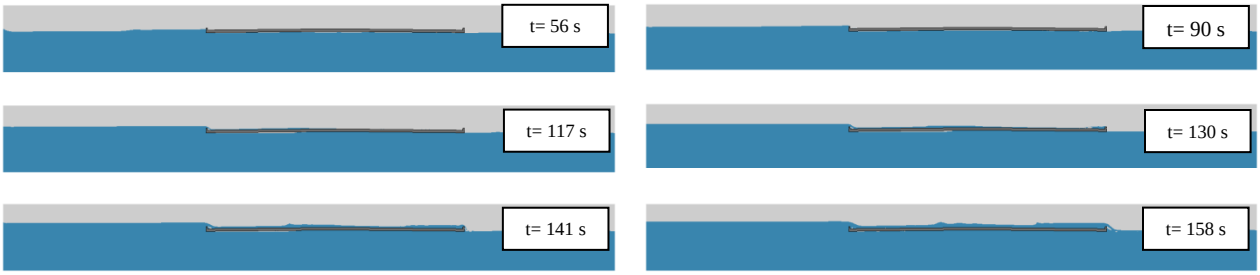

Figure D-22. Screen captures of Agua Hedionda Lagoon Bridge, Water surface elevation 10 ft above bridge elevation, Initial impact time period.

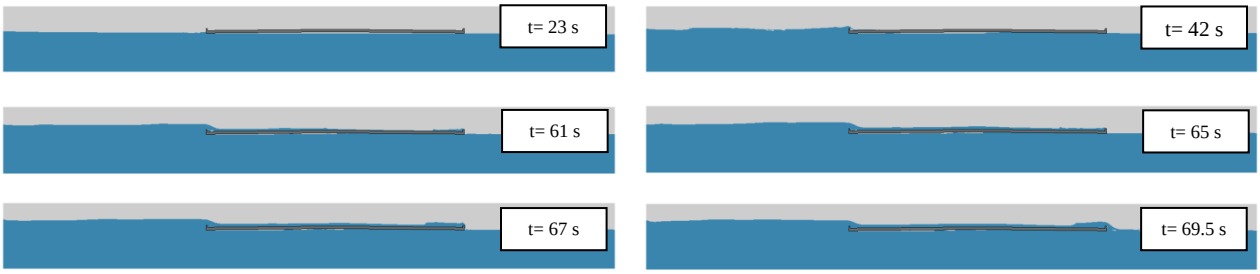

Figure D-23. Screen captures of Agua Hedionda Lagoon Bridge, Water surface elevation 15 ft above bridge elevation, Initial impact time period.

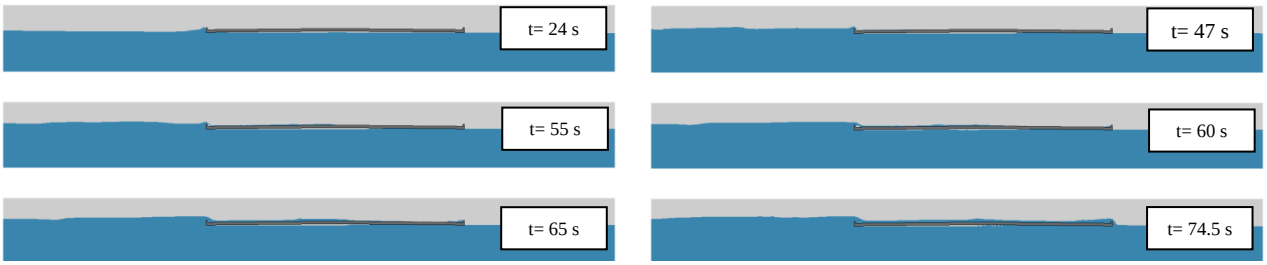

Figure D-24. Screen captures of Agua Hedionda Lagoon Bridge, Water surface elevation 20 ft above bridge elevation, Initial impact time period.

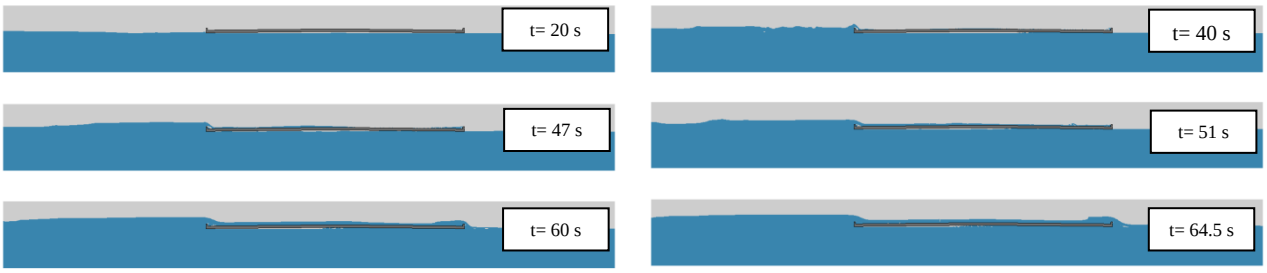

Figure D-25. Screen captures of Agua Hedionda Lagoon Bridge, Water surface elevation 25 ft above bridge elevation, Initial impact time period.

E. Appendix E. Drawings of Selected Bridges

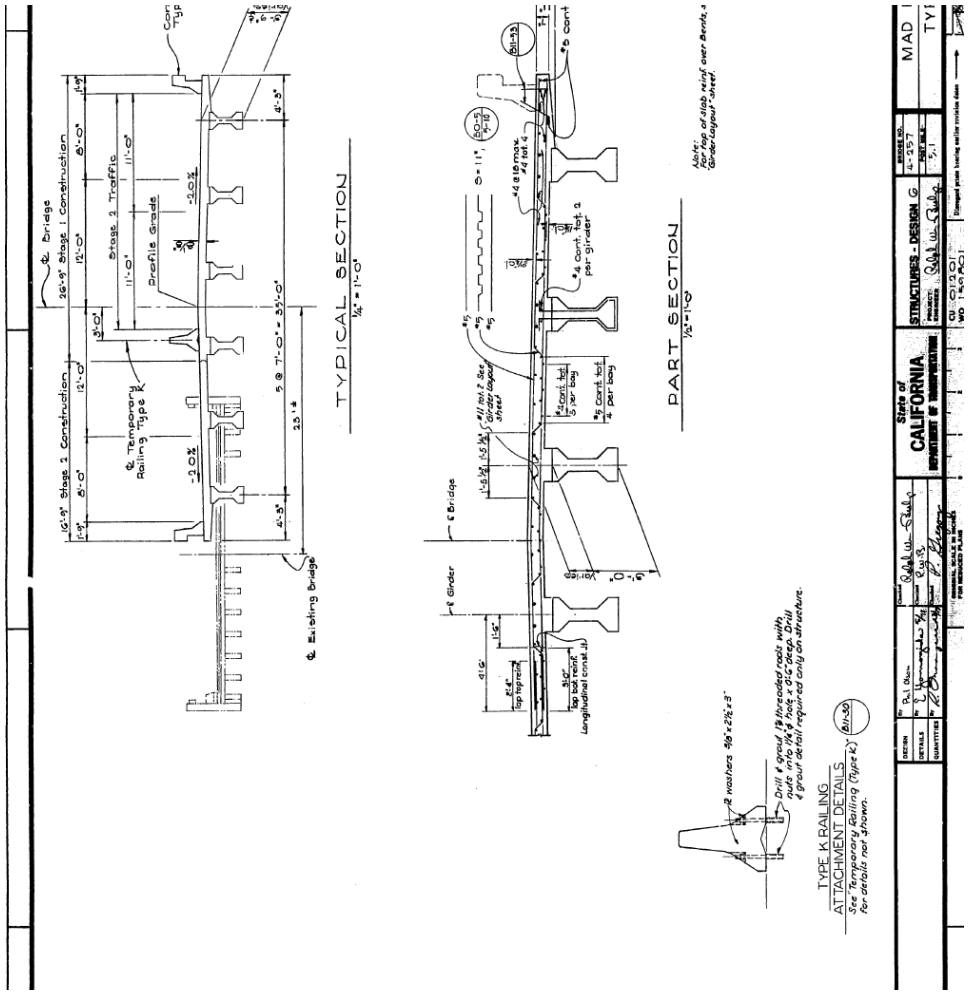

Figure E-1. Drawing of Mad River Slough Bridge.

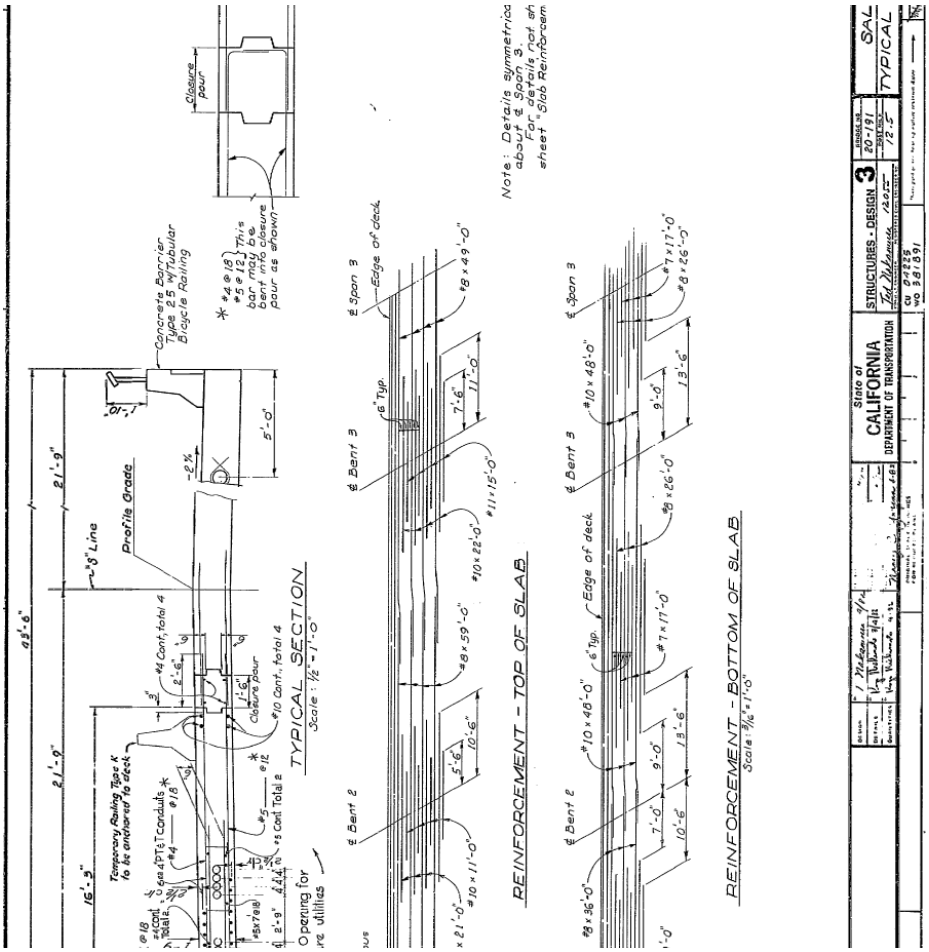

Figure E-2. Drawing of Salmon Creek Bridge.

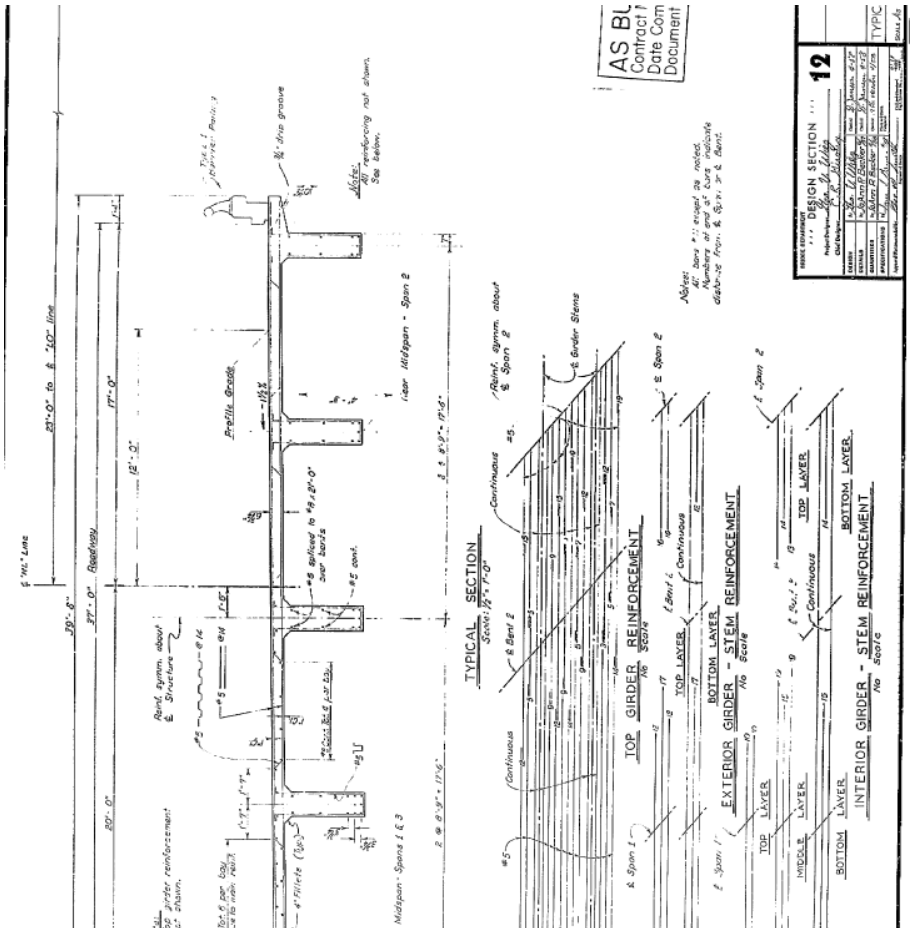

Figure E-3. Old Creek Bridge.

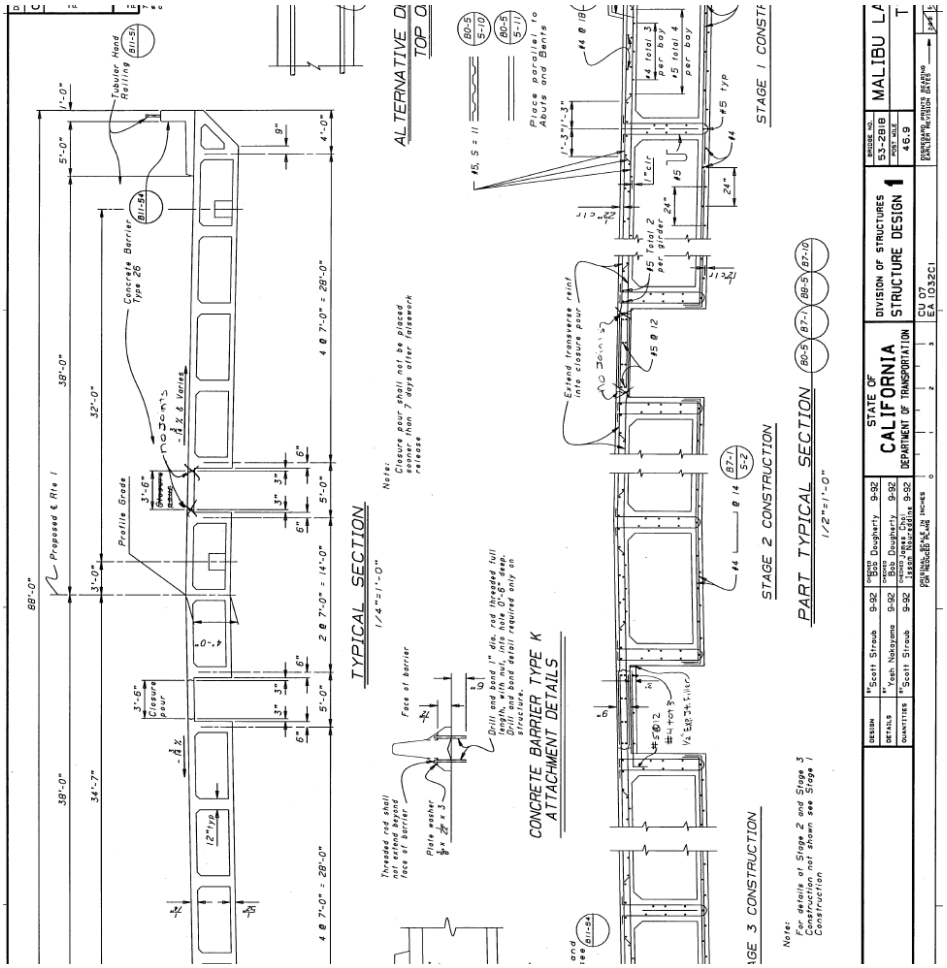

Figure E-4. Malibu Lagoon Bridge.

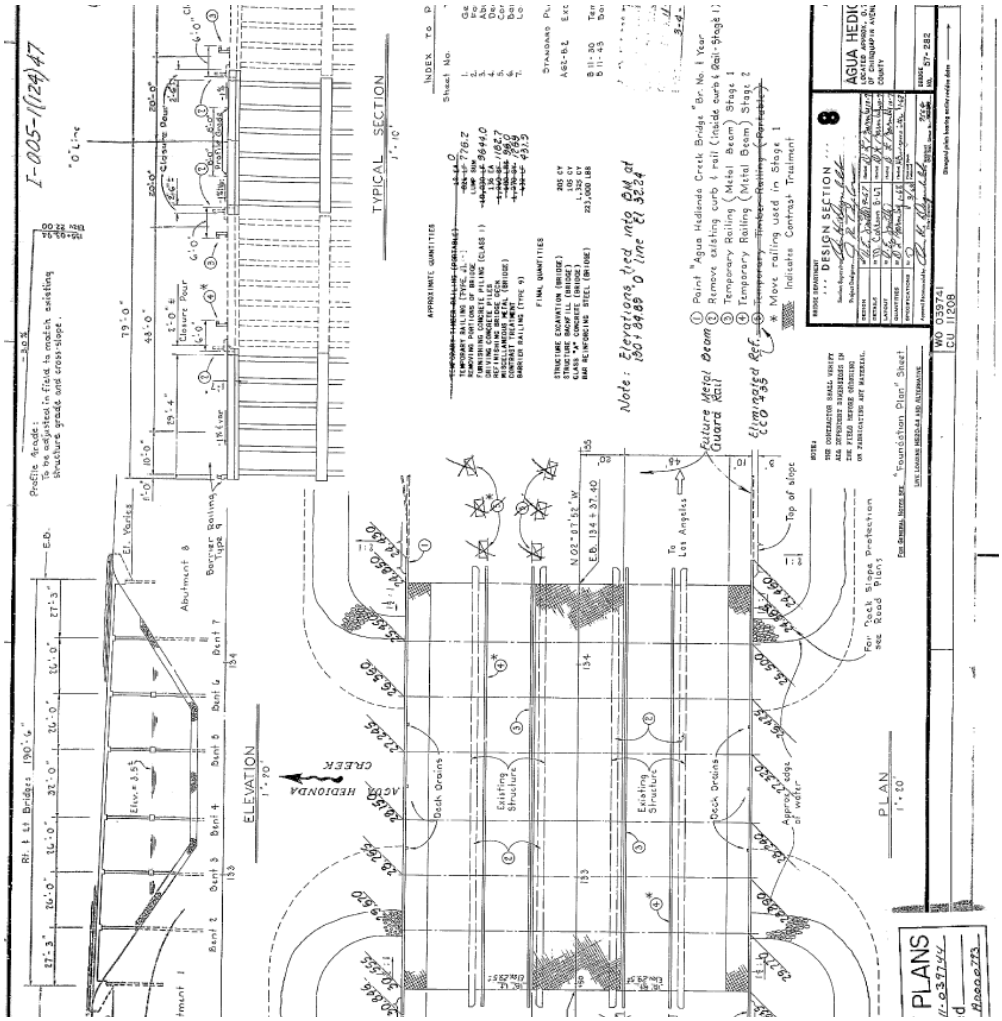

Figure E-5. Agua Hedionda Lagoon Bridge.